Steady state crack growth in viscoelastic solids: a comparative study

Chung-Yuen Hui[1*], Bangguo Zhu[1,2], Rong Long[3*]

[1]Sibley School of Mechanical and Aerospace Engineering, Field of Theoretical and Applied Mechanics, Cornell University, Ithaca, New York, 14853, USA

[2]Department of Modern Mechanics, University of Science and Technology of China, Hefei, Anhui, 230027, China

[3]Department of Mechanical Engineering, University of Colorado Boulder, Boulder, Colorado, 80309, USA

*Corresponding Authors: ch45@cornell.edu, rong.long@colorado.edu

Abstract

We compare the predictions of different theories on the steady state growth of a Mode I crack in linear viscoelastic solids. The theories studied in this work included those by Knauss, Schapery, Persson and Brener. The comparisons focus on the fractional dissipation rate and the relationship between crack growth velocity and fracture energy. Analytical solutions are carried out using realistic constitutive models such as the Generalized Maxwell Solid (GMS) and the Power Law Solid (PLS). These theories are tested against two different sets of experimental data reported in the literature. We also present new results such as the strain field directly ahead of the crack tip, the residual strain on the crack surfaces and the crack opening displacement (COD). We use the expressions for COD to study the shape and size of the "viscoelastic trumpet" proposed by de Gennes. Using a new approach, we study the shape and size of the viscoelastic dissipation zone around the crack tip and discuss its dependence on the crack growth velocity.

Keywords: Viscoelasticity, fracture, steady-state crack growth, dissipation zone, energy release rate, crack opening displacement.

Nomenclature (Greek followed by English alphabets; in alphabetical order**):**

α length of the cohesive zone or fracture process zone.

α^K length of the cohesive zone in Knauss's theory (see eqs. (4a) and (10b)).

α^S effective length of the cohesive zone in Schapery's theory (see eq. (11b))

α^{PB} length of the fracture process zone in Persson and Brener's theory (eqs. (4b) and (12d)).

$\hat{\alpha}^{PB}$ $\equiv \alpha^{PB}/2\pi$.

β $\equiv \alpha/vt_c$, dimensionless parameter given in eq. (8c).

β_n $\equiv \alpha/vt_n$, dimensionless parameter for the generalized Maxwell solid.

β^K dimensionless parameter given in eq. (10b).

β_n^K β^K defined using retardation time t_n of a generalized Maxwell solid (see eq. (18b)).

β_{ave}^K β^K defined using the average retardation time t_c^{ave} of a generalized Maxwell solid (see eq. (18f)).

β^S dimensionless parameter given in eq. (11b).

β_n^S β^S defined using retardation time t_n of a generalized Maxwell solid (see eq. (19a)).

β_{ave}^S β^S defined using the average retardation time t_c^{ave} of a generalized Maxwell solid (see eq. (19b)).

β^{PB} dimensionless parameter given in eq. (12d).

β_n^{PB} β^{PB} defined using retardation time t_n of a generalized Maxwell solid (see eq. (20a)).

β_{ave}^{PB} β^{PB} defined using the average retardation time t_c^{ave} of a generalized Maxwell solid (see eq. (20c)).

χ_{cod} viscoelastic effect parameter on crack opening displacement (see eq. (56a)).

χ_{strain} viscoelastic effect parameter on strain field (see eq. (36b)).

χ_{strain}^* viscoelastic effect parameter for ε_{22}^* (* indicates non-interacting model).

δ_0 critical crack opening displacement of the Dugdale-Barenblatt cohesive zone model.

δ_+ $= \delta_+(t)$, Dirac delta function (see Table 1).

ε_{22} normal strain perpendicular to the crack calculated using the exact stress field with the Dugdale-Barenblatt cohesive zone.

ε_{22}^∞ limiting value of ε_{22} in a fully relaxed solid.

ε_{22}^* normal strain perpendicular to the crack calculated using the non-interacting model stress field.

$\varepsilon_{22}^{\infty *}$ limiting value of ε_{22}^{*} in a fully relaxed solid.

η dimensionless dummy integration variable.

γ Euler's constant = 0.5772156649...

Γ Gamma function.

κ $\equiv 1 - J_0 / J_\infty = 1 - E_\infty / E_0$.

Λ $\equiv G_D/G = (G - G_0)/G$, fractional dissipation rate.

Λ^K fractional dissipation rate according to Knauss's theory (see eq. (10a)).

Λ^S fractional dissipation rate according to Schapery's theory (see eq. (11a)).

Λ^{PB} fractional dissipation rate according to Persson and Brener's theory (see eq. (12c) and (13a)).

Λ^{dG} fractional dissipation rate according to de Gennes's theory (see eq. (13b)).

ω frequency of oscillatory deformation in viscoelastic solids.

ω_c $\equiv 2\pi v/\alpha^{PB}$, cut-off frequency near the crack tip in Persson and Brener's theory.

ω_{max} $\equiv 2\pi v/\alpha$, cut-off frequency near the crack tip in de Gennes's theory (see eq. (2)).

Φ_D local dissipation rate (see eq. (61)).

$\bar{\Phi}_D$ Normalized local dissipation rate (see eq. (67)).

Ψ integral function defined in eq. (38b).

Ψ_{PL} integral function defined in eq. (42b).

φ function defined in eq. (50b).

φ_D angular function in eq. (68a).

ρ total dissipation rate inside a square centered at crack tip divided by G_D, $\rho \le 1$

σ_D constant cohesive stress in the Dugdale-Barenblatt cohesive zone model.

σ_m maximum cohesive stress in a general cohesive zone model.

σ_{PB} critical cohesive stress in Persson and Brener's theory.

σ_{ij} in-plane stress components (i, j = 1 or 2).

$\hat{\sigma}_{ij}$ angular variation of the Mode-I crack tip stress field (see eq. (5)).

θ angular coordinate of the polar coordinate system centered at the crack tip.

ξ dimensionless dummy integration variable.

ζ = (3 – 4ν) for plane strain and = (3 – ν)/(1 + ν) for plane stress where ν is the Poisson's ratio (assumed to be 0.5 in this work).

a_n coefficients in the generalized Maxwell solid (see eq. (16a)).

b substitution symbol defined in eq. (60d).

c_m dimensionless parameter in eq. (31a).

c_D constant of order one in eq. (68b) and (68c).

C_{PB} creep compliance function in Persson and Brener's definition (see Table 1).

d lower bound of α at zero crack velocity, related to α through $\alpha = Gd/G_0$.

d^K lower bound of α^K at zero crack velocity (see eq. (10b)).

d^S lower bound of α^S at zero crack velocity (see eq. (11b)).

d^{PB} lower bound of α^{PB} at zero crack velocity (see eq. (12d)).

$\hat{d}^{PB}$ $\equiv d^{PB}/2\pi$.

E^* complex modulus in the frequency domain: $E^* = E^*(\omega)$.

E^*_{loss} imaginary part of the complex modulus E^*.

$E^*_{storage}$ real part of the complex modulus E^*.

E^*_{PB} complex modulus in Persson and Brener's definition (see Table 1).

E_0 instantaneous tensile modulus.

E_∞ relaxed tensile modulus.

F function given in eq. (6c).

F' derivative of $F(\bar{X})$; given in eq. (6b).

${}_2F_1$ Gauss Hypergeometric function (see eq. (22a)).

G applied energy release rate; $= K_I^2 / E_\infty$ for plane stress; $= 3K_I^2 / 4E_\infty$ for plane strain.

G_0 intrinsic fracture energy; $= \sigma_D \delta_0$ in Dugdale-Barenblatt model.

G_D $\equiv G - G_0$, the dissipative energy release rate due to viscoelasticity.

$\bar{G}$ $\equiv G/G_0$, normalized energy release rate.

H_1 Hankel transform of order one (see eq. (13a)).

I integral function defined in eq. (18c).

$J(t)$ creep function under uniaxial tension.

J_0 $= J(t = 0) = 1/E_0$, instantaneous creep compliance.

J_∞ $= J(t = +\infty) = 1/E_\infty$, long-term creep compliance.

J_1 Bessel function of the first kind of order one (see eq. (13a)).

J^* complex compliance in the frequency domain: $J^* = J^*(\omega)$.

$J^*_{storage}$ real part of the complex compliance J^*.

ΔJ $\Delta J(t) = J(t) - J_\infty \le 0$ (see eq. (6d)).

$\Delta\tilde{J}$ $\Delta\tilde{J}(t/t_c) = \Delta J(t)$.

K_I applied stress intensity factor.

L length of a square centered at crack tip to for integrating the local dissipation rate.

$\bar{L}$ L normalized by size of cohesive or fracture zone, α.

L_t length scale of the "viscoelastic trumpet" (see eq. (1)).

m exponent parameter of a power law solid (see eq. (17)), $0 < m < 1$.

M Kummer's Confluent Hypergeometric function (see eq. (18c)).

N number of viscous branches in a generalized Maxwell solid (see eq. (16a)).

Q integral function defined in eq. (55b).

R radial coordinate of the polar coordinate system centered at the crack tip.

t_c creep retardation time under uniaxial tensile creep test.

t_c^{ave} average creep retardation time of a generalized Maxwell solid (see eq. (16c)).

t_n creep retardation times of a generalized Maxwell solid (n = 1, 2, ..., N).

t_R relaxation time under uniaxial tensile relaxation test ($< t_c$).

u_{cod} crack opening displacement.

$\bar{u}_{cod}$ $\equiv u_{cod} / \delta_0$, normalized crack opening displacement.

v crack growth velocity.

$\bar{v}$ $\equiv v t_c / d$, generic normalized crack growth velocity.

$\bar{v}^K$ $\equiv v t_c / d^K$, normalized crack growth velocity in Knauss's theory.

$\bar{v}^S$ $\equiv v t_c / d^S$, normalized crack growth velocity in Schapery's theory.

$\bar{v}^{PB}$ $\equiv v t_c / \hat{d}^{PB} = 2\pi v t_c / d^{PB}$, normalized crack growth velocity in Persson and Brener's theory.

v_c $\equiv d / t_c$, reference crack velocity used to define $\bar{v}$; a material constant.

$\dot{W}_e$ elastic stress work rate

X horizontal coordinate of the moving Cartesian system centered at the crack tip.

$\bar{X}$ $\equiv X / \alpha$, normalized horizontal coordinate.

Y vertical coordinate of the moving Cartesian system centered at the crack tip.

Abbreviations:

1D: One-dimensional

2D: Two-dimensional

COD: Crack Opening Displacement

DB: Dugdale-Barenblatt

FDR: Fractional Dissipation Rate

GMS: Generalized Maxwell Solid

K: Knauss

LHS: Left Hand Side

PB: Persson and Brener

PLS: Power Law Solid

RHS: Right Hand Side

S: Schapery

SI: Supplementary Information

SS: Standard Solid

SSC: Small Scale Creep

1. Introduction and Historical Perspective

Interest in the fracture of viscoelastic materials has been around since the 1960s. The subject was brought into the attention of engineers and mechanicians due to the increasing use of polymer as engineering materials. There was also an intense interest in the reliability of viscoelastic solid propellant in rockets [1]. The main contributors to theoretical development in this period are Williams [2], Mueller and Knauss [3]. In these earlier works, crack growth is assumed to occur in discrete jumps. A continuous crack growth theory where a 2D crack growing quasi-statically under steady state in a Maxwell solid was given by Kostrov and Nikitin [4] in 1970. Here it is interesting to note that Willis [5], in 1967, obtained the exact solution of a steady state Mode III semi-infinite crack growing *dynamically* in an infinite linear viscoelastic medium driven by surface traction translating rigidly with the growing crack. Willis used a Dugdale-Barenblatt (DB) cohesive zone model [6,7] to quantify local failure at the crack tip. The viscoelasticity in his medium was modeled using the standard linear solid, where there is a single relaxation time. A more comprehensive theory of fracture in linear viscoelastic solids, together with experiments, was published by Knauss in 1973 [8]. In this work, he developed an exact expression for the crack opening displacement for a steadily growing plane stress/plane strain crack in a linear viscoelastic solid with an arbitrary creep function. In this formulation, Knauss considered the small-scale creep (SSC) problem where viscoelastic dissipation is confined to a small region near the crack tip. The geometry is shown in Fig.1. He used a cohesive model more sophisticated than the DB model to eliminate the stress singularity at the crack tip. In his model, a material point experiences a constant cohesive stress as it enters the cohesive zone tip, which then decays to zero linearly at the crack tip. The relation between the crack growth velocity and the applied stress intensity factor was obtained by enforcing the fracture criterion that the crack opening displacement (COD) must be equal to the critical opening displacement where the cohesive stress vanishes. In this work we focus on a special case of this model, i.e., the DB model where the cohesive stress is constant throughout the cohesive zone (see the inset of Fig.1A).

In 1975, Schapery published a series of papers [9–11] where he removed many of the restrictions in Knauss's theory. For example, his theory accounts for non-steady state crack growth and allows for a much wider class of cohesive zone models. More importantly, he also provided closed-form, approximate expressions for the relationship between crack growth velocity and the stress intensity factor [10] which can be difficult to determine in Knauss's formulation (to be elaborated below). Here one should also mention the work of Graham, an applied mathematician who extended the classical correspondence principle applicable to stationary cracks to growing and closing crack problems with moving boundaries [12]. For example, a straightforward application of Graham's theory shows that the stress field in Knauss's SSC problem is given by the classical DB model where the material is elastic outside the cohesive zone. This stress field depends only on the cohesive stress and is *independent of any other material properties*. For completeness, we have included the full stress field for the DB model in Section S1 of the Supplementary Information (SI).

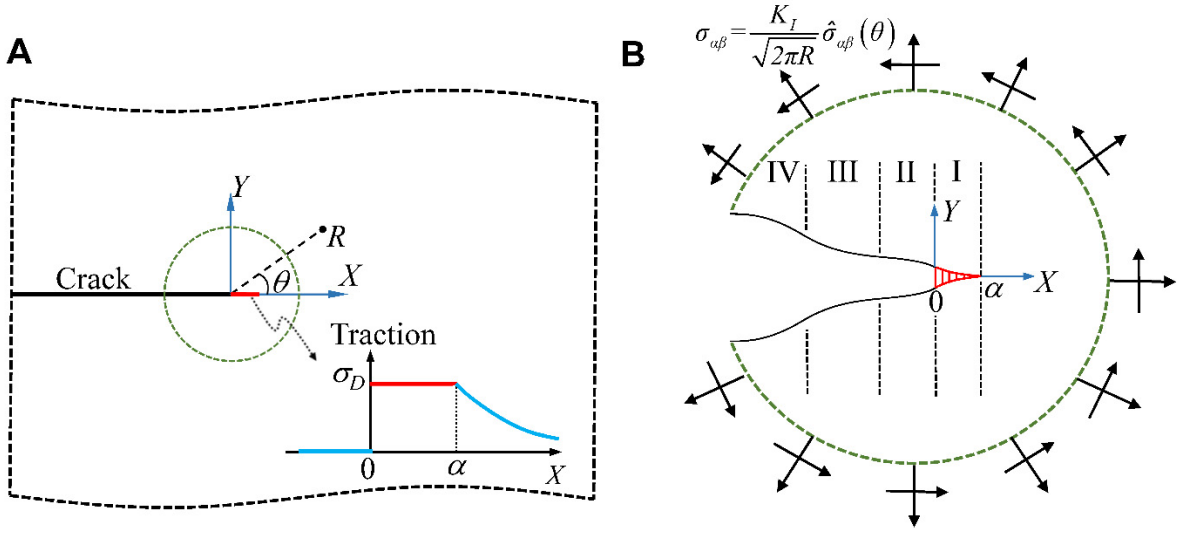

Figure 1 Geometry of the SSC problem. (A) A semi-infinite crack in an infinite viscoelastic solid. The crack tip is subjected to a DB cohesive zone at $0 \le X \le \alpha$ with a constant cohesive stress σ_D. (B) Zoomed-in view of the circular area centered at the crack tip. The crack opening profile under sufficiently fast growth velocity consists of four regions: I) fracture process zone; II) "hard solid" region; III) "liquid" trumpet region; IV) "soft solid" region. The outer boundary of the circular area is subjected to tractions prescribed by the *K*-field.

As noted by Rice [13], the presence of singular fields at the growing crack tip will create a paradox in which the local energy available for fracture is independent of the crack velocity v. This is because the local stress rate at the crack tip is proportional to the spatial gradient of stress multiplied by v. Therefore, the presence of a singular stress field will result in infinite stress rate at the crack tip. Thus, as long as $v > 0$, there is always a glassy region surrounding the crack tip. The extended correspondence principle states that local energy release rate in this glassy region is given by K_I^2 / E_0 where E_0 is the instantaneous or glassy Young's modulus. This means that the local energy release rate is independent of crack velocity – a paradox. The use of cohesive zone model eliminates the stress singularity and resolves this paradox.

The acceptance of Knauss's and Schapery's theories is not without controversy. It is interesting to note that a different approach to the crack growth problem was proposed by Christensen in 1979 [14]. In Christensen's approach, he avoided the use of cohesive zone model or a local fracture criterion. Instead, he used energy balance to separate the total energy of the system into the energy dissipated by the viscoelastic solid and the energy available for separation at the crack tip. The difficulty with this approach is that the *energy dissipation rate* (i.e., energy dissipated per unit length of crack extension) diverges due to the infinite strain rate at the crack tip. This difficulty is not fully appreciated at the time because of the mathematical difficulty of evaluating the energy dissipation rate in closed form. As we shall see later, there are two ways to compute this dissipation rate. Readers interested in historical perspective are encouraged to consult the lively correspondence between Christensen and McCartney debating the role of energy

balance [15–18]. The story ended well: in 1983, Christensen and McCartney co-published a paper [19] reconciling their differences and agreed that a bounded stress at the crack tip is necessary to apply energy balance. It is perhaps because of this controversy that the energy balance approach (which must be equally valid) is abandoned in favor of the cohesive zone approach. As we shall see, the energy balance approach will be resurrected by physicists. In any case, it is reasonable to conclude that by the end of 1983 most of the key elements of linear viscoelastic fracture have been agreed upon by the mechanics community.

In the late nineteen eighties and nineties, spurred by the interest in soft condensed matter physics, physicists started to develop their own versions of viscoelastic fracture theory. In the theories of Knauss [8] and Schapery [9], little attention is given to the amount of dissipation and where it occurs. In 1996, de Gennes published his seminal paper on soft adhesives [20]. In this work, he considered the same geometry as that in Knauss's 1973 paper: a semi-infinite steady state crack growing under SSC condition, but with a new twist. To simplify the analysis, he assumed crack growth occurs in a standard solid with a single relaxation time t_R. de Gennes did not solve the continuum equations; instead, he used scaling analysis and energy balance to reveal two results concealed in Knauss's and Schapery's theories: the first of these results indicates that, for sufficiently fast cracks, the crack opening profile can be roughly divided into four regions[1] (see Fig.1B): I). a very small "nonlinear" region around the crack tip where linear viscoelasticity breaks down; this region is essentially the fracture process zone and corresponds to the cohesive zone in the theories of Knauss [8] and Schapery [9]; II) a "hard solid" region immediately outside the "nonlinear" region where the material is glassy and the crack opening is small; III) next to the "hard solid" region is the "liquid" trumpet region where the material behaves like a viscous fluid; IV) the "liquid" region is joined by a "soft solid" region where the material is fully relaxed at its rubbery state. de Gennes proposed that most of the dissipation takes place in the "liquid" trumpet region. His scaling argument suggested that the length of the "liquid" trumpet region, L_t, is

$$L_t \sim \left(E_0 / E_\infty\right) v t_R , \tag{1}$$

where v is the crack velocity, E_0 and E_∞ are the glassy and relaxed Young's modulus respectively. Note that in this paper the subscripts "0" and "∞" for the modulus refer to the time domain, in contrast to a number of literature [20–22] where these subscripts refer to the frequency domain. In other words, E_0 and E_∞ is equivalent to the elastic modulus at infinite and zero frequency, respectively. For highly dissipative viscoelastic solids, $E_0 / E_\infty \approx 10^2 \sim 10^3$. The second result (equation (20) in de Gennes [20]) is that the dissipation part of the energy release rate G_D scales as:

$$G_D \equiv G - G_0 \sim K_I^2 \int_0^{\omega_{\max}} \mathrm{Im}\left(\frac{1}{E^*(\omega)}\right)\frac{d\omega}{\omega}, \tag{2}$$

[1] Only three regions are illustrated in de Gennes [20]; the nonlinear zone is too small to include. The "nonlinear" region was later added to the trumpet diagram by Saulnier et al. [21].

where G is the applied energy release rate outside the viscoelastic dissipation region (i.e., in the "soft solid" region), G_0 is the energy release rate delivered to the fracture process zone (equal to the intrinsic fracture energy during quasi-static crack growth), K_I is the stress intensity factor and $E^*(\omega)$ is the complex modulus under uniaxial tension[2]. The frequency ω in the integral of eq. (2) represents the cyclic loading rate at a material point as the crack grows and scales with the crack velocity v as $\omega \sim v/R$, where R is the distance between the material point and the crack tip. The introduction of a cutoff frequency $\omega_{max} \sim v/\alpha$ in eq. (2), where α is the size of the "*nonlinear*" *zone*, not only prevents the *divergence* of the dissipation integral but also brings in the dependence on crack velocity v. This expression highlights the difficulty with Christensen's approach [14]: the dissipation rate will diverge unless a cutoff length is introduced. Indeed, the divergence of the dissipation rate and the paradox raised by Rice [13] are one and the same issue.

In de Gennes's theory, existence of the "liquid" trumpet region relies on a sufficiently fast crack growth velocity v. In this regime, the size of the trumpet is given by eq. (1) which is independent of the cohesive zone properties, suggesting a decoupling between local fracture process and bulk dissipation. However, as the crack slows, the size of the trumpet is expected to decrease and eventually vanish. As this happens, the "soft solid" region starts to interact with the "nonlinear" zone. de Gennes's theory has very little to say about this regime. Specifically, de Gennes suggested that most of the energy dissipation takes place in the liquid trumpet region: at slow velocities, energy dissipation can be neglected. This turns out to be inaccurate, as noted by Saulnier et al. in their 2004 paper [21]. The scaling theory of Saulnier et al. [21] indicates that the regime of slow velocities can be important since considerable energy dissipation may take place in the "soft solid" region due to its large volume. However, the potential interaction between local fracture process and bulk dissipation for low crack velocities cannot be studied using a purely energetic model where the stress outside the fracture process zone is unaffected and given by the elastic field. Finally, de Gennes considered an infinite domain, so his theory may break down when the size of trumpet exceeds the specimen dimension. This finite specimen effect was considered by Saulnier et al. [21]. In this work, we focus on the SSC problem with an infinite domain (see Fig.1), and thus do not account for the finite specimen effect either.

The dissipation rate expression obtained by de Gennes [20] (with a similar one given by Saulnier et al. [21]) is based on scaling analysis and a standard linear solid model. Therefore, it is difficult to apply this expression to provide quantitative information such as the relation between crack velocity and the applied energy release rate. A useful form of such relation, valid for any linear viscoelastic solids, was derived by Persson and Brener (PB) [22]. Similar to de Gennes [20] and Saulnier et al. [21], the "nonlinear" zone is treated as a black box and the stress distribution is assumed to follow the elastic K-field *all the way to the boundary of the "nonlinear" zone.* PB did not study the crack opening profile and the viscoelastic trumpet. Instead, they focused on evaluating the total viscoelastic dissipation rate around the moving crack tip. They ignored the angular variation of the stress field when evaluating the dissipation integral. The effect of angular variations is approximately accounted for by adjusting an integration constant so that the energy

[2] We modified de Gennes's notation. He used the shear complex modulus while we used tensile complex modulus. This does not affect eq. (2) from a scaling perspective.

release rate at high velocities is given by $(E_0 / E_\infty)G_0$, where G_0 is the intrinsic fracture energy. However, in contrast to de Gennes [20] and Saulnier et al. [21] *where the size of the "nonlinear" zone α is assumed to be a constant*, α in PB's theory is not constant *and is directly proportional to the applied energy release rate G*. In this respect there is little difference between the cohesive zone model of Knauss and Schapery and the "nonlinear" zone description of PB, since in both approaches the size of the cohesive or "nonlinear" zone can be predicted using a critical stress criterion. More specifically, dimensional consideration implies that the size of cohesive zone α must scale with the maximum stress in the cohesive zone model, σ_m, by

$$\alpha \sim E_\infty G / \sigma_m^2 . \tag{3}$$

For the DB cohesive zone assumed in Knauss's theory, the cohesive zone size α^K is

$$\alpha^K = \frac{\pi K_I^2}{8\sigma_D^2}, \tag{4a}$$

where $K_I^2 \sim E_\infty G$ since the far field is in the fully relaxed elastic limit. In the PB model, the "nonlinear" or fracture zone size α^{PB} is given by the critical stress condition

$$\frac{K_I}{\sqrt{2\pi\alpha^{PB}}} = \sigma_{PB} \Rightarrow \alpha^{PB} = \frac{K_I^2}{2\pi\sigma_{PB}^2}, \tag{4b}$$

where σ_{PB} is the critical stress in PB's theory and is analogous to σ_D in the cohesive zone model. A comparison between eq. (4a) and (4b) shows that the two approaches differ by a numerical constant. Here we note that the size of cohesive zone in both models is independent of modulus if K_I is prescribed instead of G. Another difference between PB's theory [22] and that by de Gennes [20] or Saulnier et al. [21] is on how to relate K_I to the energy release rate: PB applied the relation that $K_I^2 \sim E_\infty G$ while de Gennes and Saulnier et al. assumed $K_I^2 \sim E_0 G_0$. While the two are equivalent in the limit of high crack velocity, the latter (i.e., $K_I^2 \sim E_0 G_0$) may not be accurate at low crack velocity due to the lack of a "hard solid" region. However, this difference does not appear to affect the scaling relation between G and v at low crack velocity, as discussed in Section 3.1.

Since the dependence of fracture energy G on crack velocity v can be directly measured from experiments, attention was chiefly directed to predicting the relation between G and v. Unfortunately, these relations are usually given in integral form, as will be summarized below for different theories, and these integrals can be difficult to evaluate. As a result, it is not always possible to obtain analytic formula connecting G and v. Schapery's approximate theory can be used to produce these formulae. However, his theory is not widely appreciated and there is no careful study of its accuracy. One of our goals is to provide a comparative study on the theories by Knauss, Schapery and PB. Amongst these theories, the only one that does not involve approximation (in the sense that the solution satisfies all the field equations exactly) is Knauss's theory. Schapery's theory is approximate since he assumed the second derivative of the logarithm of creep compliance function with respect to the logarithm of time is small. In addition, he used

an approximate method to compute the crack opening displacement inside the cohesive zone. PB's calculation is approximate since they assumed that the elastic K-field of stress is valid all the way to the boundary of the fracture process zone, ignoring the interaction between fracture processes and the continuum fields outside. They also ignored the angular variation of the stress fields when evaluating the dissipation integral.

In 1994, Gent and Lai [23] took thin sheets of different elastomers, adhered them together by C-C or S-S interfacial bonds, and then peeled them apart at various rates and temperatures. They noted that the experimental G versus v curves for different elastomers can be collapsed into a single master curve. They also plotted the storage shear modulus μ^* against the oscillation frequency ω and found that these curves resemble the master curve of G versus v. As noted by Gent and Lai, this result is consistent with the theory of Knauss [8]. By comparing their G versus v master curve (see Figure 13 of [23]) with the μ^* versus ω curve (upper curve in Figure 16 of [23]), they obtained a set of lengths (each length corresponds to different G), which were suggested to represent the size of the fracture zone. In Figure 17 of their paper, they found the size of this fracture zone increases from 10^{-11} m to 10^{-9} m as the fracture energy increases from G_0 (intrinsic fracture energy as $v \to 0$) to the high velocity limit. In a later 1996 paper, Gent [24] identified this length scale as the dissipation zone size with a reference to Knauss's work: "*Knauss assumed that energy is dissipated in a small region of length δ ahead of the crack tip…. But values of δ obtained in this way are only about 1 Å, far too small to represent the actual size of a dissipation zone."* This paper started a controversy which remains until today.

Therefore, despite the ingenuity and efforts expended on viscoelastic fracture, the theory is rather inconclusive when it comes to the *shape* and *size* of the dissipative zone. The problem is that only the *total* dissipation rate is known, which is insufficient to determine the shape of the dissipation zone. What is needed is the *local dissipation rate*. Determination of this rate is a formidable task. This is compounded by the fact that a precise definition of the dissipation zone has not been given. In a viscoelastic solid, *energy dissipation starts once the material is stressed*, so energy is dissipated at all points and all times. This is in stark contrast to elastic-plastic solids where the onset of dissipation is clearly defined by the yield criterion. Moreover, a problem inherent in linear viscoelastic theory is that it does not address the amount of internal dissipation. For example, given the relaxation function, viscoelastic theory allows one to uniquely determine the tension in a bar during a constant strain rate test. However, one cannot determine the amount of energy dissipated until the bar is returned to its initial stress-free state – e.g., by specifying the unloading history. *Additional assumptions* are required to determine the amount of energy dissipated during *any part of the loading history*. In this paper, we will state these assumptions and compute the dissipation rate at a material point. This approach will allow us to determine the size and shape of the dissipation zone.

Aside from the *paradox* of the dissipation zone size, the different approaches and approximations adopted in different theories present difficulties to practitioners. Are there significant differences between theories? Which theory should one use to interpret data? Here we note that the formulation of Knauss [8] and Schapery [9,10] is in the *time domain*, that is, the tensile creep compliance function $J(t)$ is required for calculations. On the other hand, de Gennes

[20], Saulnier et al. [21] and PB [22] present their results in the *frequency domain*, where the complex modulus $E^*(\omega)$ is used to characterize viscoelasticity. Here it is important to note that the characteristic time in the creep compliance function is the retardation time (t_c) which is typically much larger than the characteristic relaxation time (t_R) in a relaxation test. For example, in a standard Maxwell solid, $t_c = E_0 t_R / E_\infty$, thus the retardation time can be three orders of magnitude larger than the relaxation time. Therefore, the characteristic time scale in the theories of Knauss [8] or Schapery [9,10] is much larger than that in the theories of de Gennes [20], Saulnier et al. [21] and PB [22]. Of course, in principle, one should be able to go back and forth between time and frequency domains. In practice, this is easier said than done. In this paper, we provide a simple transformation which express the dissipation rate of PB (similarly that of de Gennes) in the time domain (see eq. (13a) in Section 2.2). We also suggest a simple and accurate method to predict relation between crack velocity and fracture energy from rheological data (see eq. (35d) in Section 3.1).

A goal of this work is to carry out a detailed comparison of these theories and to highlight differences and similarities. The comparisons are carried out for two general classes of viscoelastic solids which we believe to be more realistic. The first is a Generalized Maxwell Solid (GMS) where the creep functions can be represented by a Prony series. The second is a Power Law Solid (PLS). We also present new results that is not available in the literature, such as the residual strain on the crack surface and the strain distribution directly ahead of the crack tip. In particular, we develop a procedure to compute the size and shape of the dissipation zone.

The physical quantities we seek to compare between different theories are categorized into the six sections listed below, followed by conclusions in Section 8. To limit the scope of comparison, we will focus on results for the SSC problem (i.e., infinite domain) with linear viscoelasticity and the *plane stress* condition unless otherwise specified.

- **Section 2**: viscoelastic dissipation during steady state crack growth.
- **Section 3***:* relation between the crack growth velocity v and the applied energy release rate G.
- **Section 4**: strain distribution directly ahead of the cohesive zone tip.
- **Section 5**: residual strain behind the crack tip.
- **Section 6**: crack opening displacement (COD).
- **Section 7**: shape and size of dissipation zone.

We believe many of the difficulties arise because analytical solutions are difficult to obtain, which is particularly true with Knauss's formulation. Therefore, we have given considerable efforts to obtain exact closed-form solutions. Surprisingly, we have found many exact closed-form results, most of which in terms of special functions. The advantages of using special functions are two-fold. First, properties of these special functions, such as series expansion, asymptotic behaviors, and connection with other special functions are well documented (see [25] for example). Second, just like trigonometric functions, these special functions can be readily evaluated using standard numerical software packages.

2. Viscoelastic Dissipation during Steady State Crack Growth

Among the many theories reviewed in the previous section, we use Knauss's [1,8] and PB's theories [22] to represent the cohesive zone and energy balance approaches, respectively, because both theories provide *quantitative* formulae to relate the energy release rate G and the crack growth velocity v. We also include Schapery's theory in the discussion due to its closed-form solution. In the following, we use the superscripts *K, S, PB* to denote quantities associated with Knauss, Schapery and PB's approach, respectively. We have not included the theories by de-Gennes [20] and Saulnier et al. [21] in the comparison since they are based on scaling relations.

2.1 Fracture criterion: COD versus energy balance

In this section we show that *the cohesive zone approach of Knauss and Schapery using a COD-based fracture criterion is equivalent to the energy balance approach of PB*. Figure 1B illustrates a Mode-I steady state crack growing with a constant velocity v in a linear incompressible viscoelastic medium under the SSC condition. In SSC, the traction boundary condition is prescribed by the linear elastic K-field for Mode-I cracks [26,27]:

$$\sigma_{ij}\left(R\to\infty,\theta\right)=\frac{K_I}{\sqrt{2\pi R}}\hat{\sigma}_{ij}\left(\theta\right),\quad R=\sqrt{X^2+Y^2},\quad \theta=\tan^{-1}\left(Y/X\right) \tag{5}$$

where K_I is the applied stress intensity factor, R, θ are polar coordinates corresponding to the translational coordinate system X-Y centered at the moving crack tip, $\hat{\sigma}_{ij}(\theta)$ are angular variations of the Mode-I crack tip stress field, and the subscripts i, j range from 1 to 2 (i.e., 1 and 2 represents the X and Y directions, respectively). In the SSC problem, the material in the far field ($R\to\infty$) is fully relaxed with relaxed Young's modulus E_∞.

In Knauss's theory, the fracture process zone is represented by a cohesive zone (see Fig.1A). To simplify the formulation while retaining the essential mechanics, we specialize the cohesive zone to a DB model with *constant traction* σ_D. The COD is zero at the right end of the cohesive zone (i.e., $X=\alpha$) and increases as one moves towards the $-X$ direction. Crack growth occurs when the maximum total COD reaches a critical value δ_0 which also defines the left end of the cohesive zone where the traction on the crack surfaces first vanishes (i.e., the crack tip at $X=0$). The intrinsic fracture energy G_0 is related to the cohesive parameters as $G_0=\sigma_D\delta_0$. To apply the COD-based fracture criterion, Knauss calculated the COD by applying the correspondence principle and elastic crack tip stress field. In normalized form, the opening displacement u_{cod} of the *upper* crack surface in Knauss's theory can be written as

$$\bar{u}_{cod}\left(\bar{X}\le 1\right)\equiv\frac{u_{cod}}{\delta_0}=\frac{\left(\zeta+1\right)3K_I\sqrt{\alpha}}{2\delta_0\sqrt{2\pi}}\left\{J_\infty F(\bar{X})-\int_{\bar{X}}^{1}\Delta J\left(\frac{\alpha}{v}\left(\xi-\bar{X}\right)\right)F'\left(\xi\right)d\xi\right\}, \tag{6a}$$

where

$$F'(\bar{X})=-\frac{1}{4}\ln\left|\frac{\sqrt{1-\bar{X}}+1}{\sqrt{1-\bar{X}}-1}\right|, \tag{6b}$$

$$F(\bar{X}) = \frac{\sqrt{1-\bar{X}}}{2} - \frac{\bar{X}}{4}\ln\left|\frac{\sqrt{1-\bar{X}}+1}{\sqrt{1-\bar{X}}-1}\right|. \tag{6c}$$

In eq. (6a), we have normalized the *one-sided* crack opening displacement u_{cod} by δ_0, the critical opening displacement in the DB model where the traction on the crack surfaces first vanishes. The horizontal coordinate X is normalized by the *cohesive zone length,* α. $J(t)$ is the creep function under uniaxial tension and

$$\Delta J(t) \equiv J(t) - J_\infty, \tag{6d}$$

where $J_\infty \equiv J(t = +\infty) = 1/E_\infty$, and ζ is a constant related to the Poisson's ratio. Assuming incompressibility (i.e., Poisson's ratio = 0.5), $\zeta = 1$ for plane strain and = 5/3 for plane stress. Knauss [1] argued that since cohesive zone size can be much smaller than the thickness even for thin sheet fracture specimens, one should implement a local plane strain condition in eq. (6a) by setting $\zeta = 1$. Here for theoretical purpose, we retain the possibility of plane stress condition within the cohesive zone by allowing the specimen thickness to be sufficiently small. The first term in eq. (6a) is the COD in a purely elastic solid with relaxed or long-time tensile modulus $1/J_\infty = E_\infty$ subjected to the same remote K-field. The integral term accounts for viscoelastic effects during crack growth. Note that since ΔJ and $F'(\xi)$ are less than or equal to zero, the integral in eq. (6a) is always positive. Thus, the COD, u_{cod}, is always smaller than its counterpart in a relaxed solid under the same remote load since the material stiffens due to crack growth.

To relate the COD-based fracture criterion to the energy balance, we first note that K_I is related to the applied energy release rate G through the following equations due to the SSC condition and incompressibility (i.e., Poisson's ratio = 1/2):

$$G = \frac{K_I^2}{E_\infty} = J_\infty K_I^2 \qquad \text{(plane stress)}, \tag{7a}$$

$$G = \frac{3K_I^2}{4E_\infty} = \frac{3J_\infty K_I^2}{4} \qquad \text{(plane strain)}. \tag{7b}$$

The cohesive zone length α is related to K_I and σ_D in eq. (4a) where α is denoted as α^K to emphasize that it is according to Knauss's theory. Substituting eq. (4a) into eq. (6a) and using eq. (7a) or (7b), we obtain the following equation *which is valid for both plane stress and plane strain conditions*:

$$\bar{u}_{cod}\left(\bar{X} \le 1\right) = \frac{G}{G_0}F(\bar{X}) - \frac{G}{G_0}\frac{1}{J_\infty}\int_{\bar{X}}^{1}\Delta J\left(\frac{\alpha}{v}\left(\xi - \bar{X}\right)\right)F'(\xi)\,d\xi, \tag{7c}$$

The *fracture or crack growth condition* is met when the one-sided COD reaches $\delta_0/2$ at the crack tip where $\bar{X} = 0$. Using $F(\bar{X} = 0) = 1/2$, the fracture condition obtained by setting the LHS of eq. (6a) to 1/2 and evaluating at $\bar{X} = 0$ is

$$G_0 = G - \frac{2G}{J_\infty}\int_0^1 \Delta J\left(\frac{\alpha}{v}\xi\right)F'(\xi)\,d\xi\,. \tag{8a}$$

Since G is the applied energy release rate and G_0 is the intrinsic fracture toughness, the integral term in eq. (8a) must be the energy dissipated per unit crack extension, G_D. *Thus, the COD fracture criterion and the energy balance equation are equivalent* and that the integral term in (8a) represents dissipation per unit crack extension. We can rewrite eq. (8a) as

$$G_0 = G\left(1-\Lambda(\beta)\right), \qquad \Lambda = \frac{2}{J_\infty}\int_0^1 \Delta\tilde{J}\left(\frac{\alpha\xi}{vt_c}\right)F'(\xi)\,d\xi\,, \tag{8b}$$

where Λ *is the fraction of energy dissipated per unit crack extension*, referred to as the *Fractional Dissipation Rate* (FDR) hereafter. *For dimensional consistency, we have normalized the time t in the creep function* ΔJ *by a characteristic creep retardation time* t_c *so that* $\Delta J \equiv \Delta\tilde{J}\,(t/t_c)$. This normalization leads to an important dimensionless parameter β defined as

$$\beta \equiv \frac{\alpha}{vt_c}\,, \tag{8c}$$

where α is the length of the cohesive zone. Recall that α in Knauss's theory, denoted as α^K, is related to the stress intensity factor K_I in eq. (4a). Equation (8c) indicates that β is the time for the crack to move one cohesive (fracture) zone length divided by the retardation time. Thus, a small β means fast crack growth and vice versa. Although the energy balance theory of PB does not explicitly include a cohesive zone, we interpret α as the length of the fracture process zone which is defined by a prescribed critical stress σ_{PB} and the stress intensity factor K_I in eq. (4b). By comparing eq. (4a-4b), the β in Knauss's and PB's theories differ to within a numerical factor of order 1 due to different ways of estimating α, or equivalently, different definition of cohesive stress. If there is a chance of confusion, we will label β and α by a superscript, e.g., β^K and α^K refers to β and α in Knauss's theory.

In the following, we normalize the applied energy release rate G by the intrinsic toughness G_0, i.e.,

$$\bar{G} = G / G_0\,. \tag{9a}$$

Since the cohesive zone length α *increases linearly with the energy release rate* G (see eq.(4a,b) and eq.(7a,b)) and hence also depends on the crack growth velocity v, it is convenient to define a fracture length scale d that is *independent of* v. This is done by defining

$$d \equiv \alpha / \bar{G}\,. \tag{9b}$$

Physically, d is the size of the cohesive or fracture zone as crack velocity v goes to zero, i.e., the minimum size of the cohesive or fracture process zone. Equation (9b) allows us to define a material velocity $v_c \equiv d / t_c$, which will be used to normalize the crack velocity v, i.e.,

$$\overline{v} = \frac{v}{d / t_c}. \tag{9c}$$

Recall that the definition of α is based on the stress field and thus is the same under both plane stress and plane strain, but the definitions of d under plane stress and plane strain may differ by a constant coefficient. Take Knauss's theory for example. Equation (4a) for α^K is valid for both plane stress and plane strain. However, using eq. (4a), (7a) and (7b), we find that $d^K = \pi G_0/(8J_\infty\sigma_D^2)$ under plane stress and $d^K = \pi G_0/(6J_\infty\sigma_D^2)$ under plane strain. In practice, the cohesive stress σ_D for a given material is often unknown and hence treated as a fitting parameter, which is equivalent to treating d^K as a fitting parameter. In this regard, the difference in the definition of d^K does not practically affect the fitting process. For theoretical rigorousness, we will assume plane stress condition in the following unless otherwise specified.

2.2 Fractional dissipation rate (FDR)

Having established the equivalence between the cohesive zone approach and the energy balance approach, we next show that the different theories based on these two approaches are essentially different ways of calculating or approximating Λ in the form of a 1D integral. The FDR from the theories of Knauss, Schapery and PB is summarized in the following. As mentioned earlier, our summary will focus on results under the plane stress condition.

In **Knauss**'s theory**,** the FDR Λ^K is given by eq. (8b), which is rewritten below using the dimensionless parameter β^K :

$$\Lambda^K = \frac{2}{J_\infty}\int_0^1 \Delta\tilde{J}\left(\beta^K\xi\right)F'\left(\xi\right)d\xi \tag{10a}$$

$$\beta^K = \frac{\alpha^K}{vt_c},\ \ \alpha^K \equiv \bar{G}d^K,\ d^K = \frac{\pi G_0}{8J_\infty\sigma_D^2}. \tag{10b}$$

In **Schapery**'s theory, the integral in eq. (8b) is approximated by the closed-form expression (see derivation in Section S2 of the SI):

$$\Lambda^S = -\frac{\Delta\tilde{J}\left(\beta^S\right)}{J_\infty} \tag{11a}$$

$$\beta^S = \frac{\alpha^S}{vt_c},\ \alpha^S \equiv \bar{G}d^S,\quad d^S = \lambda\frac{\pi G_0}{8J_\infty\sigma_D^2}, \tag{11b}$$

where λ in d^S is approximately 1/3. Note that α^S and d^S should be interpreted as the effective cohesive zone length, since the factor of $\lambda \approx 1/3$ is absorbed into α^S and d^S to unify notation (see Section S2 of the SI for detail). Had λ not been absorbed, α^S and d^S would be the same as their counterparts in Knauss's theory (see eq. (10b)).

In **Persson and Brener**'s theory, the FDR Λ^{PB} is calculated through the energy balance approach and is given by

$$\Lambda^{PB} = \frac{2E^*_{PB}(\omega=0)}{\pi}\int_0^1 \frac{\sqrt{1-\xi^2}}{\xi}\,\mathrm{Im}\left[\frac{1}{E^*_{PB}\left(2\pi v\xi/\alpha^{PB}\right)}\right]d\xi\ , \tag{12a}$$

where $E^*_{PB}(\omega)$ is the *complex modulus* in tension defined by PB and ω is the oscillatory frequency. Also, the factor $2\pi v/\alpha^{PB}$ in eq. (12a) corresponds to cut-off frequency ω_c in PB's paper. Here we caution the reader that the viscoelastic functions in PB differ from their usual definitions in the literature (e.g., Ferry [28], Christensen [29]). Serious errors can occur if one is not aware of these differences. We have carefully studied PB's paper and these differences, as detailed in Section S3 of the SI and summarized in Table 1. In particular, we denote the quantities used by PB with the subscript "*PB*" and use a superscript ***** to denote complex modulus in the frequency domain to avoid confusion.

	Standard notation	PB's notation
Creep function	$\varepsilon(t)=\int_{-\infty}^{t} J(t-t')\frac{d\sigma(t')}{dt'}dt'$	$\varepsilon(t)=\int_{-\infty}^{t} C_{PB}(t-t')\sigma(t')dt'$
Conversion	$C_{PB}(t)=\frac{dJ(t)}{dt}+\delta_+(t)J_0$	
Complex creep compliance	$J^*(\omega)=J_\infty+i\omega\int_0^\infty[J(t)-J_\infty]e^{-i\omega t}dt$	$C^*_{PB}(\omega)=J^*(-\omega)$
Complex modulus	$E^*(\omega)=1/J^*(\omega)$	$E^*_{PB}(\omega)=1/C^*_{PB}(\omega)$

Table 1 Conversion of viscoelastic properties between the standard and PB's notation. $J(t)$ and $C_{PB}(t)$ are the creep compliance functions in the standard notation and PB's notation, respectively. $E^*(\omega)$ and $E^*_{PB}(\omega)$ are the complex moduli in the standard notation and PB's notation, respectively. $\delta_+(t)$ is the Dirac delta function. Derivation of conversion is given in Section S3 of the SI.

It is interesting to compare the dissipative energy release rate G_D obtained by de Gennes [20] in eq. (2) with that of PB. Using the normalization $\xi = \omega/\omega_{max} = \omega\alpha/v$ and eq. (7a), we can rewrite eq. (2) as

$$\frac{G_D}{G} \sim E^*(\omega=0)\int_0^1 \frac{1}{\xi}\,\mathrm{Im}\left(\frac{1}{E^*(\xi v/\alpha)}\right)d\xi\ , \tag{12b}$$

knowing that $E^*(\omega=0) = E_\infty = 1/J_\infty$. Besides the obvious difference in the pre-factor, the weight function $\sqrt{1-\xi^2}$ is absent from the scaling model of de Gennes. However, from a *scaling* perspective, the two expressions are practically identical. To cast PB's FDR expression into a form similar to eq. (10a), we note that $E^*_{PB}(\omega=0) = E_\infty = 1/J_\infty$ and introduce a characteristic time

t_c (i.e., the creep retardation time) in the complex modulus: $E^*_{PB}(\omega) \equiv \tilde{E}^*_{PB}(\omega t_c)$. Therefore, eq. (12a) can be rewritten as

$$\Lambda^{PB} = \frac{2}{\pi J_\infty}\int_0^1 \frac{\sqrt{1-\xi^2}}{\xi}\,\mathrm{Im}\left[\frac{1}{\tilde{E}^*_{PB}\left(\xi/\beta^{PB}\right)}\right]d\xi\,, \tag{12c}$$

$$\beta^{PB} \equiv \frac{\alpha^{PB}}{2\pi v t_c}, \alpha^{PB} = \bar{G}d^{PB}, d^{PB} = \frac{G_0}{J_\infty \sigma^2_{PB}}\quad, \tag{12d}$$

Here we note that β^{PB} in eq. (12d) is defined with an extra factor of $1/2\pi$ in comparison to its counterpart in eq. (10b) and (11b). To be consistent, we divided the size of cohesive zone in PB's model by a factor of 2π: $\hat{\alpha}^{PB} = \alpha^{PB}/2\pi$ or equivalently $\hat{d}^{PB} = d^{PB}/2\pi$, so that $\beta^{PB} \equiv \hat{\alpha}^{PB}/vt_c$. This is equivalent to increasing the fracture stress in PB's theory by a factor of $\sqrt{2\pi}$.

We emphasize two important results:

a) The FDR expressions of Knauss and Schapery are based on the *creep compliance* in the *time* domain, whereas PB employs the *complex modulus* in *frequency* domain to evaluate the FDR. We found an elegant expression converting one to the other. In the time domain, PB's dissipation rate can be written as the Hankel transform of the standard creep function $\Delta\tilde{J}(t/t_c)$, as derived in Section S4 of the SI. Specifically

$$\Lambda^{PB}\left(\beta^{PB}\right) = -\frac{1}{J_\infty}\int_0^\infty \frac{\Delta\tilde{J}(\eta)}{\eta} J_1\left(\frac{\eta}{\beta^{PB}}\right)d\eta = -\frac{1}{J_\infty}\sqrt{\frac{\beta^{PB}}{2\pi}}H_1\left(\frac{\Delta\tilde{J}(\eta)}{\eta^{3/2}}, \frac{1}{\beta^{PB}}\right)\,, \tag{13a}$$

where J_1 is the Bessel function of the first kind of order one and H_1 is the *Hankel transform* of order one. The FDR by de Gennes as expressed in eq. (12b) can also be written in the time domain following similar derivation, which has an even simpler form:

$$\Lambda^{dG} = -\frac{1}{J_\infty}\int_0^\infty \left[\frac{1-\cos\left(vt/\alpha\right)}{t}\right]\Delta J(t)dt\,. \tag{13b}$$

b) The size of fracture process zone or cohesive zone, α, in different approaches differs by a numerical constant and is *directly proportional* to the applied energy release rate G. The minimum size $\alpha\left(v\to 0\right) = d$ is reached as crack velocity approaches zero and G approaches the intrinsic fracture energy G_0. Indeed, the theories of Knauss, Schapery and PB share a common result:

$$\frac{\alpha\left(v\to\infty\right)}{\alpha\left(v\to 0\right)} = \frac{G\left(v\to\infty\right)}{G\left(v\to 0\right)} = \frac{E_0}{E_\infty}\,, \tag{14}$$

implying that the size of the cohesive zone can increase by three orders of magnitudes as the crack velocity increases. In contrast, in the theory of de Gennes [20] and Saulnier et al. [21], α is assumed to be a constant, which has been recognized by Saulnier et al. [21] as a limitation in their model.

2.3 Material model: Generalized Maxwell Solid (GMS) and Power Law Solid (PLS):

The results in Section 2.1-2.2 are valid for any incompressible linear viscoelastic solids. To make our discussions more relevant to applications, we consider two broad classes of material models: Generalized Maxwell solid (GMS) and Power Law solid (PLS). In a GMS, the creep or relaxation function can be expressed using a Prony series. This series is widely used in finite element analysis and engineering applications. A difficulty with the GMS model is that many terms of the Prony series is often needed to model real material behavior. In practice, it is often found that the PLS, which has much fewer material parameters, fits data well [30,31] for a wider range of frequencies in a rheology test. In the following, we denote a dimensionless material parameter κ that measures bulk dissipation

$$\kappa \equiv 1 - \frac{J_0}{J_\infty} = 1 - \frac{E_\infty}{E_0}, \tag{15}$$

where $J_0 \equiv J(t=0) = 1/E_0$. Note dissipation is zero when $\kappa = 0$ since material is purely elastic. For highly viscoelastic solids, κ is slightly less than one.

In GMS, the creep function is represented as a *Prony* Series [32]

$$J(t) = J_\infty - (J_\infty - J_0)\sum_{n=1}^{N} a_n e^{-t/t_n}, \qquad \sum_{n=1}^{N} a_n = 1, \tag{16a}$$

where t_n are characteristic *retardation times*; they are arranged so that $t_1 < t_2 < ... < t_N$. The a_n's are weights indicating the compliance contribution for different retardation mechanisms. In the viscoelastic fracture literature, theoretical results are often confined to the *standard solid* (SS) where there is one characteristic retardation time t_1 which we shall denote by t_c. For this case, eq. (16a) reduces to

$$J(t) = J_\infty - (J_\infty - J_0) e^{-t/t_c}. \tag{16b}$$

Finally, since $\sum_{n=1}^{N} a_n = 1$, we define an *average retardation time* t_c^{ave} by

$$\frac{1}{t_c^{ave}} \equiv \sum_{n=1}^{N} \frac{a_n}{t_n} \tag{16c}$$

Later, we shall see that t_c^{ave} is the appropriate time scale for defining β in the FDR Λ.

For PLS, we assume the following form of creep function:

$$J(t) = J_\infty - \frac{(J_\infty - J_0)}{(1 + t/t_c)^m}, \quad 0 < m < 1. \tag{17}$$

A very similar power law solid model was proposed by Williams [33].

Our focus is on evaluating the FDR in eq. (10a), (11a) and (12a) for these two classes of viscoelastic models. The evaluation of these integrals and associated asymptotic behaviors are tedious, they are given in the SI. In the following, we indicate closed-form solutions by the

notation "(closed form)". If the solution is in closed form and can be written in terms of elementary functions, we use the notation "(elementary)".

2.4 Evaluation of FDR for GMS

In this section, we summarize the FDR by Knauss, Schapery and PB for GMS using the creep function in eq. (16a).

In **Knauss**'s theory, the FDR is given by

$$\Lambda^K = 2\kappa \sum_{n=1}^{N} a_n I\left(\beta_n^K\right), \qquad \text{(closed form)} \tag{18a}$$

$$\beta_n^K \equiv \frac{\alpha^K}{vt_n} = \frac{\bar{G}d^K}{vt_n}, \tag{18b}$$

$$I(\beta) \equiv -\int_0^1 e^{-\beta\xi} F'(\xi)\, d\xi = \frac{\sqrt{\pi}}{4} \sum_{i=0}^{\infty} \frac{(-1)^i \beta^i}{(i+1)\Gamma(i+3/2)} = \frac{1}{4\eta} \lim_{\varepsilon \to 0} \left[\Gamma(\varepsilon) \left[M\left(\varepsilon, \frac{1}{2}, -\beta\right) - 1 \right] \right]. \tag{18c}$$

In eq. (18c), β is the generic form of β_n^K, M is the Kummer's *Confluent Hypergeometric function* and Γ is the *Gamma* function (see Section S5 of SI). The series in eq. (18c) has infinite radius of convergence[3]. Since $t_1 < t_2 < ... < t_N$, we have $\beta_1^K > \beta_2^K > ... > \beta_N^K$. To facilitate the application of eq. (18a), we derived the following asymptotic results (see Section S6 of SI)

$$\Lambda^K\left(\beta_N^K >> 1\right) \approx \kappa \sum_{n=1}^{N} \left[a_n \left(\frac{\ln\left(\beta_n^K\right)}{2\beta_n^K} + \frac{(2\ln 2 + \gamma)}{2\beta_n^K} - \frac{1}{4\left(\beta_n^K\right)^2} + ... \right) \right], \quad \sum_{n=1}^{N} a_n = 1, \tag{18d}$$

$$\Lambda^K\left(\beta_1^K << 1\right) = \kappa \left(1 - \frac{\beta_{ave}^K}{3} + \sum_{n=1}^{N} \frac{4a_n \left(\beta_n^K\right)^2}{45} + ... \right), \tag{18e}$$

where $\gamma = 0.5772156649...$ is the Euler constant and

$$\beta_{ave}^K \equiv \frac{\bar{G}d^K}{vt_c^{ave}}. \tag{18f}$$

In **Schapery**'s theory, the FDR is given by

$$\Lambda^S = \kappa \sum_{n=1}^{N} a_n e^{-\beta_n^S}, \qquad \beta_n^S \equiv \frac{\alpha^S}{vt_n} = \frac{\bar{G}d^S}{vt_n} \qquad \text{(elementary)}. \tag{19a}$$

[3] The function I is entire as $\Gamma(\varepsilon)$ has a simple pole at $\varepsilon = 0$, while $[M(\varepsilon, 1/2, -\beta) - 1]$ has a simple zero at $\varepsilon = 0$, hence I has a removable singularity at the origin, as evident by the power series expansion.

In the limit of large β_n^S (low crack velocity), Λ^S decays exponentially. In the limit of small β_n^S, the asymptotic result is

$$\Lambda^S\left(\beta_1^S << 1\right) = \kappa\left(1 - \beta_{ave}^S + ..\right),\ \beta_{ave}^S \equiv \frac{\bar{G}d^S}{vt_c^{ave}}. \tag{19b}$$

In **PB**'s theory, the FDR is given by (see Section S7 of the SI):

$$\Lambda^{PB} = \kappa\sum_{n=1}^{N} a_n\left[\sqrt{1+\left(\beta_n^{PB}\right)^2} - \beta_n^{PB}\right],\ \beta_n^{PB} \equiv \frac{\bar{G}\hat{d}^{PB}}{vt_n} \qquad \text{(elementary)}. \tag{20a}$$

The following asymptotic behaviors can be readily obtain using eq. (20a):

$$\Lambda^{PB}\left(\beta_N^{PB} >> 1\right) \approx \kappa\left[\frac{1}{2}\sum_{n=1}^{N}\frac{a_n}{\beta_n^{PB}} + O\left(\beta_N^{PB}\right)^{-3}\right] \approx \frac{\kappa}{2\beta_{ave}^{PB}} \tag{20b}$$

$$\Lambda^{PB}\left(\beta_1^{PB} << 1\right) = \kappa\left(1 - \beta_{ave}^{PB} + ...\right), \qquad \beta_{ave}^{PB} \equiv \frac{\bar{G}\hat{d}^{PB}}{vt_c^{ave}}. \tag{20c}$$

Before we compare the FDR from different approaches, we note an important observation: the FDR is a function of β_n only[4]. Comparison of eq. (18e), (19b) and (20c) shows that for large crack velocities ($\beta_n << 1$) all three theories are practically identical. The difference between theories occurs at small velocities ($\beta_n >> 1$). In this regime, Schapery's approximation eq. (19a) considerably underestimates the FDR due to the rapid exponential decay. However, it must be noted that Schapery's approximation is designed for realistic material behavior so it is not expected to be accurate for the SS. The relevant comparison is between eq. (18d) and (20c). As noted in the introduction, in this regime there can be significant interaction between the fracture process zone and the continuum field surrounding it. In Knauss's formulation, this interaction is accounted for by the cohesive zone model. However, this interaction is neglected in PB's model. According to eq. (18d) in Knauss's theory, the dominant behavior at low velocity is:

$$\Lambda^K\left(\beta_N^K >> 1\right) \approx \kappa\sum_{n=1}^{N} a_n\frac{\ln\left(\beta_n^K\right)}{2\beta_n^K}, \tag{21}$$

which states that the FDR for low velocities (where $\bar{G} \approx 1$) scales with v as $\Lambda^K\left(\beta_N^K >> 1\right) \approx -v\ln v$. In contrast, PB's theory predicts that the FDR for low velocities is directly proportional to v, which is valid for any GMS, *regardless of the number of terms in the Prony series*. This is because $(\beta_n^{PB})^{-1} \propto v$ for all n (see eq. (20b)). It is also interesting to note that eq. (20b) suggests that the region of linear behavior is quite large, since the next order term in the asymptotic series is $(\beta_N^{PB})^{-3} \propto v^3$. This result is consistent with the scaling analysis of Saulnier et al. [21] where it was proposed that the dissipation rate increases linearly with the crack velocity until the full

[4] Straightly speaking, Λ/κ is a function of β_n only.

development of the trumpet. On the other hand, if the interaction between the fracture process zone and the continuum field is taken into consideration, as in Knauss's model, this conclusion is not entirely true (e.g., see inset of Fig.2). In eq. (18d), we carried out asymptotic expansion to the third order to show that the quadratic term $(\beta_n^K)^{-2}$ in the series is not zero, which, together with the fact that the dominance of the logarithmic term at very small velocities, suggests the linear region can be significantly reduced.

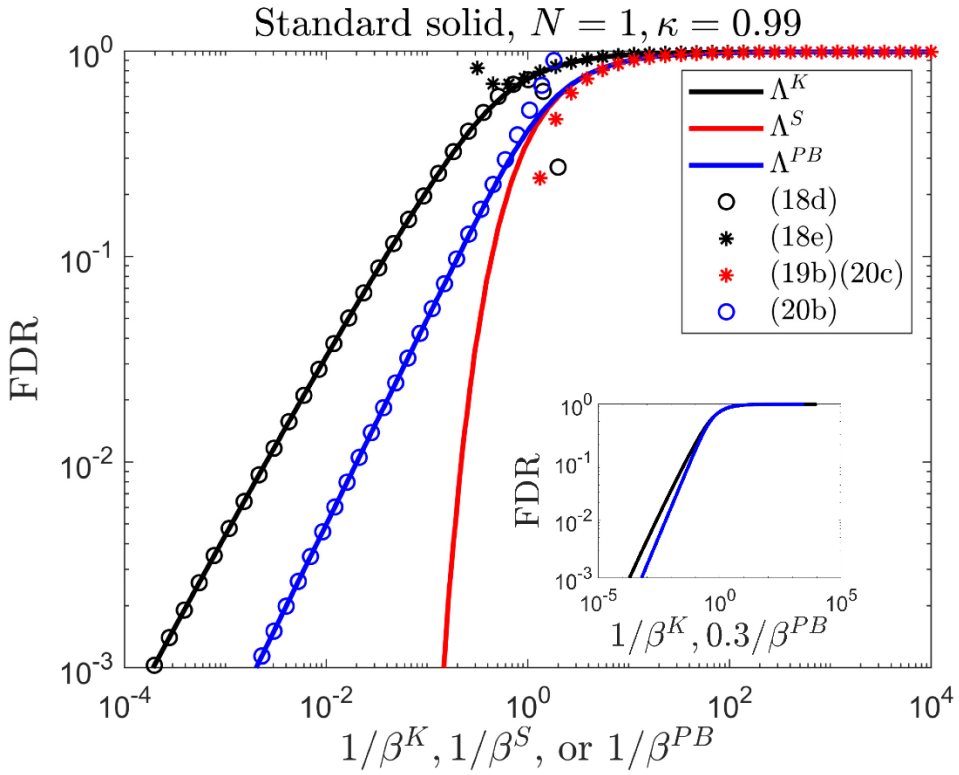

Figure 2 FDR for a Standard Solid (N=1) with κ = 0.99. Full solutions based on the theories of Knauss, Schapery and PB are represented by solid lines, whiles the symbols represent asymptotic solutions. The inset shows that PB's theory can be brought into reasonable agreement with Knauss's theory, except at very low velocities, by plotting Λ against $0.3/\beta^{PB}$, i.e., by shifting the PB curve to the left by log(1/0.3).

Figure 2 plots the FDR according to Knauss, Schapery and PB for standard solid where N =1. In this case, there is only one retardation time and hence one β_n, i.e., $\beta \equiv \beta_1$ where superscript K, S or PB is added to distinguish the three theories. The full solutions are shown as solid lines and the asymptotic behaviors at large and small $1/\beta$ are represented as symbols. All three theories show the same trend for large $1/\beta$ (large velocity). However, the three theories are quite different for small $1/\beta$ (small velocities). In particular, Schapery's theory deviates from the trends exhibited by Knauss's and PB's theories at small velocities. Note that the three term expansions for large β (i.e., small $1/\beta$) in eq. (18d) is very accurate for $\beta \geqslant 1$, while eq. (18e) is accurate for $\beta < 1$. Hence these asymptotic expressions in eq. (18d) and (18e) *can be used to compute the FDR for the entire*

range of β. The resemblance between Knauss's and PB's curves suggests that one can adjust the critical stress σ_{PB} in PB's theory, and hence $\hat{d}^{PB}$ and β^{PB}, to bring the two theories into better agreement. The inset in Fig.2 shows that this is possible if we shift the PB (blue solid curve) to the left by log(1/0.3). However, as shown in the insert of Fig.2, the asymptotic behavior of PB's theory at low velocity differs from that of Knauss's theory even after the shift. As mentioned above, this is due to interaction between the fracture process zone and the continuum field, giving rise to the logarithmic dependence on velocity in Knauss's theory (see eq. (21)).

2.5 Evaluation of FDR for PLS

The evaluation of FDR for PLS is summarized in this section. Unlike the Prony Series for GMS, the creep function of PLS assumed in eq. (17) only involves a single time scale t_c, which corresponds to a single β in the FDR solution.

In **Knauss**'s theory, the FDR is given by (see Section S8 of the SI for derivation):

$$\Lambda^K = \frac{\kappa}{2(1-m)\beta^K}\lim_{\varepsilon\to 0}\left[\Gamma(\varepsilon)\left\{{}_2F_1\left(-1+m,\varepsilon,\frac{1}{2}+\varepsilon,-\beta^K\right)-1\right\}\right], \text{ (closed form)}, \quad (22a)$$

where ${}_2F_1$ is the *Gauss Hypergeometric* function. Using the series expansion of eq. (22a), we found the following asymptotic behaviors (see Section S9 of the SI for derivation):

$$\Lambda^K\left(\beta^K << 1, m\right) \approx \kappa\left(1-\frac{m}{3}\beta^K + ..\right), \quad (22b)$$

$$\Lambda^K\left(\beta^K >> 1, m\right) \approx \frac{\kappa}{2(1-m)}\frac{\sqrt{\pi}\Gamma(1-m)}{\Gamma(3/2-m)}\left(\beta^K\right)^{-m} . \quad (22c)$$

A more detailed asymptotic solution for $\beta^K >> 1$ with additional higher order terms is provided in Section S7 of SI. Interestingly, we found that eq. (22a) can be reduced to elementary functions in the special case of $m = 1/2$ (see Section S10 of the SI), i.e.,

$$\Lambda^K\left(\beta^K, m=\frac{1}{2}\right) = \frac{2\kappa}{\sqrt{\beta^K}}\left[\sin^{-1}\sqrt{\frac{\beta^K}{1+\beta^K}} - \frac{\ln\sqrt{1+\beta^K}}{\sqrt{\beta^K}}\right] \quad \text{(elementary)}. \quad (23a)$$

In this special case, the asymptotic behaviors become (Section S10 of the SI)

$$\Lambda^K\left(\beta^K << 1, m=\frac{1}{2}\right) = \kappa\left[1-\frac{\beta^K}{6}+...\right], \quad (23b)$$

$$\Lambda^K\left(\beta^K >> 1, m=\frac{1}{2}\right) \approx \frac{2\kappa}{\sqrt{\beta^K}}\left[\frac{\pi}{2} - \frac{\ln\sqrt{\beta^K}}{\sqrt{\beta^K}} - \frac{1}{\sqrt{\beta^K}} + ...\right]. \quad (23c)$$

In **Schapery**'s theory, the FDR is determined by substituting the power law creep function in eq. (17) into eq. (11a):

$$\Lambda^S = \frac{\kappa}{\left(1+\beta^S\right)^m} \qquad \text{(elementary).} \tag{24a}$$

The asymptotic behaviors of eq. (24a) are

$$\Lambda^S\left(\beta^S << 1, m\right) = \kappa\left(1 - m\beta^S + ...\right) \quad , \tag{24b}$$

$$\Lambda^S\left(\beta^S >> 1, m\right) = \kappa\left(\beta^S\right)^{-m}\left(1 - \frac{m}{\beta^S} + ...\right) \quad . \tag{24c}$$

In **PB**'s theory, we calculate the FDR using the Hankel transform expression given by eq. (13a), which gives (see 6.563 on Page 685 of [34] and Page 23 of [35] for the Hankel transform of $(1+\eta)^{-m}/\eta$):

$$\begin{aligned}\Lambda^{PB} &= \kappa\int_0^\infty \frac{1}{\left(1+\eta\right)^m}\frac{J_1\left(\eta/\beta^{PB}\right)}{\eta}d\eta \\ &= \frac{\pi\kappa}{\Gamma\left(m\right)\sin m\pi}\left\{-\sum_{k=0}^{\infty}\frac{\left(-1\right)^k\left(2k\right)!\left(2\beta^{PB}\right)^{-\left(1+2k\right)}}{\left(k!\right)\left(k+1\right)!\Gamma\left(2k+2-m\right)} + \sum_{k=0}^{\infty}\frac{\left(2\beta^{PB}\right)^{-\left(k+m\right)}\Gamma\left(m+k\right)\sin\left(\frac{m+k}{2}\pi\right)}{\left(k!\right)\Gamma\left(\frac{k+3+m}{2}\right)\Gamma\left(\frac{k+m+1}{2}\right)}\right\}\end{aligned} \tag{25a}$$

(closed form)

The asymptotic behavior for large β^{PB} can be directly obtained from eq. (25a), i.e.,

$$\Lambda^{PB}\left(\beta^{PB} >> 1, m\right) \approx \frac{\pi\kappa}{\Gamma\left(m\right)\sin m\pi}\left\{\frac{\left(2\beta^{PB}\right)^{-m}\Gamma\left(m\right)\sin\left(\frac{m}{2}\pi\right)}{\Gamma\left(\frac{3+m}{2}\right)\Gamma\left(\frac{m+1}{2}\right)} - \frac{\left(\beta^{PB}\right)^{-1}}{\Gamma\left(2-m\right)} + ...\right\} \tag{25b}$$

The behavior for small β^{PB} can be obtained from literature on asymptotic behavior of Hankel transforms [36]:

$$\Lambda^{PB}\left(\beta^{PB} << 1, m\right) \approx \kappa\left(1 - m\beta^{PB} + ...\right). \tag{25c}$$

Similar to the results for GMS, in the regime of high crack velocity ($\beta << 1$), all approaches give similar results. Indeed, eq. (25c), (24b) and (22b) are practically identical, with the understanding that β in different theories differs by a numerical factor of order 1. Likewise, in the regime of low crack velocity ($\beta << 1$), all three theories predict that

$$\Lambda \sim \beta^{-m} \propto v^m. \tag{26}$$

Note that Schapery's theory, which disagrees with the other two theories in the low velocity regime for GMS, is doing just as well as Knauss's or PB's theory for the PLS in terms of the scaling trend. More interesting is the difference between the prediction of the GMS and the PLS in the low crack velocity regime. For PLS, the FDR in all three theories scales with the velocities to the power m, whereas for a GMS, the FDR scales with the crack velocity v as $-v\ln v$ (Knauss) or v (PB). It is interesting to note that the FDR for PLS and GMS scales with v in essentially the same way in the high crack velocity regime. Figure 3 plots the FDR against β for $m = 1/2$. The full solutions are plotted as solid lines and the asymptotic behavior for small and large β are represented by symbols. The insert in Fig.3 shows that all three theories can be brought into close agreement by horizontal shifting in the log-log plot. Comparison of these theories for different values of m (m = 0.25, 0.5 and 0.75) is shown in Fig. S1 in Section S11 of the SI.

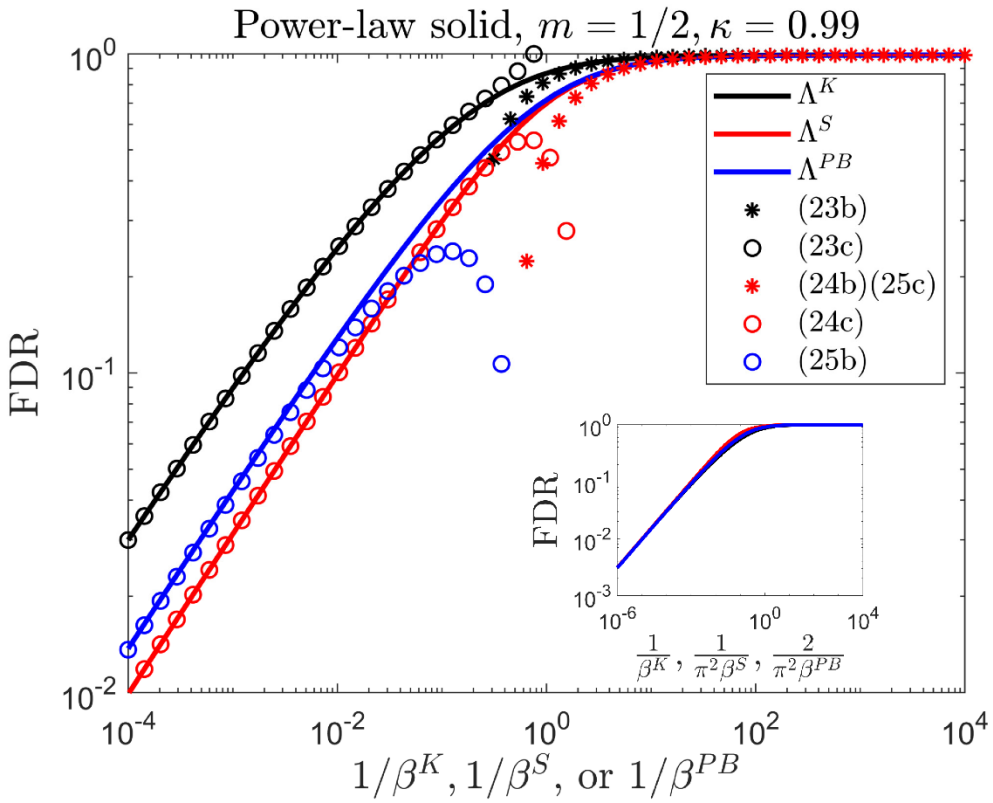

Figure 3 FDR for a PLS with $m = 1/2$ and $\kappa = 0.99$. The solid lines represent full solutions based on the theories of Knauss, Schapery and PB, while the symbols represent asymptotic solutions. The inset shows that all three theories can be brought into agreement by a horizontal shift to the left in the log-log plot by a factor of $\log(\pi^2)$ (for Schapery) and $\log(\pi^2/2)$ (for PB) .

3. Energy Release Rate and Crack Growth Velocity

Once the FDR is computed, the relationship between the normalized energy release rate $\bar{G} \equiv G / G_0$ and the normalized crack velocity $\bar{v} \equiv v t_c^{ave} / d$ can be determined by solving the energy balance equation:

$$\bar{G} = \left(1 - \Lambda\right)^{-1} \quad . \tag{27}$$

Equation (27) is a nonlinear algebraic equation. For example, for GMS the arguments of Λ, $\beta_n = \bar{G} t_c^{ave} / \bar{v} t_n$, depend on both $\bar{G}$ and $\bar{v}$. As a result, there is no closed form solution in general. However, numerically this relation can be determined easily. Indeed, since Λ depends only on β, given the viscoelastic material parameters, we can assign β_n to compute $\bar{G}$ using eq. (27) and eq. (18)-(21). Once $\bar{G}$ is known, we simply compute $\bar{v}$ using $\bar{v} = \bar{G} t_c^{ave} / \beta_n t_n$. This procedure generates a plot of $\bar{v}$ versus $\bar{G}$ without solving any nonlinear equation.

3.1 Solutions for GMS

In this section, we seek closed-form solutions that relate $\bar{G}$ and $\bar{v}$ based on the theories of Knauss, Schapery and PB. If no closed form solution exists, we provide the asymptotic behavior. For GMS, we only present results for the SS where $N = 1$, $t_c \equiv t_1$, and $\beta \equiv \beta_1$. Here we note that some authors use relaxation time t_R in *a relaxation test as the characteristic material time* [20,21]. In general, the relaxation time t_R is much smaller than the retardation time t_c. For example, for an SS, $t_R = (E_\infty / E_0) t_c$, which can be three orders of magnitude smaller than t_c.

In **Knauss**'s theory, the FDR in eq. (18b) (N =1) does not permit a closed form solution for eq. (27). Therefore, we provide the asymptotic behaviors below using eq. (18d) and (18e):

$$\bar{G} \approx 1 + \left[1 + \frac{\kappa \bar{v}^K}{2}\right]\left(-\ln \bar{v}^K + \left(2 \ln 2 + \gamma\right)\right)\frac{\kappa \bar{v}^K}{2} \quad , \quad \bar{v}^K \equiv \frac{v d^K}{t_c} << 1 , \tag{28a}$$

$$\bar{v}^K \approx \frac{\left(1 + J_\infty / J_0\right)\left(\bar{G}^2 / 3\right)}{J_\infty / J_0 - \bar{G}}, \qquad \bar{v}^K >> 1 . \tag{28b}$$

Recall that γ in eq. (28a) is the Euler's constant.

In **Schapery**'s theory, closed-form solution is found by substituting eq. (19a) (N =1) into eq. (27), which gives

$$\bar{v}^S = \frac{\bar{G}}{\ln\left(\kappa\left(\frac{\bar{G}}{\bar{G} - 1}\right)\right)}, \ \bar{v}^S \equiv v d^S / t_c \qquad \text{(closed form)}. \tag{29a}$$

This solution has the following asymptotic behaviors:

$$\bar{G} \approx 1 + \kappa e^{-1/\bar{v}^S} \qquad \bar{v}^S << 1, \tag{29b}$$

$$\bar{v}^S \approx \frac{\left(1+J_\infty / J_0\right)\bar{G}^2}{J_\infty / J_0 - \bar{G}} \qquad \bar{v}^S >> 1. \tag{29c}$$

In **PB**'s theory, closed-form solution is also found by substituting eq. (20a) ($N = 1$) into eq. (27), which gives

$$\bar{v}^{PB} = \frac{\left(\bar{G}-1\right)/\kappa}{1-\left(\dfrac{\bar{G}-1}{\bar{G}\kappa}\right)^2}, \quad \bar{v}^{PB} \equiv \frac{vt_c}{\hat{d}^{PB}} \qquad \text{(closed form).} \tag{30a}$$

The asymptotic behaviors of eq. (30a) are

$$\bar{G} \approx 1+\kappa\bar{v}^{PB} \qquad \bar{v}^{PB} << 1, \tag{30b}$$

$$\bar{v}^{PB} \approx \left(1-\frac{\bar{G}-1}{\kappa\bar{G}}\right)^{-1}\bar{G}, \qquad \bar{v}^{PB} >> 1. \tag{30c}$$

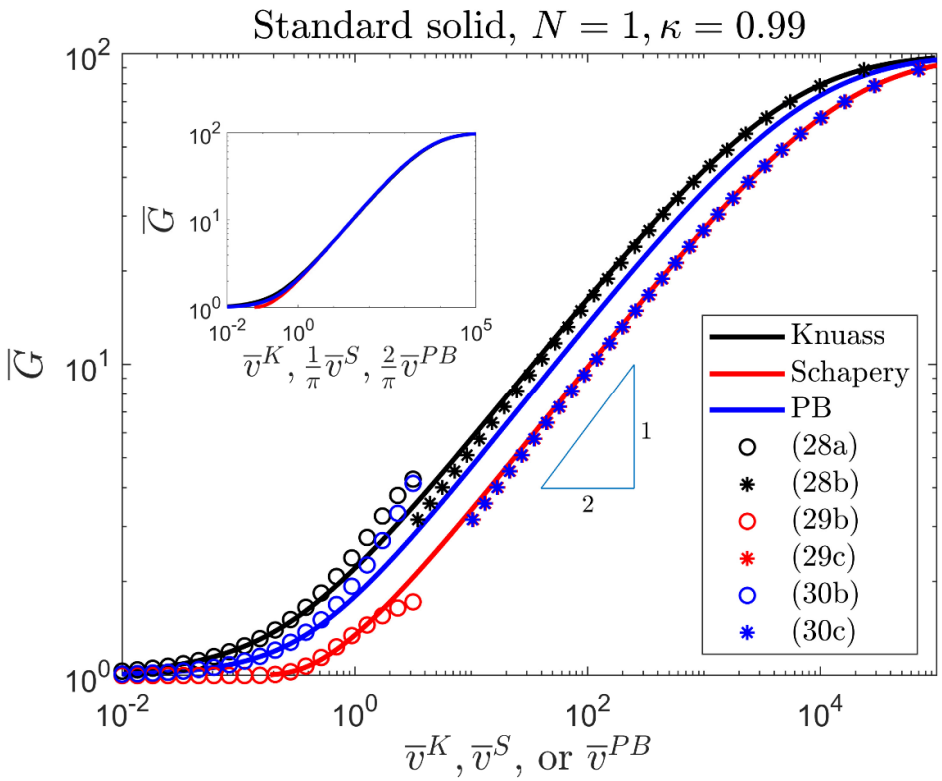

Figure 4 Normalized energy release rate $\bar{G}$ versus normalized crack velocity $\bar{v}$ for an SS with κ = 0.99. Solid lines represent full solutions based on the theories of Knauss (numerical), Schapery (eq. (29a)) and PB (eq. (30a)), while symbols represent asymptotic solutions. The inset shows that the three theories can be brought into reasonable agreement by shifting the Schapery and PB curves to the left by $\log(\pi)$ (Schapery) and $\log(\pi/2)$ (PB), respectively.

For all three theories, $\bar{G}$ approaches 1 in the limit of low crack velocity ($\bar{v}$ <<1), and approaches $J_\infty/J_0 = E_0/E_\infty$ in the limit of high crack velocity ($\bar{v}$ >>1), as expected. To illustrate the asymptotic solutions, we plot the $\bar{G}$ versus $\bar{v}$ in Fig.4 for an SS using the three theories. From Section 2.4, these theories are expected to exhibit different behaviors in the regime of low crack velocity, as confirmed by eq. (28a), (29b) and (30b). In particular, Schapery's theory underestimates $\bar{G}$ for low crack velocities. For high crack velocities, the prediction for different theories is practically identical up to constant coefficients. It should be noted that by plotting $\bar{v}^K$, $\bar{v}^S$, and $\bar{v}^{PB}$ on the same axis, we have implicitly assumed that $d^K = d^S = \hat{d}^{PB}$. Given that the definitions of d^K, d^S and $\hat{d}^{PB}$ differ by constants of order one and the cohesive stress (i.e., σ_D or σ_{PB}) is unknown, d^K, d^S and $\hat{d}^{PB}$ can be interpreted as independent fitting parameters. Changing their values is equivalent to shifting the $\bar{G}$ versus $\bar{v}$ curves horizontally in the log-log plot. As illustrated in the insert of Fig.4, the theories of Knauss, Schapery and PB can be brought into good agreement (except at low crack velocities) by shifting the Schapery and PB curves to the left.

3.2 Solutions for PLS

In this section we summarize solutions for PLS. In **Knauss**'s theory, closed-form solution relating $\bar{G}$ and $\bar{v}^K$ is not available. Instead, we get the following asymptotic solutions by substituting eq. (22b) and (22c) into eq. (27) (see Section S12 of the SI for derivation).

$$\bar{v}^K \approx \left(\frac{\bar{G}-1}{c_m}\right)^{1/m} \bar{G}^{(m-1)/m},\ c_m = \frac{\kappa}{2(1-m)}\frac{\sqrt{\pi}\Gamma(1-m)}{\Gamma(3/2-m)},\quad \bar{v}^K \equiv \frac{vd^K}{t_c} << 1, \tag{31a}$$

$$\bar{v}^K \approx \left(\frac{m\kappa}{3}\frac{J_\infty}{J_0}\right)\frac{\bar{G}^2}{(J_\infty/J_0)-\bar{G}},\qquad \bar{v}^K >> 1, \tag{31b}$$

where Γ is the Gamma function.

In **Schapery**'s theory, closed-form solution is found by combining eq. (24a) and (27):

$$\bar{v}^S = \frac{\bar{G}}{\left(\frac{\kappa\bar{G}}{\bar{G}-1}\right)^{1/m}-1},\quad \bar{v}^S \equiv \frac{vd^S}{t_c} \qquad \text{(elementary)}. \tag{32a}$$

The asymptotic behaviors of eq. (32a) are given by

$$\bar{v}^S \approx \left(\frac{\bar{G}-1}{\kappa}\right)^{1/m},\qquad \bar{v}^S << 1 \tag{32b}$$

$$\bar{v}^S \approx m\kappa\left(\frac{J_\infty}{J_0}\right)^2\left(1-\frac{J_0}{J_\infty}\bar{G}\right)^{-1}, \qquad \bar{v}^S >> 1 \tag{32c}$$

Derivation of eq. (32c) is given in Section S13 of the SI.

In **PB**'s theory, closed-form solution is not available. The asymptotic behavior in the low crack velocity limit is obtained using eq. (25b):

$$\bar{v}^{PB} \approx \left(\frac{\bar{G}-1}{c_{PB}}\right)^{1/m}, \quad c_{PB} = \frac{\pi 2^{-m}\kappa}{2\Gamma\left(\frac{m+1}{2}\right)\Gamma\left(\frac{3+m}{2}\right)\cos(m\pi/2)}, \quad \bar{v}^{PB} \equiv \frac{v\hat{d}^{PB}}{t_c} = \frac{vd^{PB}}{2\pi t_c} << 1. \tag{33a}$$

The asymptotic behavior under high crack velocity limit similar to eq. (32c) since eq. (25c) is identical to eq. (24b), i.e.,

$$\bar{v}^{PB} \approx m\kappa\left(\frac{J_\infty}{J_0}\right)^2\left(1-\frac{J_0}{J_\infty}\bar{G}\right)^{-1}, \qquad \bar{v}^{PB} >> 1 \qquad . \tag{33b}$$

Similar to SS, in all three theories $\bar{G}$ approaches 1 in the limit of $\bar{v}$ <<1 and approaches $J_\infty / J_0 = E_\infty / E_0$ in the limit of $\bar{v}$ >>1.

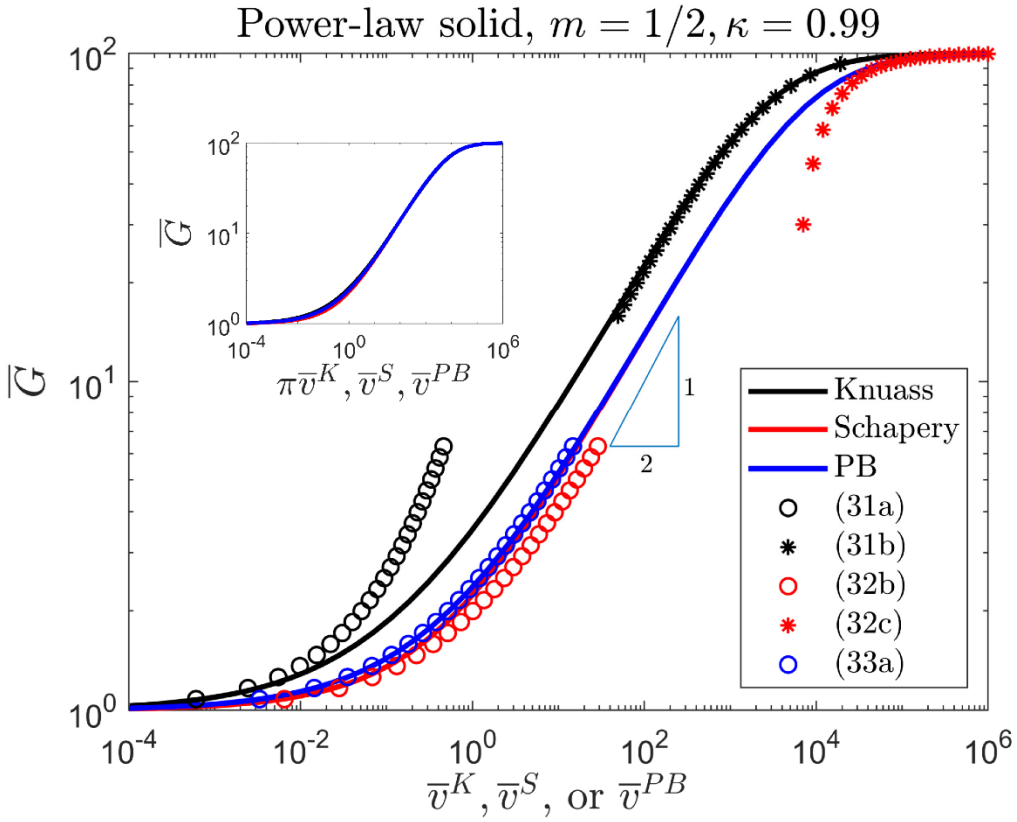

Figure 5 Normalized energy release rate $\bar{G}$ versus normalized crack velocity $\bar{v}$ for a PLS with m = 1/2 and κ = 0.99. Solid lines represent full solutions based on the theories of Knauss (numerical),

Schapery (eq. (32a)) and PB (numerical), while symbols represent asymptotic solutions. Note that the Schapery and PB curves are very close to each other; only a small difference is observed in the low crack velocity regime. The inset shows that all theories can be brought into agreement by shifting the Knauss curve to the right by a factor of $\log(\pi)$.

It is interesting to compare the PLS model with the SS model. Note that in the low crack velocity limit, all theories predict the same scaling (with different scaling constants) for the PLS, which is

$$\overline{v} \sim \left(\overline{G}-1\right)^{1/m} \quad . \tag{34}$$

Equation (34) suggests the difference between the three theories in the low crack velocity regime can be mostly attributed to the *limitation of the SS model, which has only one characteristic relaxation time*. To demonstrate this point, we plot the normalized energy release rate versus normalized crack velocity in Fig.5 (log-log) for PLS with m = 1/2. The asymptotic results in eq. (31) to (34) are also plotted as symbols to indicate their regions of validity. Notably, all three curves exhibit a middle section with a slope slightly less than 0.5 (≈ 0.47), which is consistent with eq. (34) implying that for $1 < \overline{G} << J_\infty / J_0$, $\overline{v} \sim (\overline{G}-1)^{1/m} \sim \overline{G}^2$. The inset shows that all theories can be brought into agreement by shifting horizontally.

Although the solutions for relating $\overline{G}$ and $\overline{v}$ are based on the creep compliance function in the time domain, $\Delta J(t)$, we note a practical disadvantage, i.e., it can be time-consuming to obtain the creep compliance function. It is easier to determine complex modulus $E^*(\omega)$ from small strain rheological tests or Dynamical Mechanical Analysis. Here we highlight a useful result which allows quick estimate of fracture behavior from the complex modulus data. Specifically, one can obtain the complex compliance $J^*(\omega)$ from the complex modulus using the identity: $J^*(\omega) = 1/E^*(\omega)$, and further estimate $\Delta J(t)$ using the approximation[5]:

$$\Delta J\left(t\right) = J\left(t\right) - J_\infty \simeq J^*_{storage}\left(\omega = \frac{2}{\pi t}\right) - J^*\left(\omega = 0\right) \equiv \Delta J^*_{storage}\,, \tag{35a}$$

where $J^*_{storage}(\omega)$ is the storage compliance, i.e., the real part of $J^*(\omega)$. Using $J^*(\omega) = 1/E^*(\omega)$, we have

$$J^*_{storage}\left(\omega\right) - J^*\left(\omega = 0\right) = \frac{E^*_{storage}\left(\omega\right)}{\left|E^*\left(\omega\right)\right|^2} - \frac{1}{E_\infty}\,, \tag{35b}$$

where $E_\infty = E^*(\omega = 0) = 1/J^*(\omega = 0)$. For example, Schapery's theory can be easily casted in the *frequency domain* using eq. (11a), (35a) and (35b),

[5] This approximation is often used to convert storage modulus to creep compliance (see equation 4.60 on Page 142 of Christensen [29]). We are not aware of any study on its limitations.

$$\Lambda^S = -\frac{\Delta\tilde{J}\left(\beta^S\right)}{J_\infty} \approx -\frac{\Delta J^*_{storage}\left(2/\left(\pi\beta^S t_c\right)\right)}{J_\infty} = 1 - \frac{E_\infty E^*_{storage}\left(2/\left(\pi\beta^S t_c\right)\right)}{\left|E^*\left(2/\left(\pi\beta^S t_c\right)\right)\right|^2}, \tag{35c}$$

where β^S is defined in eq. (11b). Using eq. (35c) and (27), the relation between energy release rate $\bar{G}$ and crack velocity $\bar{v}$ can be written as

$$\bar{G} \approx \frac{\left|E^*\left(2/\left(\pi\beta^S t_c\right)\right)\right|^2}{E_\infty E^*_{storage}\left(2/\left(\pi\beta^S t_c\right)\right)} = \frac{\left|E^*\left(2v/\left(\pi\bar{G}d^S\right)\right)\right|^2}{E_\infty E^*_{storage}\left(2v/\left(\pi\bar{G}d^S\right)\right)}. \tag{35d}$$

Although the length d^S, i.e., the minimum fracture process zone size, can be calculated from the cohesive stress σ_D using eq. (11b), it is more convenient to determine d^S by fitting experimental data (see Section 2.7 for example) since σ_D is unknown. Note for the limits of low and high velocities, eq. (35d) is exact and reduces to $\bar{G} = 1$ and $\bar{G} = E^*(\omega = \infty)/E_\infty = E_0/E_\infty$, respectively. If the storage modulus is much larger than the loss modulus in the domain of interest, one can further make the approximation[6]

$$\bar{G} \approx E^*_{storage}\left(\frac{2}{\pi\beta^S t_c}\right)/E_\infty = E^*_{storage}\left(\frac{2v}{\pi\bar{G}d^S}\right)/E_\infty. \tag{35e}$$

3.3 Comparison with experimental data

We end this section by two examples which compare the theories of Knauss, Schapery and PB to experimental data in the literature.

In the first example, we use the GMS model with $N = 5$ to fit the storage and loss modulus of a styrene-butadiene copolymer, which was given in Figure14 of Gent and Lai [23]. Details of the fitting are given in Section S14 of the SI. This fit provides us with the material constants in eq. (16a). We then use eqs. (18a), (19a) ,(20a) and (27) to predict the relationship between $\bar{G}$ and $\bar{v}$, which is compared with the experimental data in Gent and Lai [23]. The comparison between theory and experimental data based on the three different theories (Knauss, Schapery and PB) is shown in Fig.6. Recall $\bar{v}$ is normalized by d/t_c^{ave}, where d is related to the minimum fracture process or cohesive zone size and is specialized to d^K, d^S and $\hat{d}^{PB}$ for the theories of Knauss, Schapery and PB, respectively. We determine d by shifting the theoretical $\bar{G}$ and $\bar{v}$ curve horizontally in a log-log plot to minimize the difference between theory and experiment. This procedure also allows us to determine the size of the cohesive or fracture process zone using eq. (10b) and compare with the result in Figure 17 of Gent and Lai [23] which was obtained based on

[6] In theory, the loss modulus can be obtained using the Kramer-Kronig relation if the storage modulus is known. In practice, the loss modulus can be obtained quickly using the approximation $E^*_{loss}(\omega) \cong \left(\frac{\pi\omega}{2}\right)\left(dE^*_{storage}(\omega)/d\omega\right)$ (see equation 4.54 on Page 141 of Christensen [29]).

various approximations. We found a good fit for all three theories by choosing $d^K = d^S = \hat{d}^{PB}$ = 0.1 nm, consistent with Gent and Lai [23]. Although d^K, d^S and $\hat{d}^{PB}$ can be treated as independent fitting parameters to further optimize the fit for each theory, this is not pursued here since the results in Fig.6 are already illustrative of the three theories' behaviors. Figure 6 shows that the Schapery model given by eq. (19a) is surprisingly good, despite its simplicity. The oscillation in the Schapery curve is due to the limitation of the GMS model where each term in the Prony series is a decaying exponential with different time constants. The fit would have been smoother if more terms of the Prony series are chosen.

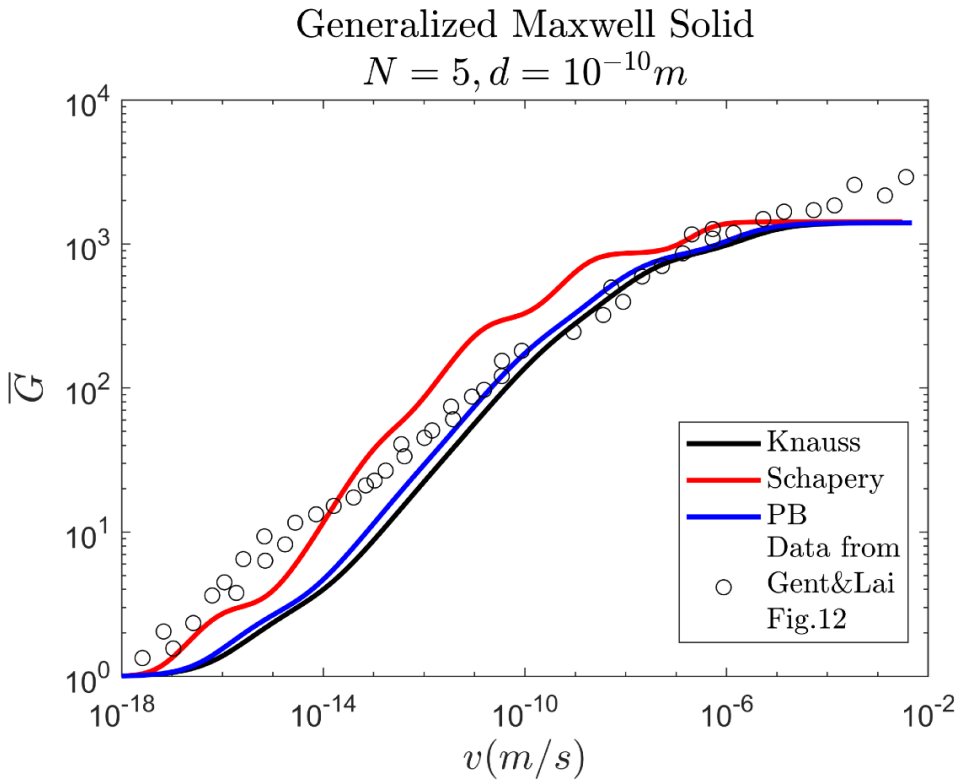

Figure 6 Comparison of normalized energy release rate $\overline{G}$ versus crack velocity v using the GMS model. Experimental data (circles) are extracted from Figure 12 in Gent and Lai [23]. The solid lines are given by Knauss's, Schapery's and PB's theories.

In the second example, we use the creep compliance and fracture data for a polyurethane elastomer called Solithane 113 provided in the review article of Knauss [1]. To further test the theory, we use the PLS model to fit the experimental creep compliance curves provided in Figure 3 of Knauss [1], as shown in Section S15 of the SI. The parameters which give best fit to creep compliance data are: J_0 = 6.0256 × 10^{-7} Pa^{-1}, J_∞ = 3.4914 × 10^{-4} Pa^{-1}, t_c = 0.1446 s, and m = 0.2523. Since we have verified that the theories of Knauss, Schapery and give similar $\overline{G}$ versus normalized crack velocity $\overline{v}$ (to within a shift factor), we use Schapery's theory eq. (32a) to

predict the $\overline{G}$ versus $\overline{v}$ behavior for its simplicity. We then compare the predicted behavior with the experimental data in Knauss [1], which is given in Figure 12 in his paper[7]. The only unknown parameter is d^S defined in eq. (11b). From eq. (32a) and the definition of $\overline{v} = vt_c / d^S$, we found $d^S = 0.9$ nm by shifting Schapery's theory along the horizontal axis ($\log \overline{v}$) to obtain the best fit to the experimental data. Comparison between the theory and experimental data is shown in Fig.7.

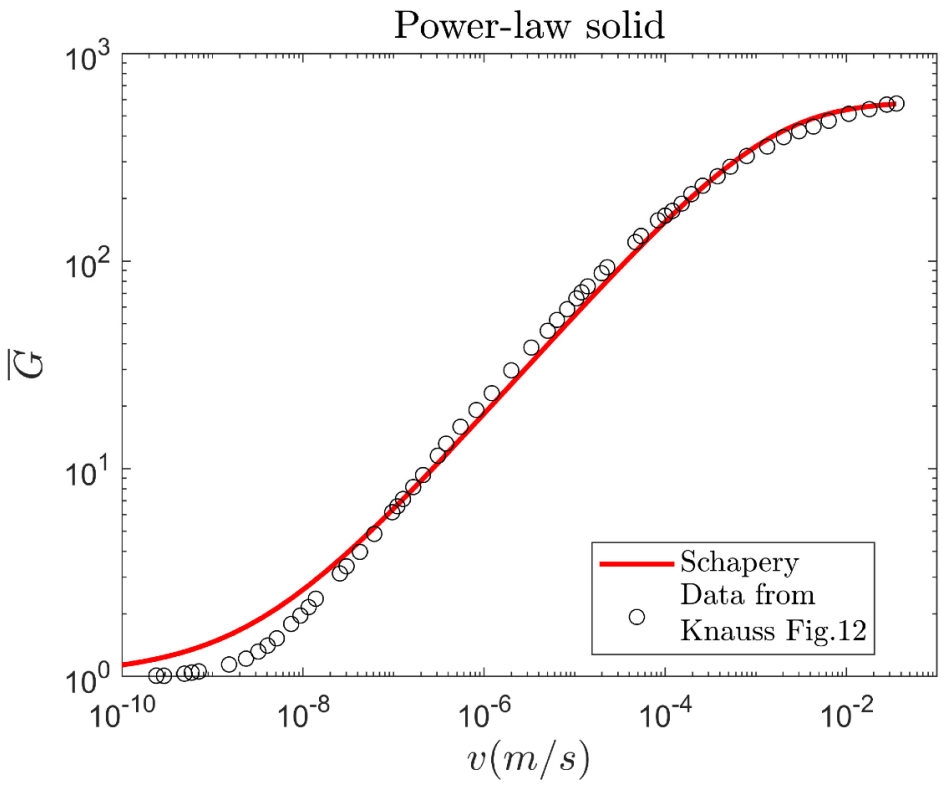

Figure 7 Comparison of normalized energy release rate $\overline{G}$ versus crack velocity v using the PLS model. Experimental data (circles) are extracted from Figure 12 of Knauss [1], and the solid line represents Schapery's theory based on a PLS model determined by fitting the creep compliance data in Knauss [1].

4. Strain distribution directly ahead of the cohesive zone tip

Our review of the literature shows that little attention is paid to the deformation field of a growing crack in viscoelastic solids. Analytical solutions revealing the displacement or strain fields surrounding a crack under steady state propagation not only provide theoretical insights towards the viscoelastic fracture mechanics, but also enable a new avenue for experimental validation, since the displacement and strain fields can be directly measured. For example, de

[7] Knauss reported fracture strain versus crack velocity. We have converted his fracture strain to toughness (see Section S15 of SI)

Gennes' examination of the Crack Opening Displacement (COD) has led to the "viscoelastic trumpet" model highlighting the physics of viscoelastic dissipation. On the experimental side, digital image correlation has been applied to measure the strain fields associated with a propagating crack in elastomers and hydrogels [37–43]. More recently, a method based on tracking randomly distributed tracer particles has been demonstrated to be capable of accurately measuring the large deformation fields around a crack in soft elastomers [44]. Later, in Section 7, we will see that the strain distribution is needed to compute the local dissipation rate. In this and the next two sections, we will focus on three aspects of the crack deformation fields:

- Distribution of the normal strain ε_{22} (i.e., perpendicular to the crack) directly ahead of the cohesive zone tip ($X \geq \alpha$, $Y = 0$) in Section 4.
- Residual strain behind the crack tip ($X < \alpha$, $Y = 0$) in Section 5.
- Crack opening displacement in Section 6.

To avoid redundancy, we will limit our discussions to the plane stress condition, since extension of the solutions to the plane strain condition is straightforward.

In Section 2, we discussed that in the limit of low crack velocity, the fracture process zone may interact with bulk viscoelasticity and hence alter the crack tip field. Such interaction is accounted for in Knauss's theory via the cohesive zone [1,8], but is not captured in the energetic theories (e.g., PB [22], de Gennes [20] and Saulnier et al. [21]). Under the SSC condition, the correspondence principle of linear viscoelasticity dictates the crack tip stress field in a viscoelastic solid is identical to that in an elastic solid. However, the crack tip strain field is expected to be affected by viscoelasticity. To quantify the effect of viscoelasticity on the crack tip strain field, we use the distribution of ε_{22} directly ahead of the cohesive zone tip, $\varepsilon_{22}(X \geq \alpha, Y = 0)$, as a benchmark problem. For Mode-I cracks, it is known that material points directly ahead the crack tip ($Y = 0$) is under equi-biaxial tension: $\sigma_{22} = \sigma_{11}$. Combining this feature, the steady state condition and the incompressibility constraint (i.e., Poisson's ratio = 1/2), we obtain the following strain distribution in plane stress[8]:

$$\varepsilon_{22}\left(X \geq \alpha, Y = 0\right) = -\frac{1}{2}\int_X^\infty J\left(\frac{X' - X}{v}\right)\frac{\partial \sigma_{22}}{\partial X'}dX' = \underbrace{\frac{J_\infty}{2}\sigma_{22}\left(X\right)}_{\varepsilon_{22}^\infty} - \frac{1}{2}\int_X^\infty \Delta J\left(\frac{X' - X}{v}\right)\frac{\partial \sigma_{22}}{\partial X'}dX' . \quad (36a)$$

The first term on the RHS of eq. (36a) represent the strain distribution of the *fully relaxed* solid, which is referred to as ε_{22}^∞ and is larger than the actual strain ε_{22}. To highlight the effect of viscoelasticity, we define a dimensionless quantity χ_{strain} which is the relative difference between ε_{22}^∞ and ε_{22},

$$\chi_{strain}\left(\bar{X} \geq 1\right) = \frac{\varepsilon_{22}^\infty\left(\bar{X} \geq 1, Y = 0\right) - \varepsilon_{22}\left(\bar{X} \geq 1, Y = 0\right)}{\varepsilon_{22}^\infty\left(\bar{X} \geq 1, Y = 0\right)} . \quad (36b)$$

[8] For plane strain, multiply the RHS by a factor of 3/4.

Note that we normalized X by the cohesive zone size α, i.e., $\bar{X} \equiv X/\alpha$. In general, χ_{strain} is a monotonically decreasing function of $\bar{X}$ for $\bar{X} \geq 1$ and also depends on the crack velocity.

To evaluate eq. (36a), we need to determine the creep function $\Delta J(t)$ and the stress distribution $\sigma_{22}(\bar{X})$. The former is specified according to the two viscoelastic models: GMS and PLS, as detailed in Section 2.3. The latter depends on whether the cohesive zone is explicitly included. For example, if the DB cohesive zone model with a constant traction σ_D is included (as in Knauss's theory), we have the following stress distribution using the stress field in Section S1 of the SI:

$$\sigma_{22}\left(X \geq \alpha, Y = 0\right) = \frac{2\sigma_D}{\pi} \tan^{-1} \sqrt{\frac{\alpha}{X - \alpha}} \ . \tag{37a}$$

In contrast, in PB's theory, $\sigma_{22}(X)$ is given by the K-field all the way until the fracture process zone. To facilitate comparison, we will also use σ_D to denote the critical stress and α to denote the fracture process zone size. In this case, the stress distribution is

$$\sigma_{22}^{*}\left(X \geq \alpha, Y = 0\right) = \frac{K_I}{\sqrt{2\pi X}} = \sigma_D \sqrt{\frac{\alpha}{X}} \ , \tag{37b}$$

where we added an asterisk superscript to σ_{22} to distinguish it from that in eq. (37a) and used the relation $\sigma_D = K_I / \sqrt{2\pi\alpha}$. We shall call this the non-interacting model and will label quantities associated with it by *. We will implement both stress distributions and compare the resultant strains to illustrate the interaction between cohesive zone and bulk viscoelasticity.

4.1 Solutions for GMS

We first consider the stress distribution in eq. (37a) and find that (see Section S16 of the SI)

$$\varepsilon_{22}\left(\bar{X} \geq 1, Y = 0\right) = \varepsilon_{22}^{\infty}\left(\bar{X} \geq 1, Y = 0\right) - \frac{\sigma_D}{2\pi E_\infty} \kappa \sum_{n=1}^{N} a_n \exp\left(\beta_n \bar{X}\right) \Psi\left(\bar{X}, \beta_n\right), \tag{38a}$$

where $\beta_n \equiv \alpha / v t_n$ and

$$\Psi\left(\bar{X}, \beta_n\right) \equiv \int_{\bar{X}}^{\infty} \frac{e^{-\beta_n \eta}}{\eta \sqrt{\eta - 1}} d\eta \ , \tag{38b}$$

$$\varepsilon_{22}^{\infty}\left(\bar{X} \geq 1, Y = 0\right) = \frac{\sigma_D}{2\pi E_\infty} \left\{ \pi - 2 \tan^{-1}\left(\sqrt{\bar{X} - 1}\right) \right\} = \frac{\sigma_D}{\pi E_\infty} \tan^{-1}\left(\frac{1}{\sqrt{\bar{X} - 1}}\right). \tag{38c}$$

The second term on the RHS of eq. (38a) measures the deviation from the elastic strain due to viscoelasticity. Using eq. (38a) and (38c), eq. (36b) becomes

$$\chi_{strain}\left(\bar{X}\geq 1\right)\equiv\frac{\kappa\sum_{n=1}^{N}a_n\exp\left(\beta_n\bar{X}\right)\Psi\left(\bar{X},\beta_n\right)}{\pi-2\tan^{-1}\left(\sqrt{\bar{X}-1}\right)}. \tag{39a}$$

For SS, $N=1$, $a_1=1$, and there is only one retardation time $t_c=t_1$. Consequently, eq. (39a) reduces to

$$\chi_{strain}\left(\bar{X}\geq 1\right)\equiv\frac{\kappa\exp\left(\beta\bar{X}\right)\Psi\left(\bar{X},\beta\right)}{\pi-2\tan^{-1}\left(\sqrt{\bar{X}-1}\right)}, \tag{39b}$$

where $\beta=\alpha/vt_c$.

For general GMS, we find that for $\bar{X}>>1$, the asymptotic behavior of eq. (39a) is given by (see Section S17 of the SI)

$$\chi_{strain}\approx\frac{\kappa}{2\bar{X}}\sum_{n=1}^{N}\frac{a_n}{\beta_n}=\frac{\kappa}{2X}v\sum_{n=1}^{N}a_nt_n\ \text{ for }\ \bar{X}>>1, \tag{39c}$$

where we have used the definitions $\bar{X}=X/\alpha$ and $\beta_n=\alpha/vt_n$. Equation (39c) tells us that it takes a distance from the cohesive zone tip much greater than $v\sum_{n=1}^{N}a_nt_n$ to reach the relaxed state. The characteristic distance emerging in eq. (39c), $v\sum_{n=1}^{N}a_nt_n$, is independent of the cohesive zone size and depends only the crack velocity. The faster the crack velocity, the larger this distance is. The above result for χ_{strain} is valid for a plane strain crack as well since χ_{strain} is the ratio of strains and the constant factor of 3/4 needed for the plane strain case does not appear in χ_{strain}.

It is useful to consider the strain at the cohesive zone tip (i.e., $\bar{X}=1$). At this point, eq. (38a) can be reduced to

$$\varepsilon_{22}\left(\bar{X}=1,Y=0\right)=\frac{\sigma_D}{2E_\infty}\left[1-\kappa\sum_{n=1}^{N}a_n\exp\left(\beta_n\right)erfc\left(\sqrt{\beta_n}\right)\right], \tag{40a}$$

where we have used the identity (see Section S16 of the SI):

$$\Psi\left(\bar{X}=1,\beta_n\right)=\pi\,erfc\left(\sqrt{\beta_n}\right), \tag{40b}$$

and *erfc* is the complementary error function. Accordingly, eq. (39b) becomes

$$\chi_{strain}\left(\bar{X}=1\right)=\kappa\sum_{n=1}^{N}a_n\exp\left(\beta_n\right)erfc\left(\sqrt{\beta_n}\right). \tag{40c}$$

It is worth noting that in the limit of high crack velocity (i.e., $\beta_1<<1$), $\chi_{strain}(\bar{X}=1)$ approaches κ. This is consistent with the expectation that at high crack velocity the cohesive zone is surrounded by materials in the unrelaxed elastic limit with modulus E_0.

Next, we use the stress distribution in eq. (37b) (i.e., the *K*-field) to calculate the strain directly ahead of the fracture process zone tip (i.e., $X \geq \alpha$ and $Y = 0$) and for χ_{strain}. The resulting expressions are simpler (see Section S18 of the SI for detailed derivation):

$$\varepsilon_{22}^{*}\left(\bar{X}\geq 1, Y=0\right)=\frac{\sigma_D}{2E_\infty\sqrt{\bar{X}}}\left[1-\kappa\left\{1-\sum_{n=1}^{N}a_n\sqrt{\pi\bar{X}\beta_n}\exp\left(\beta_n\bar{X}\right)erfc\left(\sqrt{\beta_n\bar{X}}\right)\right\}\right], \tag{41a}$$

$$\chi_{strain}^{*}\left(\bar{X}\right)=\kappa\left\{1-\sum_{n=1}^{N}a_n\sqrt{\pi\bar{X}\beta_n}\exp\left(\beta_n\bar{X}\right)erfc\left(\sqrt{\beta_n\bar{X}}\right)\right\}. \tag{41b}$$

where $\beta_n \equiv \alpha / vt_n$ and we have added an asterisk superscript to ε_{22} and χ_{strain} to distinguish from those from that in eq. (38a) and (39a). Unlike eq. (39a) where χ_{strain} is a function of both $\bar{X}$ and β_n, here χ_{strain}^{*} depends only on $\beta_n\bar{X}$, which is independent of the fracture process zone size α. Hence, there are obvious differences between eq. (38a) and (41a) near the cohesive zone tip due to interaction between fracture process zone and the viscoelastic continuum fields, especially at low crack velocities. In particular, the strain at the cohesive tip is given by

$$\varepsilon_{22}^{*}\left(\bar{X}=1, Y=0\right)=\frac{\sigma_D}{2E_\infty}\left[1-\kappa\left\{1-\sum_{n=1}^{N}a_n\sqrt{\pi\beta_n}\exp\left(\beta_n\right)erfc\left(\sqrt{\beta_n}\right)\right\}\right], \tag{41c}$$

which is clearly different from its counterpart in eq. (40a). However, far ahead of the cohesive zone tip (i.e., $\bar{X}$ >>1), we expect χ_{strain} and χ_{strain}^{*} to agree. This is confirmed in Section S19 of the SI, where we show that the asymptotic behavior of χ_{strain}^{*} for large $\bar{X}$ is the same as eq. (39c).

Figure 8 compares the strain distribution predicted by eq. (38a) and eq. (41a) using the SS (N=1) as an example. In this case, there is only one retardation time $t_c = t_1$ and hence one β (i.e., $= \alpha/vt_c$). To facilitate comparison, we normalize ε_{22} and ε_{22}^{*} by σ_D/E_∞. We found that if we multiply eq. (41a) by a factor of $2/\pi$, then Knauss's and PB's theories are in good agreement with each other, as shown in Fig.8. This factor is not coincident: eq. (37a) suggests that σ_{22} approaches $(2/\pi)\sigma_D\sqrt{\alpha / X}$ when $X >> \alpha$. Comparing this behavior with eq. (37b), we can see that far ahead of the cohesive zone tip σ_{22} is equal to $2/\pi$ times σ_{22}^{*}. Multiplying eq. (41a) by $2/\pi$ ensures that the stress far ahead of the cohesive zone tip is given by the same stress intensity factor K_I. After the vertical shift, we still expect deviations between eq. (38a) and (41a) near the cohesive zone tip $\bar{X}$ = 1, because the effects of interaction between fracture process zone and bulk viscoelasticity are not accounted for in eq. (41a). However, Fig.8 shows that such deviations are not significant. These differences depend on β and can be explored by examining the asymptotic behavior of eq. (40a) and (41c) (see Section S20 of the SI). The curves for different β can be collapsed into a single master curve if we plot $\varepsilon_{22} / \varepsilon_{22}^{\infty} = 1 - \chi_{strain}^{*}$ (or $\varepsilon_{22}^{*} / \varepsilon_{22}^{*\infty} = 1 - \chi_{strain}^{*}$) versus $\beta\bar{X}$ as shown in the insert of Fig.8. Although this is expected for eq. (41b), it is interesting to see that it also approximately holds for eq. (39a) except the small deviations at the cohesive zone tip $\bar{X}$ = 1.

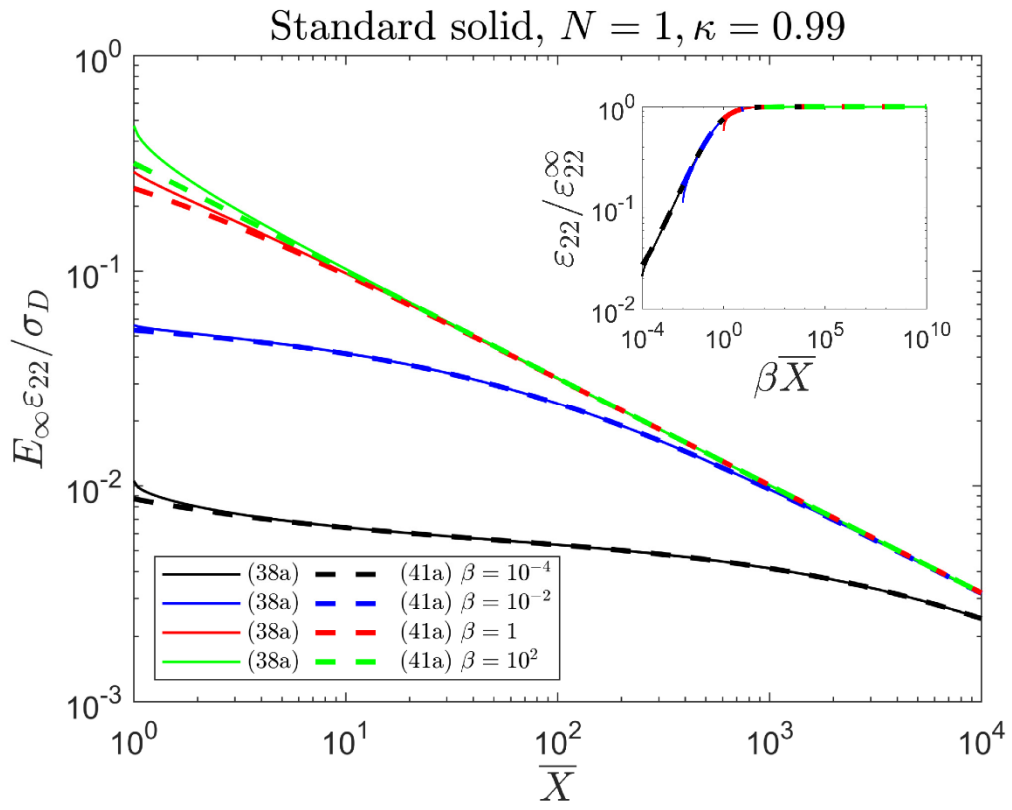

Figure 8 Normalized strain distribution $E_\infty \varepsilon_{22} / \sigma_D$ and $E_\infty \varepsilon_{22}^* / \sigma_D$ directly ahead of the cohesive zone tip ($\overline{X} \geq 1$) for SS with $N = 1$, $\kappa = 0.99$ and 4 different β. The strain in eq. (41a) is multiplied by $2/\pi$ to bring it into agreement with eq. (38a) for $\overline{X} >> 1$. The inset shows that by plotting $\varepsilon_{22} / \varepsilon_{22}^\infty = 1 - \chi_{strain}$ (or $\varepsilon_{22}^* / \varepsilon_{22}^{*\infty} = 1 - \chi_{strain}^*$) versus $\beta \overline{X}$ all curves for different β collapsed into a single curve.

4.2 Solutions for PLS

In this section we present results for PLS. We start with the stress in eq. (37a) and find that ε_{22} directly ahead of the cohesive zone tip is given by

$$\varepsilon_{22}\left(\overline{X} \geq 1, Y = 0\right) = \frac{\sigma_D}{\pi E_\infty}\left[\left(\frac{\pi}{2} - \tan^{-1}\left(\sqrt{\overline{X} - 1}\right)\right) - \frac{\kappa}{2}\Psi_{PL}\left(\overline{X}, \beta, m\right)\right], \tag{42a}$$

where $\beta = \alpha / v t_c$ and

$$\Psi_{PL}(\overline{X}, \beta, m) \equiv \int_{\overline{X}}^{\infty} \frac{1}{\left[1 + \beta(\eta - \overline{X})\right]^m} \frac{1}{\eta\sqrt{\eta - 1}} d\eta \,. \tag{42b}$$

As in the GMS, the first term in eq. (42a) is the elastic strain of a fully relaxed solid (i.e., $\varepsilon_{22}^{\infty}$) and the second represents the reduction in strain due to viscoelasticity. Using eq. (36b), we find

$$\chi_{strain}\left(\bar{X}\geq 1\right)=\frac{\kappa\Psi_{PL}\left(\bar{X},\beta,m\right)}{\pi-2\tan^{-1}\left(\sqrt{\bar{X}-1}\right)}. \tag{42c}$$

For general *m*, we have not been able to obtain a closed-form solution in terms of well-known special functions. However, there is a special case where the integral in eq. (42b) can be evaluated exactly: *m* = 1/2. In this case, χ_{strain} is found to be (see Section S21 of the SI)

$$\chi_{strain}\left(\bar{X}\geq 1,\beta,m=1/2\right)=\frac{2\kappa}{\pi-2\tan^{-1}\left(\sqrt{\bar{X}-1}\right)}\sqrt{\frac{1}{\bar{X}\beta-1}}\ln\left(\frac{\sqrt{\frac{\bar{X}\beta-1}{\beta}}+1}{\sqrt{\frac{\left(\bar{X}\beta-1\right)\left(\bar{X}-1\right)}{\bar{X}\beta}}+\sqrt{\frac{1}{\bar{X}\beta}}}\right),$$

$$\text{for } \bar{X}\beta>1\ , \tag{43a}$$

$$\chi_{strain}\left(\bar{X}\geq 1,\beta,m=1/2\right)$$

$$=\frac{2\kappa}{\pi-2\tan^{-1}\left(\sqrt{\bar{X}-1}\right)}\frac{1}{\sqrt{1-\beta\bar{X}}}\left[\sin^{-1}\left(\sqrt{\frac{1-\beta\bar{X}}{\beta+1-\beta\bar{X}}}\right)-\sin^{-1}\left(\sqrt{\frac{1-\beta\bar{X}}{\beta+1-\beta\bar{X}}\left(1-1/\bar{X}\right)}\right)\right],$$

$$\text{for } \bar{X}\beta<1 \tag{43b}$$

These two expressions are continuous at $\beta\bar{X}=1$ where

$$\chi_{strain}\left(\bar{X}\beta=1,m=1/2\right)=\frac{2\kappa}{\pi-2\tan^{-1}\left(\sqrt{\left(1-\beta\right)/\beta}\right)}\frac{1-\sqrt{1-\beta}}{\sqrt{\beta}}\ . \tag{43c}$$

The asymptotic behaviors of χ_{strain} in case of *m* =1/2 can be readily found using eq. (43a) and (43b). For $\beta>>1$ (i.e., slow crack velocity), the χ_{strain} in eq. (43a) simplifies to

$$\chi_{strain}\left(\bar{X}\geq 1,\beta\gg 1,m=\frac{1}{2}\right)\approx\frac{2\kappa}{\pi-2\tan^{-1}\left(\sqrt{\bar{X}-1}\right)}\sqrt{\frac{1}{\bar{X}\beta}}\ \ln\left(\frac{\sqrt{\bar{X}}+1}{\sqrt{\bar{X}-1}+\sqrt{\frac{1}{\bar{X}\beta}}}\right). \tag{44a}$$

As expected, for slow crack growth, the contribution to the strain from viscoelastic flow is insignificant, even at the cohesive zone tip ($\bar{X}$ = 1). For $\beta<<1$ (i.e., fast crack velocity), the χ_{strain} at *a fixed* $\bar{X}$ as $\beta\rightarrow 0$ is obtained using eq. (43b):

$$\chi_{strain}(\bar{X}\geq 1,\bar{X}\beta \ll 1,m=\frac{1}{2})\approx \frac{2\kappa}{\pi-2\tan^{-1}\left(\sqrt{\bar{X}-1}\right)}\left[\frac{\pi}{2}-\sin^{-1}\sqrt{\frac{\bar{X}-1}{\bar{X}}}\right]=\kappa\,. \tag{44b}$$

Similar to the GMS, it is useful to consider the strain at the cohesive zone tip $\bar{X}=1$. For $\beta > 1$, eq. (43a) implies that

$$\chi_{strain}(\bar{X}=1,\beta>1,m=1/2)=\frac{2\kappa}{\pi}\sqrt{\frac{1}{\beta-1}}\ln\left(\sqrt{\beta-1}+\sqrt{\beta}\right). \tag{45a}$$

For $\beta < 1$, eq. (43b) implies that

$$\chi_{strain}(\bar{X}=1,\beta<1,m=1/2)=\frac{2\kappa}{\pi}\frac{\sin^{-1}\left(\sqrt{1-\beta}\right)}{\sqrt{1-\beta}}. \tag{45b}$$

In particular, eq. (45b) shows that in the high crack velocity limit ($\beta << 1$), $\chi_{strain}(\bar{X}=1)$ approaches κ, which is expected due to the unrelaxed solids surrounding the cohesive zone with high crack velocity.

Next, we use the approximate stress field in eq. (37b) based on the *K*-field outside the fracture process zone. In this case, a closed-form solution for ε_{22}^{*} directly ahead of the cohesive zone tip can be obtained for any *m* (see Section S22 of the SI).

$$\varepsilon_{22}^{*}\left(\bar{X}\geq 1,Y=0\right)=\frac{\sigma_D}{2E_\infty\sqrt{\bar{X}}}\left(1-\frac{\kappa}{2m+1}\left(\beta\bar{X}\right)^{-m}{}_2F_1\left(m,m+\frac{1}{2},m+\frac{3}{2},\frac{\beta\bar{X}-1}{\beta\bar{X}}\right)\right), \tag{46a}$$

where $\beta = \alpha/vt_c$ and ${}_2F_1$ is the hypergeometric function. Accordingly, χ_{strain}^{*} is given by

$$\chi_{strain}^{*}\left(\bar{X}\geq 1,\beta,m\right)=\frac{\kappa\left(\beta\bar{X}\right)^{-m}}{2m+1}{}_2F_1\left(m,m+\frac{1}{2},m+\frac{3}{2},\frac{\beta\bar{X}-1}{\beta\bar{X}}\right). \tag{46b}$$

Equation (46b) indicates that χ_{strain}^{*} depends only on $\bar{X}\beta$, *m* and κ, implying that in absence of interaction between cohesive zone and bulk viscoelasticity, χ_{strain}^{*} at a given *X* scales inversely with vt_c. Using the asymptotic behavior of the hypergeometric function (see Section S23 of the SI), we found the following asymptotic behaviors for χ_{strain}^{*}

$$\chi_{strain}^{*}\left(\bar{X}\geq 1,\bar{X}\beta >> 1,m\right)=\frac{\kappa\left(\beta\bar{X}\right)^{-m}}{2m+1}\frac{2\Gamma\left(m+3/2\right)\Gamma\left(1-m\right)}{\sqrt{\pi}}, \tag{47a}$$

$$\chi_{strain}\left(\bar{X}\geq 1,\bar{X}\beta <<1,m\right)\approx\kappa\,, \tag{47b}$$

where Γ is the Gamma function. Equation (47a) shows that for slow crack velocity, we need to move ahead of the cohesive zone tip by a distance of $\bar{X}\gg 1/\beta$ or $X >> vt_c$ for the viscoelastic

effect (i.e., χ^*_{strain}) to vanish. Comparing eq. (47a) with (39c), the rate of decay of χ^*_{strain} in the PLS is much slower than the GMS in this regime. Thus, the PLS predicts a much larger region where viscoelastic effect is present. Finally, for m = 1/2, the hypergeometric function eq. (46a) is elementary and is (see 15.1.13 in [25])

$$ {}_2F_1\left(\frac{1}{2},1,2,\frac{\beta\bar{X}-1}{\beta\bar{X}}\right)=2\left[1+\left(1-\frac{\beta\bar{X}-1}{\beta\bar{X}}\right)^{1/2}\right]^{-1}=2\left[1+\frac{1}{\sqrt{\beta\bar{X}}}\right]^{-1} $$

(48)

The strain distribution ε_{22} and ε^*_{22}, normalized by and σ_D / E_∞, for a PLS with m = 1/2 and κ = 0.99 and different β is shown in Fig. 9. The results of eq. (42a) and (46a) can be brought into good agreement, except near the cohesive zone tip, if the strain in eq. (46a) is multiplied by a constant factor of 2/π, which originates from the difference in the far field stress given in eq. (37a) and (37b), as already discussed for Fig.8. Similar to SS, the curves for different β collapse into a master curve (except near $\bar{X}$ = 1) when the vertical and horizontal axes are replaced by $\varepsilon_{22}/\varepsilon^{\infty}_{22}=1-\chi_{strain}$ (or $\varepsilon^*_{22}/\varepsilon^{*\infty}_{22}=1-\chi^*_{strain}$) and $\beta\bar{X}$ respectively (see Fig.9 inset).

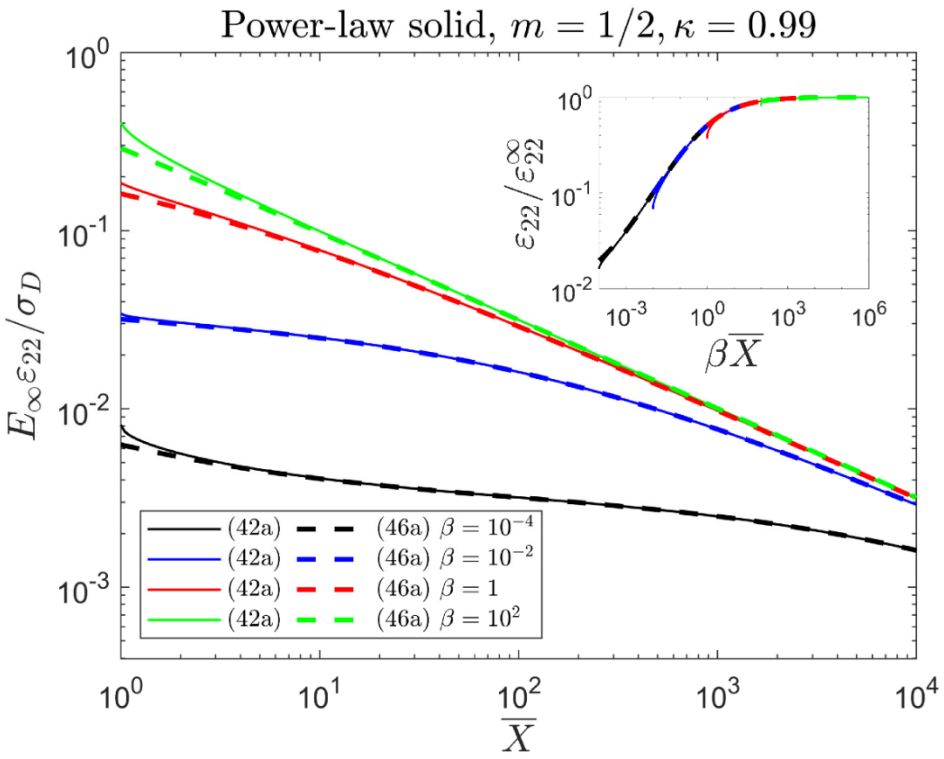

Figure 9 Normalized strain distribution $E_\infty \varepsilon_{22}/\sigma_D$ and $E_\infty \varepsilon^*_{22}/\sigma_D$ directly ahead of the cohesive zone tip ($\bar{X} \geq 1$) for PLS with m = 1/2, κ = 0.99 and 4 different β. The strain in eq. (46a) is multiplied by a constant factor of 2/π to bring it into agreement with eq. (42a) for $\bar{X} >> 1$. Inset shows that curves for different β collapsed into a master curve (except when $\bar{X}$ is close to 1) when

the vertical and horizontal axes are replaced by $\varepsilon_{22}/\varepsilon_{22}^{\infty}=1-\chi_{strain}$ (or $\varepsilon_{22}^{*}/\varepsilon_{22}^{*\infty}=1-\chi_{strain}^{*}$) and $\beta\bar{X}$ respectively.

5. Residual strain on crack surface

As a material point sweeps past the crack tip and enters the crack surface, it unloads completely but the accumulated strain takes a finite distance to vanish, the residual strain in this region can be seen in experiment [45] and reflects dissipation. In this section, we use the residual strain on the crack surfaces, $\varepsilon_{22}(X<0,\ Y=0)$, to characterize the viscoelastic effect behind the crack tip. Solutions of the residual strain requires knowledge of the detailed stress distribution within the cohesive zone, which is not available in the *K*-field based approximate stress distribution in eq. (37b). Therefore, only results based on the stress fields with the DB cohesive zone model (i.e., constant cohesive stress σ_D) will be included.

5.1 Solutions for GMS

A detail calculation shows that for GMS (see Section S24 of SI), the residual strain behind the crack tip is given *exactly* by

$$\varepsilon_{22}\left(\bar{X}<0,Y=0\right)=\frac{\sigma_D\kappa}{2E_{\infty}}\sum_{n=1}^{N}a_n\exp\left(-\beta_n\left|\bar{X}\right|\right)erf\left(\sqrt{\beta_n}\right), \tag{49a}$$

where $\bar{X}\equiv X/\alpha$ and $\beta_n\equiv\alpha/vt_n$. Equation (49a) shows that ε_{22} decays exponentially with $|\bar{X}|$ and the decaying distance is governed solely by $\beta_n|\bar{X}|$ *which is independent of the cohesive zone size* α. The maximum residual strain occurs right behind the crack tip (i.e., at $X=0$), and is given by

$$\varepsilon_{22}\left(\bar{X}=0^{-},Y=0\right)=\frac{\sigma_D\kappa}{2E_{\infty}}\sum_{n=1}^{N}a_n erf\left(\sqrt{\beta_n}\right). \tag{49b}$$

Equation (49b) shows that the magnitude of the residual strain *decreases* as the crack velocity *increases*, although the *distance of decay increases linearly with velocity* since it is directly proportional to $1/\beta_n$. Since $\beta_1>\beta_2>....>\beta_N$, the decay is controlled by the largest retardation time t_N. Hence the residual strain far behind the crack faces is:

$$\varepsilon_{22}\left(\beta_N\left|\bar{X}\right|>>1,Y=0\right)\approx\frac{\sigma_D\kappa}{2E_{\infty}}\exp\left(-\beta_N\left|\bar{X}\right|\right)erf\left(\sqrt{\beta_N}\right). \tag{49c}$$

Thus, the decay distance can be estimated by setting $\beta_N\left|\bar{X}\right|=1$ which yields $\left|X\right|=vt_N$. At this position the residual strain is 1/*e* of its maximum value at the crack tip.

5.2 Solutions for PLS

For PLS, exact solution of the residual strain distribution on the crack surface can also be obtained (see Section S25 of the SI), which is

$$\varepsilon_{22}\left(\bar{X}<0,Y=0,m\right)=\frac{\sigma_D\kappa}{2E_\infty\left[1+\beta\left|\bar{X}\right|\right]^m}\left(1-\frac{\left[1+\beta\left|\bar{X}\right|\right]^m\varphi\left(\beta,\bar{X}<0\right)}{\pi}\right) \tag{50a}$$

where $\beta = \alpha/vt_c$ and

$$\varphi\left(\beta,\bar{X}<0\right)=\beta^{-m}\frac{\Gamma\left(m+1/2\right)\Gamma\left(1/2\right)}{\Gamma\left(m+1\right)}\,{}_2F_1\left(m,m+\frac{1}{2},m+1,\frac{-\beta\left|\bar{X}\right|-1}{\beta}\right). \tag{50b}$$

Recall that ${}_2F_1$ is the hypergeometric function and Γ is the Gamma function. An equivalent form of φ is given in Section S25 of the SI. The maximum residual strain occurs just behind the crack tip at $\bar{X}=0^-$, which is

$$\varepsilon_{22}\left(\bar{X}=0^-,Y=0\right)=\frac{\sigma_D\kappa}{2E_\infty}\left(1-\frac{\varphi\left(\beta,\bar{X}=0\right)}{\pi}\right) \tag{51}$$

The asymptotic behavior of $\varepsilon_{22}^{\max}\left(\bar{X}=0^-,Y=0\right)$ for $\beta<<1$ (fast crack velocity) can be obtained directly from the series expansion of the hypergeometric function in eq. (50b), which is (see Section S26 of the SI)

$$\varepsilon_{22}\left(\bar{X}=0^-,Y=0,\beta<<1\right)\approx\frac{\sigma_D\kappa}{2E_\infty}\frac{2\Gamma\left(m+1/2\right)\sqrt{\pi}}{\Gamma(m)}\sqrt{\beta}\quad . \tag{52a}$$

Thus, the maximum residual strain vanishes as the reciprocal of the square root of the crack velocity. Similarly, the behavior of $\varepsilon_{22}\left(\bar{X}=0^-,Y=0\right)$ for $\beta>>1$ (slow crack velocity) is found to be (see Section S26 of the SI):

$$\varepsilon_{22}\left(\bar{X}=0^-,Y=0,\beta>>1\right)=\frac{\sigma_D\kappa}{2E_\infty}\left(1-\frac{1}{\sqrt{\pi}}\beta^{-m}\frac{\Gamma\left(m+1/2\right)}{\Gamma\left(m+1\right)}\right). \tag{52b}$$

Just as in the case of GMS, eq. (52a) and (52b) indicates that the *maximum residual strain* decreases as the velocity increase.

At large distances behind the crack tip (i.e., $|\bar{X}|>>1$), the residual strain should go to zero. For the special case of SS, the residual strain decays *exponentially* fast with $|\bar{X}|$ as governed by the characteristic length vt_c (see eq. (49c)). For PLS, the characteristic decay distance is still controlled by vt_c, but the rate of decay is much slower. To obtain the decay behavior, we first rewrite the residual strain distribution in eq. (50a) as (see Section S27 of the SI):

$$\varepsilon_{22}\left(\bar{X}<0, Y=0\right)=-\frac{\sigma_D \kappa}{2E_\infty\left[1+\beta\left|\bar{X}\right|\right]^m}\frac{\Gamma\left(m+1/2\right)\Gamma(-1/2)}{\pi\,\Gamma(m)}\sqrt{\frac{\beta}{\beta\left|\bar{X}\right|+1}}\,{}_2F_1\left(m+\frac{1}{2},\frac{1}{2},\frac{3}{2},\frac{\beta}{-\beta\left|\bar{X}\right|-1}\right). \quad (53a)$$

Equation (53a) is exact since we have made no assumption that distance is large. Since $\beta\left|\bar{X}\right|$ appears as a unit, one must insist $\beta\left|\bar{X}\right|>>1$ (instead of $\left|\bar{X}\right|>>1$). Therefore, for fast crack velocity (i.e., $\beta<<1$), the characteristic decay distance can be very large (i.e., $\left|\bar{X}\right|>>1/\beta$) *even though the magnitude of residual strain is small*. In the limit of $\beta\left|\bar{X}\right|>>1$, the first order behavior of eq. (53a) is (see Section S27 of the SI):

$$\varepsilon_{22}\left(\beta\left|\bar{X}\right|>>1, Y=0\right)\approx\frac{\sigma_D \kappa}{E_\infty\left(\beta\left|\bar{X}\right|\right)^{m+1/2}}\frac{\Gamma\left(m+1/2\right)}{\pi\,\Gamma(m)}\sqrt{\pi\beta}\quad . \quad (53b)$$

Recall that eq. (52a) shows the maximum residual strain is proportional to $\sqrt{\beta}$ (small) in the limit of fast crack velocity. Here eq. (53b) shows that the residual strain decays with $|\bar{X}|$ in a power law (i.e., $\sim|\bar{X}|^{-m-1/2}$) and the characteristic distance of decay scales with $1/\beta$.

Finally, for the special case of m = 1/2, the residual strain distribution is elementary (see Section S28 of the SI)

$$\varepsilon_{22}\left(\bar{X}<0, Y=0, m=\frac{1}{2}\right)=\frac{\sigma_D \kappa}{2E_\infty\left[1+\beta\left|\bar{X}\right|\right]^{1/2}}\left[1-\frac{2}{\pi}\tan^{-1}\left(\sqrt{\frac{1+\beta\left|\bar{X}\right|}{\beta}}\right)\right]. \quad (54)$$

The normalized residual strain distribution $E_\infty\varepsilon_{22}/\sigma_D$ is plotted in Fig.10 for different values of β for the case of the SS (N =1) (solid lines)and PLS (m = 1/2) (dash lines) as a comparison. The long and short times moduli for both cases are chosen to be the same.

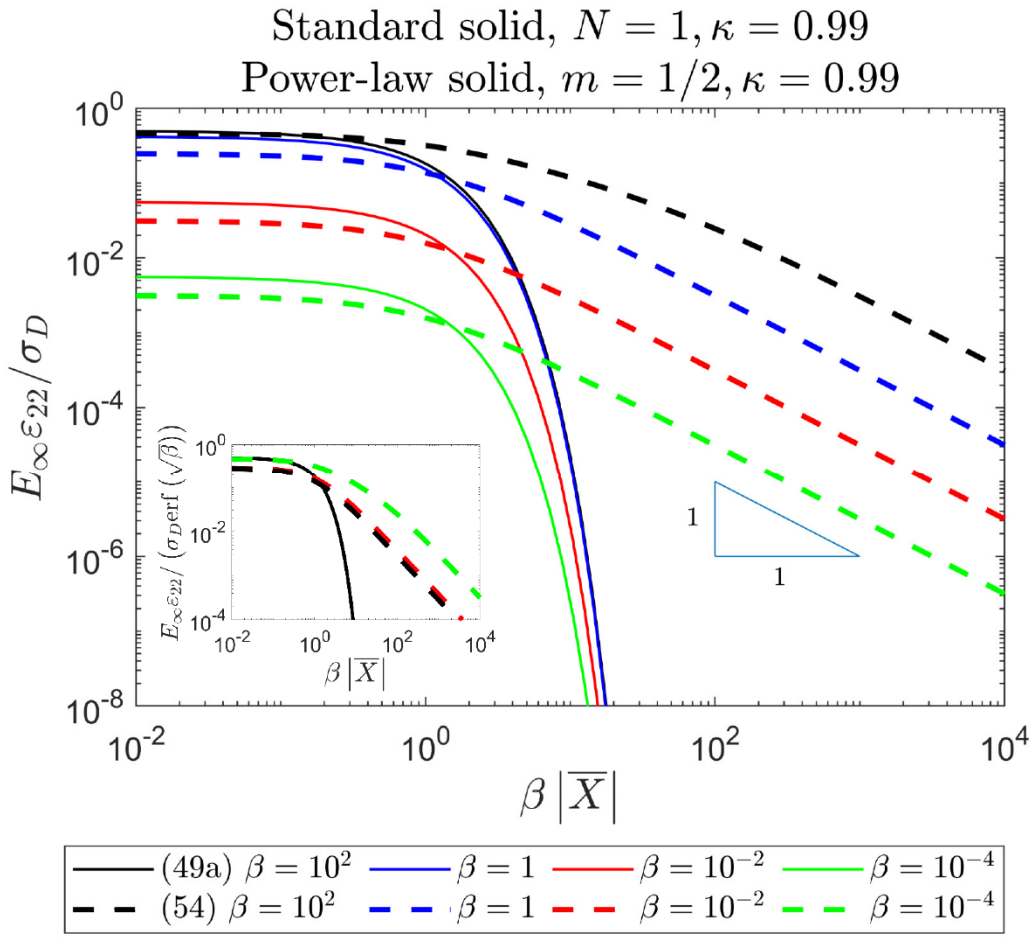

Figure 10 Normalized residual strain distribution $E_\infty \varepsilon_{22} / \sigma_D$ on crack surface ($X < 0$, $Y = 0$) for the SS and the PLS (m = 1/2) for different β. Both materials have the same short and long times modulus and E_∞/E_0 = 0.01. The solid lines represent results for the SS and the dashed lines represent results for the PLS. The inset shows that all SS curves can be collapsed into a single master curve by translating the curves vertically according to $erf\left(\sqrt{\beta}\right)$ (see eq. (49a) with N = 1). For the PLS, the curve cannot be brought exactly into a single master curve.

6. Crack opening displacement

de Gennes [20] was the first to suggest that the dissipation zone can be identified as the "liquid" trumpet region of the Crack Opening Displacement (COD), i.e., the "liquid" trumpet separates the "soft solid" region in the far field ($\overline{X} \to -\infty$) from the "hard solid" region. Here we present the COD for GMS and PLS. Like Section 5, we will only present results based on the exact stress field with the DB cohesive zone in eq. (37a), since solutions of the COD requires the detailed stress distribution in the cohesive zone, which is not available in the approximate stress field in eq.

(37b). To maintain dimensional consistency, we normalize the COD u_{cod} by the critical cohesive separation of the DB model δ_0: $\overline{u}_{cod} \equiv u_{cod} / \delta_0$.

6.1 Solutions for GMS

For the GMS, a useful form of the normalized COD $\overline{u}_{cod}$ is given by (see Section S29 of the SI)

$$\overline{u}_{cod}\left(\overline{X} \le 1\right) = \overline{G}\left[F(\overline{X}) + \kappa \sum_{n=1}^{N} a_n \left[\frac{1-\exp\left(\beta_n \overline{X}\right)}{\beta_n} \right] F'\left(\overline{X}\right) + \kappa \sum_{n=1}^{N} \frac{a_n \exp\left(\beta_n \overline{X}\right)}{4\beta_n} Q\left(\beta_n, \overline{X}\right) \right], \qquad (55a)$$

where $\overline{G} \equiv G / G_0$, $\beta_n \equiv \alpha / vt_n$, $F(\overline{X})$ and $F'(\overline{X})$ are defined in eq. (6b) and (6c), and the function $Q(\beta_n, \overline{X})$ is defined as

$$Q\left(\beta_n, \overline{X}\right) \equiv \int_{\overline{X}}^{1} \frac{e^{-\beta_n \xi} - 1}{\xi \sqrt{1-\xi}} d\xi \,. \qquad (55b)$$

The first term $\overline{u}_{cod}^{\infty} \equiv \overline{G} F(\overline{X})$ in eq. (55a) is the normalized COD of a crack in a purely elastic solid with the relaxed modulus E_∞. The second and third term in eq. (55a) represent the reduction of COD due to viscoelasticity. Unfortunately, we cannot find an expression for $Q(\beta_n, \overline{X})$ in terms of known special functions. As before, we define the relative difference χ_{cod},

$$\chi_{cod}\left(\overline{X} \le 1\right) = \frac{\overline{u}_{cod}^{\infty} - \overline{u}_{cod}}{\overline{u}_{cod}^{\infty}} = \frac{-\kappa \sum_{n=1}^{N} a_n \left[\frac{1-\exp\left(\beta_n \overline{X}\right)}{\beta_n} \right] F'\left(\overline{X}\right) - \kappa \sum_{n=1}^{N} \frac{a_n \exp\left(\beta_n \overline{X}\right)}{4\beta_n} Q\left(\beta_n, \overline{X}\right)}{F\left(\overline{X}\right)} \qquad (56a)$$

to characterize the extent of the viscoelastic trumpet. Note that $0 \le \chi_{cod} \le 1$. When $\beta_N >> 1$ (i.e., low crack velocity), χ_{cod} approaches zero. When $\beta_N << 1$ (i.e., high crack velocity), χ_{cod} approaches κ. Therefore, when χ_{cod} is small in the limit of low crack velocity, the material is fully relaxed, implying that there is no viscoelastic trumpet. The viscoelastic trumpet of de Gennes appears where χ_{cod} is not small. To illustrate this point, Fig.11 plots the COD $\overline{u}_{cod} / \overline{u}_{cod}^{\infty} = 1 - \chi_{cod}$ for SS (N=1) for different values of β. Recall the FDR $\Lambda^K = \overline{G} - 1$ depends only on β, and hence each $\overline{u}_{cod} / \overline{u}_{cod}^{\infty}$ curve corresponds to a different FDR which is also labelled on the curve. Note that since $\overline{u}_{cod}$ is normalized by $\overline{u}_{cod}^{\infty}$, the upper and lower horizontal lines $\overline{u}_{cod} / \overline{u}_{cod}^{\infty} = 1$ and $\overline{u}_{cod} / \overline{u}_{cod}^{\infty} = 1 - \kappa$ in Fig.11 represents the COD in a fully relaxed and a glassy solid respectively. The trumpet region is the curve in between these two horizontal lines. From eq. (6a), (8b) and the definition $\overline{u}_{cod}^{\infty} \equiv \overline{G} F(\overline{X})$, we must have

$$1-\chi_{cod}\left(\bar{X}=0\right)=\frac{\bar{u}_{cod}\left(\bar{X}=0\right)}{\bar{u}_{cod}^{\infty}\left(\bar{X}=0\right)}=1-\Lambda^{K}. \tag{56b}$$

Hence each of the horizontal lines in Fig.11 is associated with a particular value of FDR.

A more quantitative way to estimate the size of the "viscoelastic trumpet" is to find the location where χ_{cod} becomes small. Although eq. (55a) is valid for $\bar{X}\le 1$ (i.e., including the cohesive zone), here we focus on the COD behind the crack tip, i.e., $\bar{X}\le 0$. In Section S30 of the SI, we show that the COD for *large* $\beta_N\left|\bar{X}\right|$, which occurs either $\left|\bar{X}\right|$ is large or β_N is large or both, is given by

$$\bar{u}_{cod}\left(\bar{X}<0,\beta_N\left|\bar{X}\right|>>1\right)\approx\bar{G}\left[F(\bar{X})+\kappa\sum_{n=1}^{N}\frac{a_n}{\beta_n}F'\left(\bar{X}\right)+\kappa\sum_{n=1}^{N}\frac{a_n}{4\beta_n}\frac{-1}{\sqrt{1+\left|\bar{X}\right|}}\left(\frac{1}{\beta_n\left|\bar{X}\right|}+...\right)\right]. \tag{57a}$$

Using the asymptotic behavior of F,F', we have

$$\chi_{cod}\left(\bar{X}<0,\beta_N\left|\bar{X}\right|>>1\right)\approx\frac{\kappa}{2}\sum_{n=1}^{N}\left[\frac{a_n}{\beta_n\left|\bar{X}\right|}\left(1+\frac{1}{2\beta_n\left|\bar{X}\right|}+...\right)\right]. \tag{57b}$$

The implication from eq. (57b) is that χ_{cod} becomes small when $\beta_N\left|\bar{X}\right|$ is large, i.e., when $\left|\bar{X}\right|\sim 1/\beta_n$ or $X\sim vt_c^{ave}$. Hence the size of viscoelastic trumpet is dictated by vt_c^{ave}.

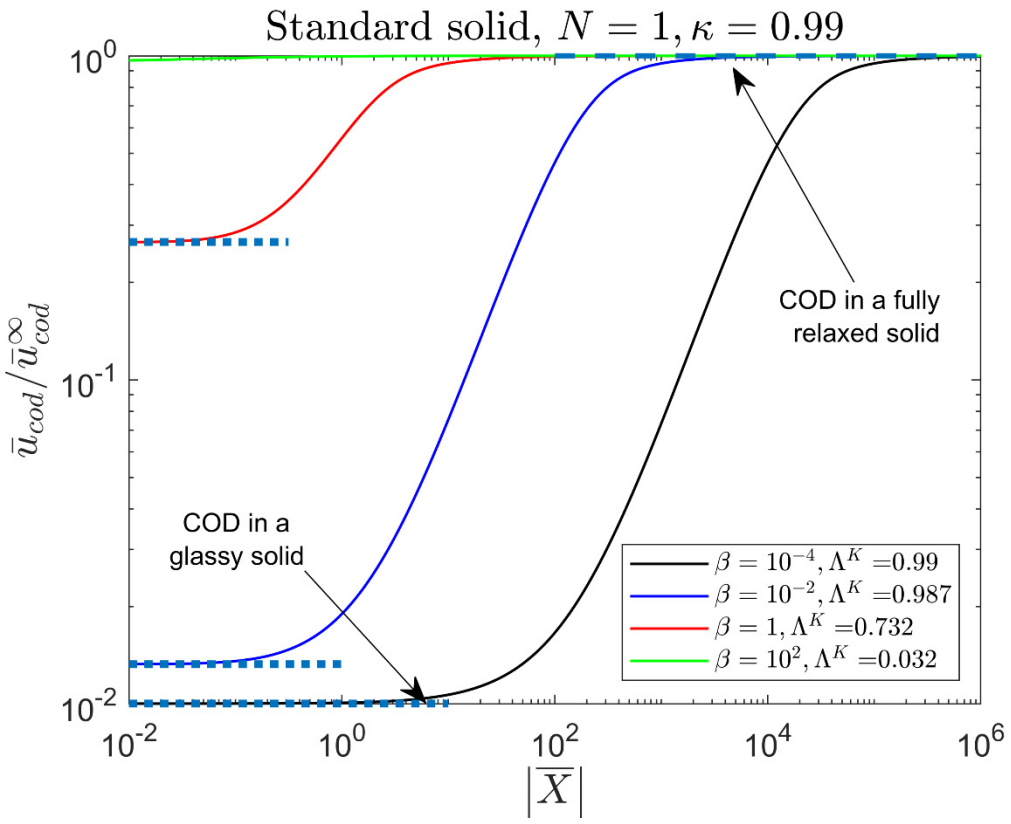

Figure 11 $\bar{u}_{cod} / \bar{u}^{\infty}_{cod} = 1 - \chi_{cod}\left(\bar{X} \le 0\right)$ versus normalized distance $|\bar{X}|$ from crack tip for SS (N=1) with κ= 0.99 and different values of β. The corresponding FDR for each curve is indicated in figure. Note that since $\bar{u}_{cod}$ is normalized by $\bar{u}^{\infty}_{cod} \equiv \bar{G}F(\bar{X})$, the upper and lower horizontal lines $\bar{u}_{cod} / \bar{u}^{\infty}_{cod} = 1$ and $\bar{u}_{cod} / \bar{u}^{\infty}_{cod} = 1 - \kappa = 10^{-2}$ represents the COD in a fully relaxed and a glassy solid respectively. The vertical coordinate of each intermediate horizontal dotted line is $1 - \Lambda^K$ according to eq. (56b).

6.2 Solutions for PLS

The normalized COD for PLS is given by

$$\bar{u}_{cod}\left(\bar{X} < 1\right) = \bar{G}\left[F(\bar{X}) + \kappa \int_{\bar{X}}^{1} \frac{F'(\eta)\, d\eta}{\left[1 + \beta\left(\eta - \bar{X}\right)\right]^m}\right], \tag{58}$$

where $\beta = \alpha/vt_c$. Following similar procedures in Section 6.1, one can evaluate χ_{cod} for PLS similarly to eq. (56a). Although it is possible to find closed-form solution for the COD in the region $\bar{X} \le -1$, the solution is complicated: we have not been able to express the solution in term of known special functions but a power series solution can be obtained (see Section S31 of the SI).

We also obtain asymptotic properties of the solution (also shown in Section S31 of the SI). In particular, for $\bar{X} < 0$ and $\beta\left|\bar{X}\right| >> 1$, we found

$$\bar{u}_{cod}\left(\bar{X}<0,\beta\left|\bar{X}\right|>>1\right)\approx \bar{G}\sqrt{\left|\bar{X}\right|}\left[1-\kappa\left\{\frac{\sqrt{\beta}}{2\left(\beta\left|\bar{X}\right|\right)^{m+1/2}}+\frac{\sqrt{\pi}\Gamma\left(2-m\right)}{2\left(1-m\right)\Gamma\left(3/2-m\right)}\frac{1}{\left(\beta\left|\bar{X}\right|\right)^{m}}\right\}\right]. \quad (59)$$

In the special case of m = 1/2, the integral in eq. (58) can be separated into two integrals and each integral can be evaluated exactly after a lengthy derivation (see Section S32 of SI), i.e.,

$$\int_{\bar{X}}^{1}\frac{F'(\eta)d\eta}{\left[1+\beta\left(\eta-\bar{X}\right)\right]^{1/2}}=\int_{0}^{1}\frac{F'(\eta)d\eta}{\left[1+\beta\left(\eta-\bar{X}\right)\right]^{1/2}}+\int_{\bar{X}}^{0}\frac{F'(\eta)d\eta}{\left[1+\beta\left(\eta-\bar{X}\right)\right]^{1/2}}\ . \quad (60a)$$

The first integral measures the effect of cohesive traction on the COD and is:

$$\int_{0}^{1}\frac{F'(\eta)d\eta}{\left[1+\beta\left(\eta-\bar{X}\right)\right]^{1/2}}=\frac{\sqrt{b}}{2\beta}\ln\left(\frac{b+\beta}{b}\right)-\frac{1}{\sqrt{\beta}}\sin^{-1}\left(\frac{\sqrt{\beta}}{\sqrt{b+\beta}}\right). \quad (60b)$$

The second integral measures the effect of far field traction on the COD:

$$\int_{\bar{X}}^{0}\frac{F'(\eta)d\eta}{\left[1+\beta\left(\eta-\bar{X}\right)\right]^{1/2}}=-\frac{\left(\sqrt{b}-1\right)}{2\beta}\ln\left|\frac{\sqrt{1+\left|\bar{X}\right|}+1}{\sqrt{1+\left|\bar{X}\right|}-1}\right|+\frac{\sqrt{b}}{2\beta}\ln\left[\frac{b+\beta\left(1+\sqrt{1+\left|\bar{X}\right|}\right)+\sqrt{b}}{b-\beta\left(\sqrt{1+\left|\bar{X}\right|}-1\right)+\sqrt{b}}\frac{b}{\left(b+\beta\right)}\right] \quad (60c)$$
$$-\frac{1}{\sqrt{\beta}}\left[\sin^{-1}\left(\frac{\sqrt{b+\beta-1}}{\sqrt{\beta+b}}\right)-\sin^{-1}\left(\frac{\sqrt{\beta}}{\sqrt{\beta+b}}\right)\right]$$

In both eq. (60b) and (60c), b is defined as,

$$b=1+\beta\left|\bar{X}\right| \quad (60d)$$

The COD for PLS with m = 1/2 is obtained using eq. (58) with the integral determined by adding eq. (60b) and (60c). This solution is plotted in Fig.12 to facilitate the comparison with that of SS (see Fig.11) for different values of β.

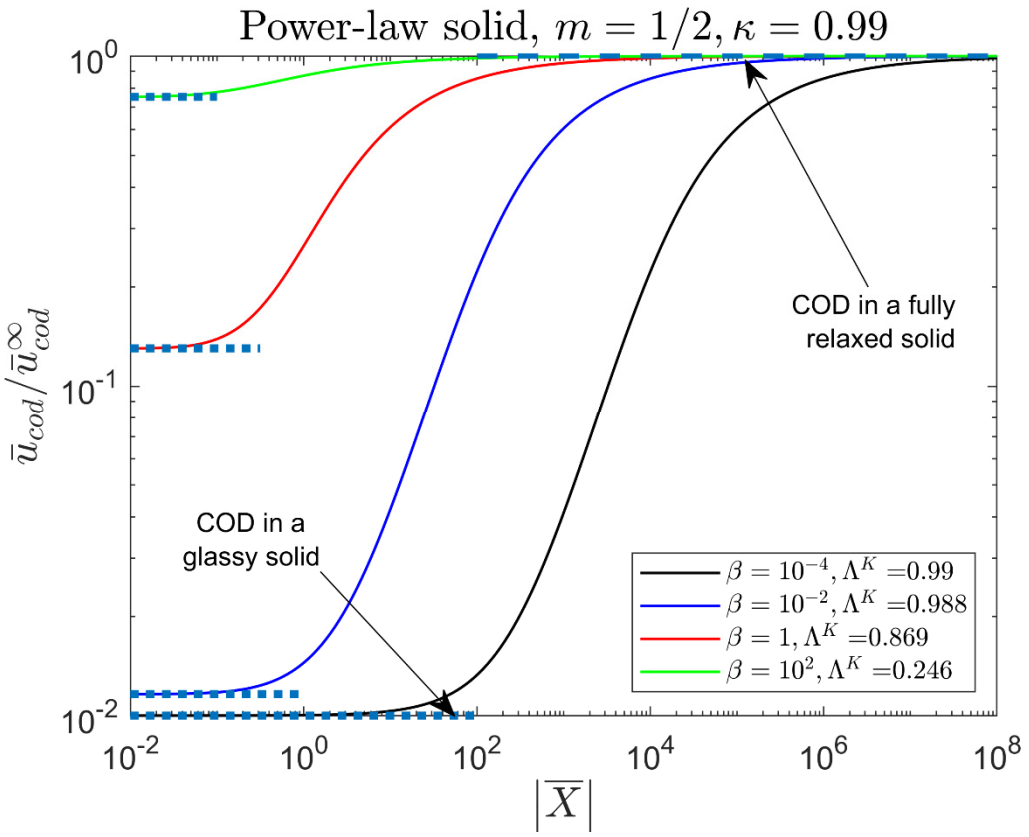

Figure 12 $\bar{u}_{cod}/\bar{u}^{\infty}_{cod}$ versus normalized distance $|\bar{X}|$ from crack tip for a PLS (m = 1/2 and κ = 0.99) and different values of β. The FDR for each curve is indicated in figure. Note that since $\bar{u}_{cod}$ is normalized by $\bar{u}^{\infty}_{cod} \equiv \bar{G}F(\bar{X})$, the upper and lower horizontal lines $\bar{u}_{cod}/\bar{u}^{\infty}_{cod} = 1$ and $\bar{u}_{cod}/\bar{u}^{\infty}_{cod} = 1-\kappa = 10^{-2}$ represents the COD in a fully relaxed and a glassy solid respectively. The vertical coordinate of each intermediate horizontal dotted line is $1-\Lambda^K$.

7. Dissipation Zone

As discussed in the introduction section, existing theories in the literature focus only on the total viscoelastic dissipation as manifested in the FDR Λ, but little is known about how dissipation is distributed around the crack tip. This is attributed to the lack of a thermodynamically based way to define energy dissipation in linear viscoelasticity. Specifically, one can define the following dissipation density per unit length of crack extension at any point within the moving coordinate system (X, Y), referred to as the local dissipation rate:

$$\Phi_D \equiv \left[\sigma_{ij}\dot{\varepsilon}_{ij} - \dot{W}_e\right]/v\,, \tag{61}$$

where $\sigma_{ij}\dot{\varepsilon}_{ij}$ is the stress power at a material point and $\dot{W}_e$ is the elastic stress power (or the time rate of change in the stored elastic energy per unit volume). However, for an arbitrary linear

viscoelastic model, in which a creep compliance function or relaxation function is prescribed, $\dot{W}_e$ is not always well defined. Certain physical assumptions are needed to define $\dot{W}_e$ and hence the local dissipation. Here we refer to a method suggested by Holzapfel [46] (see Page 286-288) to evaluate $\dot{W}_e$, which is based on the rheological representation of GMS. A GMS can be represented by parallel elements consisting of an elastic spring and a set of Maxwell elements. This physical model allows us to define $\dot{W}_e$ as time rate of change in the total elastic energies stored in the springs. Alternatively, one can also evaluate Φ_D by computing the power of energy dissipated by the dashpots. Since the calculations are quite tedious for a general GMS, we consider only the SS (N =1) and give details in Section S32 of SI.

Equipped with the definition of local dissipation for SS, we can now quantitatively discuss the dissipation zone around the crack tip. This can be achieved by evaluating Φ_D and plotting its contour, knowing that the areal integral of Φ_D over the entire plane is equal to the $G_D = G - G_0$. However, this approach can only be implemented numerically. To gain insights, we will first evaluate Φ_D directly ahead of the cohesive zone tip in Section 4.1 and discuss its physical implications, and then plot the 2D contours of Φ_D in Section 4.2.

7.1 Dissipation rate ahead of the cohesive zone tip

In this section, we evaluate the local dissipation rate Φ_D for any material point directly ahead of the cohesive zone tip. We first base our calculation on the crack tip stress fields in Knauss's theory with the DB cohesive zone and show that for SS (see Section S33 of SI)

$$\Phi_D\left(\bar{X}\geq 1, Y=0\right)=\frac{\kappa}{E_\infty v t_c}\left[\frac{\sigma_D}{\pi}\exp\left(\beta\bar{X}\right)\Psi\left(\bar{X},\beta\right)\right]^2, \tag{62}$$

where $\beta = \alpha/vt_c$ and the function $\Psi(\bar{X},\beta)$ is defined by eq. (38b). Physically, $E_\infty t_c/\kappa$ represents the effective viscosity for material points on the crack line and the term inside the square bracket is the stress acting on the dashpot. For large $\bar{X}$, the local dissipation rate Φ_D in eq. (62) is obtained from the asymptotic behavior of $\Psi(\bar{X},\beta)$ (see Section S17 of the SI):

$$\Phi_D\left(\bar{X}>>1,\beta,Y=0\right)\approx\frac{\kappa}{E_\infty v t_c}\left(\frac{\sigma_D}{\pi}\right)^2\frac{1}{\beta^2\bar{X}^3} \tag{63}$$

A simpler expression for the local dissipation rate directly ahead of the crack tip can be obtained if we use the *K*-field based approximate stress distribution in eq. (37b). In this case, the local dissipation rate can be expressed in closed form (see Section S33 of SI):

$$\Phi_D^*\left(\bar{X}\geq 1, Y=0\right)=\frac{\kappa}{E_\infty v t_c}\left[\frac{\sigma_D}{\sqrt{\bar{X}}}\left\{1-\sqrt{\pi\bar{X}\beta}\exp\left(\beta\bar{X}\right)erfc\left(\sqrt{\beta\bar{X}}\right)\right\}\right]^2, \tag{64}$$

where $\beta = \alpha/vt_c$ and we have added an asterisk superscript to Φ_D to distinguish it from that in eq. (62). The asymptotic behavior of eq. (64) for $\bar{X} >> 1$ is shown below

$$\Phi_D^*\left(\beta\bar{X}>>1, Y=0\right)\approx\frac{\kappa}{E_\infty v t_c}\left(\frac{\sigma_D}{2}\right)^2\frac{1}{\beta^2\bar{X}^3}, \tag{65}$$

which is the same as eq. (63) if a constant numerical factor $(2/\pi)^2$ is multiplied to the RHS of eq. (65). The factor $2/\pi$ is due to the difference in the far field stress prescribed by eq. (37a) and (37b), as discussed in Section 4.1. However, eq. (62) and (64) differ considerably near the cohesive zone tip. This can be seen by comparing them at the cohesive zone tip where $\bar{X}=1$. For this case,

$$\Phi_D\left(\bar{X}=1, Y=0\right)=\frac{\kappa\sigma_D^2}{E_\infty v t_c}\left[\exp\left(\beta\right)erfc\left(\sqrt{\beta}\right)\right]^2 \tag{66a}$$

whereas

$$\Phi_D^*\left(\bar{X}=1, Y=0\right)=\frac{\kappa\sigma_D^2}{E_\infty v t_c}\left[1-\sqrt{\pi\beta}\exp\left(\beta\right)erfc\left(\sqrt{\beta}\right)\right]^2. \tag{66b}$$

In the limit of high crack velocity where $\beta \to 0$, using the asymptotic behavior of the complementary error function, we obtain

$$\Phi_D\left(\bar{X}=1, Y=0\right)\approx\frac{\kappa\sigma_D^2}{E_\infty v t_c}\left(1-\frac{4\sqrt{\beta}}{\sqrt{\pi}}\right)\text{ and }\Phi_D^*\left(\bar{X}=1, Y=0\right)\approx\frac{\kappa\sigma_D^2}{E_\infty v t_c}\left(1-2\sqrt{\pi\beta}\right). \tag{66c}$$

The maximum dissipation rates at the cohesive zone tip agree in the limit of high crack velocities and exhibit similar first order asymptotic behavior. However, in the limit of low velocities (i.e., $\beta \to +\infty$), we obtain

$$\Phi_D\left(\bar{X}=1, Y=0\right)\approx\frac{\kappa\sigma_D^2}{E_\infty v t_c}\left(\frac{1}{\pi\beta}\right)\quad\text{and }\Phi_D^*\left(\bar{X}=1, Y=0\right)\approx\frac{\kappa\sigma_D^2}{E_\infty v t_c}\left(\frac{1}{2\beta}\right)^2. \tag{66d}$$

which implies that the maximum dissipation rate at the cohesive zone tip predicted by eq. (66a) vanishes much *slower* than that in eq. (66b). This result again illustrates the fact that interaction effect becomes important for slow crack growth. Hence, a non-interacting model such as the PB's theory tends to overestimate the dissipation rate.

Motivated by eq. (62), we define a normalized local dissipation rate $\bar{\Phi}_D$ as

$$\bar{\Phi}_D \equiv \Phi_D \Big/ \left(\frac{\kappa \sigma_D^2}{E_\infty v t_c} \right). \tag{67}$$

From eq. (63) and (65), we expect that a log-log plot of $\bar{\Phi}_D$ versus $\beta^{2/3}\bar{X}$ should have a slope of -3 for sufficiently large values of $\beta^{2/3}\bar{X}$. Figure 13 shows that this is indeed the case. As predicted by eq. (66c) and (66d), maximum deviation between the two theories occurs when $\bar{X}=1$ and $\beta >> 1$ (i.e., at the tip of cohesive zone under low crack velocity).

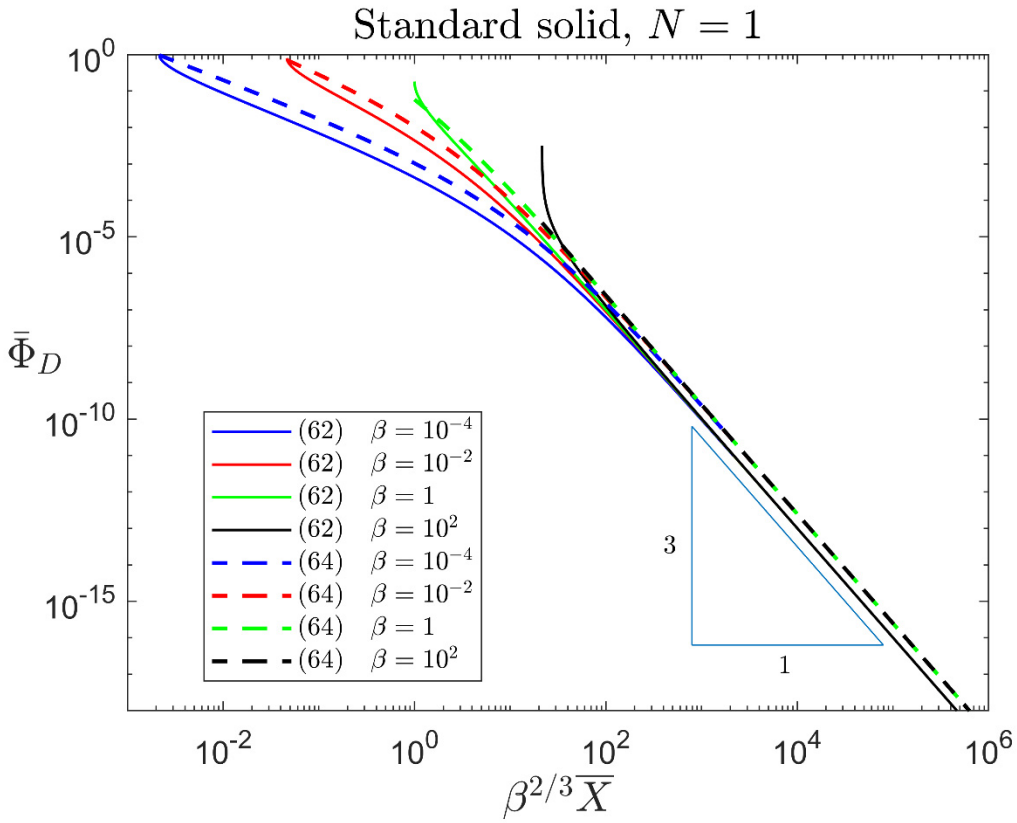

Figure 13 Normalized local dissipation rate $\bar{\Phi}_D$ defined in eq. (67) versus $\beta^{2/3}\bar{X}$ for a standard solid with $\kappa = 0.99$.

Equation (65) also allows us to gain insight in the scaling analysis of Saulnier et al. [21]. Note that the asymptotic behavior in eq. (65) also applies to $\bar{X} > 0$ and $\beta >> 1$ (i.e., low crack velocity). From a scaling perspective, we extend eq. (65) and assume the local dissipation rate *everywhere* has the form in the limit of low crack velocity ($\beta >> 1$)*:*

$$\Phi_D^*\left(\bar{R},\theta\right) \approx \frac{\kappa}{E_\infty v t_c}\left(\frac{\sigma_D}{2}\right)^2 \frac{1}{\beta^2 \bar{R}^3}\varphi_D(\theta), \quad \bar{R} \equiv \frac{R}{\alpha} \geq 1. \tag{68a}$$

The total dissipation rate is given by the areal integral of $\Phi_D^*(\bar{R},\theta)$:

$$G_D = \frac{\kappa}{E_\infty v t_c}\left(\frac{\sigma_D}{2}\right)^2 \frac{\alpha^3}{\beta^2}\int_{-\pi}^{\pi}\varphi_D(\theta)\,d\theta\int_{\alpha}^{\infty}\frac{1}{R^3}RdR = \frac{\kappa c_D}{4E_\infty v t_c}\frac{\sigma_D^2\alpha^2}{\beta^2} = \frac{\kappa c_D}{4E_\infty}\sigma_D^2 v t_c\,. \tag{68b}$$

where $c_D = \int_{-\pi}^{\pi}\varphi_D(\theta)\,d\theta$ is assumed to be a numerical constant of order 1. Using eq. (37b), we replace σ_D by $K_I/\sqrt{2\pi\alpha}$ and obtain

$$G_D = \kappa\frac{c_D}{8\pi}\frac{K_I^2}{E_\infty}\frac{v t_c}{\alpha} \sim \frac{K_I^2}{E_\infty}\frac{v t_c}{\alpha}\,, \tag{68c}$$

showing that G_D is proportional to the crack velocity v, as noted by Saulnier et al. [21]. It should be noted that the analysis above is based on eq. (65) for the non-interacting model. Indeed, it can be shown that eq. (68c) agrees with eq. (30b) in Section 3.1 for PB's theory within a constant prefactor. For the interacting model, however, since eq. (63) does not apply to the limit of $\beta >> 1$ near $\bar{X} = 1$, the scaling behavior between G_D and v under low crack velocity is not exactly linear, as confirmed eq. (28a) in Section 3.1 for Knauss's theory.

7.2 Areal distribution of local dissipation rate

To gain further insights towards the shape and size of the viscoelastic dissipation zone, we carry out a 2D analysis of the dissipation zone. This analysis is based on the exact stress field around the crack tip with a DB cohesive zone model (see Section S34 of the SI), which is valid for steady state crack growth in viscoelastic solid due to the correspondence principle. Using eq. (61) and the rheological representation of SS, we are able to calculate the local dissipation rate over the entire plane. The shape of dissipation zone can be evaluated by plotting the contours of $\bar{\Phi}_D$. An example is shown in Fig.14 for $\beta = 0.001$ and $\kappa = 0.99$.

Since $\bar{\Phi}_D$ does not vanish exactly until one moves infinitely far away from the crack tip, strictly speaking dissipation occurs everywhere. However, one can define the dissipation zone as the region within which the integral of Φ_D can account for most of the total dissipation rate G_D. To demonstrate this point, we consider a series of concentric squares centered at the crack tip but with different sizes. The side length of each square, denoted as L, is normalized by the cohesive zone length α, i.e., $\bar{L} \equiv L/\alpha$. We integrate the local dissipation rate within each square and define ρ as the ratio between the contribution from each square region and the total dissipation per unit crack extension, G_D (see Fig.14). The numerical results for ρ versus L for different β are given in Fig.15. In particular, Fig.15A illustrates the method we used to calculate the energy dissipated within the square of side length $\bar{L}$. We divided the whole domain into progressively larger square regions surrounding the crack tip, i.e., Region $(i-1) \subset$ Region (i). Then we use a set of square grids to partition each region (see grid in Region i for example). The local dissipation rate is calculated on each black point. We multiple the local dissipation rate evaluated at these points by

the area of each little square, the red one for example. The energy dissipated within each region is the sum of these energies. Verification of our areal integral scheme is shown in Section S34 of the SI. We keep increasing the size or number of regions until the sum of dissipated energy reaches a constant value which is the normalized total energy dissipation rate, as shown in Fig.15B. Since the cohesive zone size α is proportional to $\bar{G}$ ($\equiv G/G_0$) and hence varies with β, in Fig.15B we renormalize L by the minimum cohesive zone size d ($\equiv \alpha/\bar{G}$) which is a constant. As β is decreased from 10^5 to 10^{-5} (i.e., increasing crack velocity), the L required for the saturation of ρ increases from ~ $10d$ to $10^8 d$, indicating a substantial expansion of the dissipation zone size.

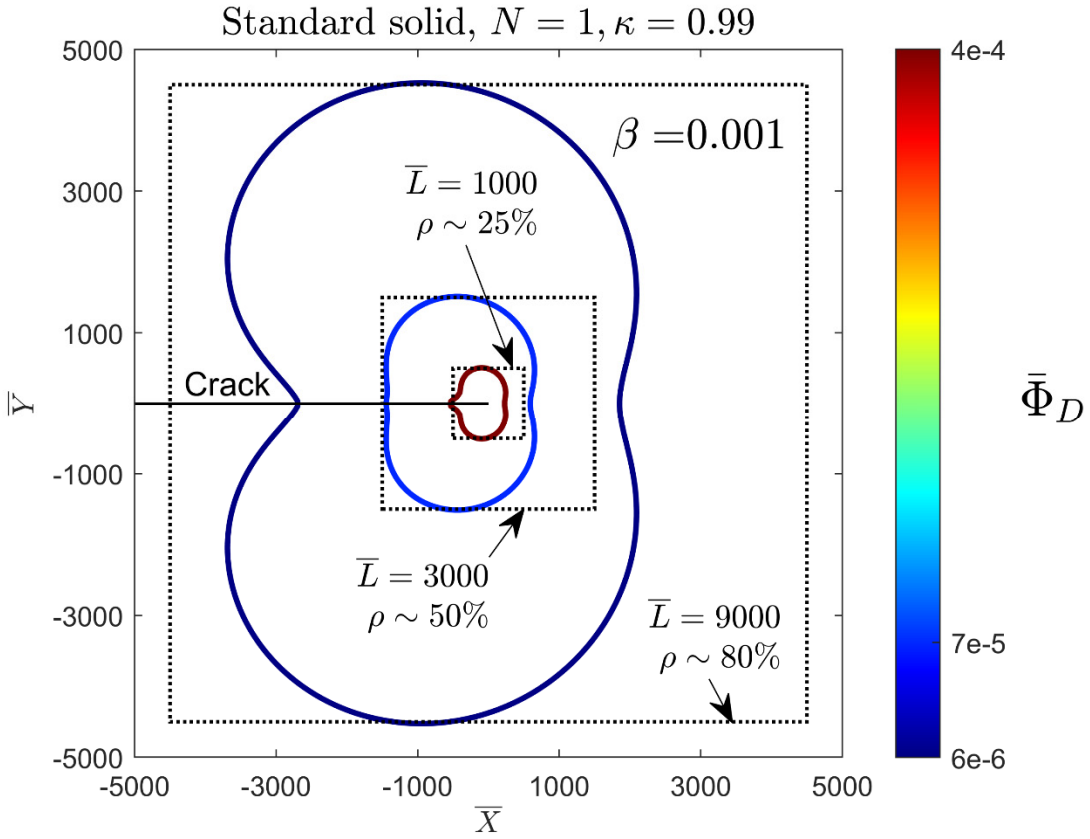

Figure 14 Contour of the local dissipation rate. The solid colored lines represent contour of normalized local dissipative rate. $\bar{L}$ is the side length of the concentric squares centered at the crack tip (normalized by α) and ρ is the ratio between the areal integral of Φ_D within the square region and the total dissipation per unit crack extension, G_D.

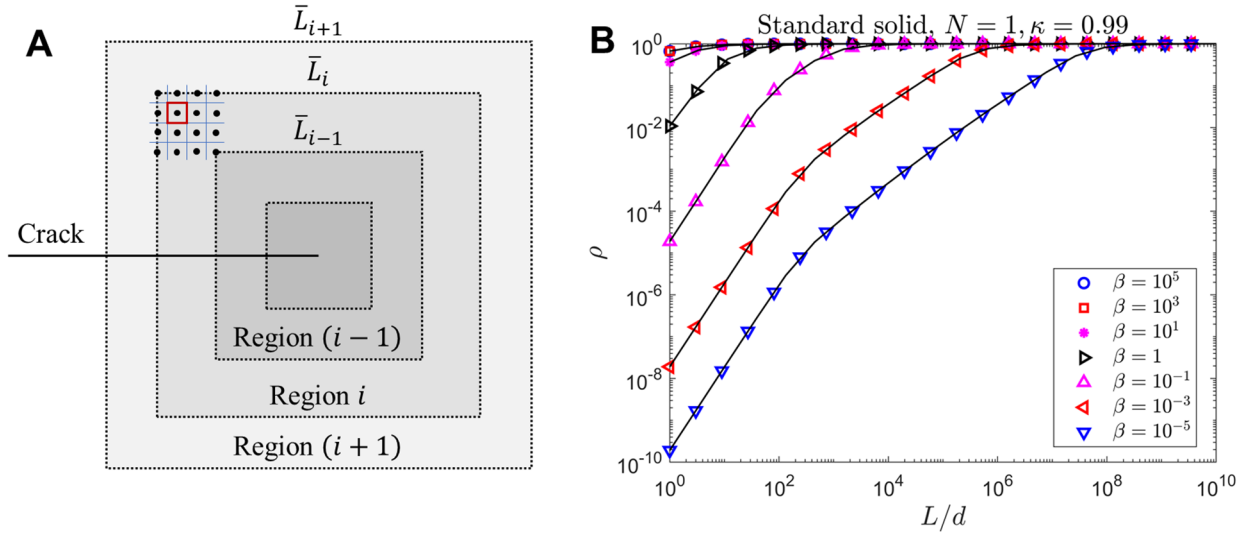

Figure 15 Size of the dissipation zone defined by relative contribution to the total dissipation rate.

8. Discussion and Conclusions

In this work, we present a quantiative comparative study on the theories for steady-state crack growth in viscoelastic solids assuming the SSC condition (i.e., infinite domain and dominance of *K*-field) and the DB cohesive zone model. Our analysis reveals that there are no significant differences between the theories of Knauss, Schapery, and PB *provided that the size of cohesive zone is regarded as a fitting parameter to experimental data*. The main difference in these theories arises from the different way of estimating the size of the fracture zone α. This results in different estimates for d, which is used to fit experimental data. The fact is that this length is controlled by the parameters in the cohesive or fracture model (e.g. the cohesive stress σ_D) and different models give different answers (up to numerical constants). This conclusion is consistent with the findings in recent works [47,48] that compared PB's theory to Schapery's theory (extended by Greenwood [49]). In addition, these models have limitations. For example, there is no particular reason why fracture process has to be concentrated on a line zone. Indeed, a recent experimental work [50] has used mechanophores to demonstrate that bond scission in elastomers are not restricted to the crack plane but can occur in a delocalized manner. Given the simplicity of Schapery's theory, we advocate its usage (see eq. (35d)). However, it must be noted that Schapery's theory is developed for realistic material behavior so it does not work well for highly idealized solids such as the SS, especially at slow crack growth velocities.

Our analysis did reveal that there are small differences in the prediction at low velocities between Knauss's and PB's theories. In this regime, the relation between fracture energy and crack velocity is sensitive to the interaction between the fracture process and continuum fields. Such interaction is accounted for in interactive theories such as Knauss, but not in non-interactive theories such as PB. This difference leads to different scaling behaviors of FDR, strain distribution and local dissipation rate in the regime of slow crack velocity. Although the interactive theory can account for the exact stress field near the cohesve zone (e.g., Knauss), its solution for the slow

crack velocity limit may depend on the detailed form of the cohesive zone. Since it is difficult to directly measure the cohesive zone parameters, predictive solution (e.g., FDR and dissipation zone) for the slow crack velocity regime remains an open question. The challenge of capturing the slow crack velocity regime is manifested in Fig.6 and 7, where the deviation between experimental data and theories appears mostly in the slow crack velocity regime.

We have obtained closed-form expressions for the residual strain directly behind the crack tip as well as the normal strain directly ahead of the cohesive zone tip using Knauss model. We also obtained closed-form expressions for the crack opening displacement and use these expressions to quantify the size of the "liquid" trumpet in de Gennes's theory. The scaling analysis of Saulnier et al. [21] shows that a significant amount of energy can be dissipated before the a full trumpet is established. Our analysis verified this result. This result reveals a weakness of de Gennes's argument, that dissipation is associated with the viscous trumpet. Indeed, if a significant energy dissipation occurs *before* the establishment of a full trumpet, there is no direct correspondence between crack opening profile and dissipation. Intuitively, one may argue that since the stress tensor on the crack surface is exactly zero, the work rate on material points there is also zero, hence dissipation must occur elsewhere other than the crack surface. Since deformation of the crack surface can be affected by stresses far away from the surface, it is far from certain that there is a direct link between dissipation and the deformed crack profile.

A key point discussed in this work is the size of dissipation zone. de Gennes suggested that the size of dissipation scales with $E_0 v t_R / E_\infty$ [20]. An estimate for $v t_R$ can be obtained using the data from Gent and Lai [23]. Their Figure 13 shows that G increases from G_0 to its high velocity limit as crack velocity v increases from 10^{-20} m/s to 10^{-2} m/s. If we estimate the characteristic relaxation time using the frequency ω_R corresponding to the peak of the $\tan\delta$ curve in their Figure 17, we obtain $t_R = 2\pi/\omega_R \approx 2\pi/10^{-2}$ s^{-1}. *Hence, in their experiments, $v t_R$ varies from 10^{-17} m to 10 m, and $E_0 v t_R / E_\infty$ is sub-angstroms at low crack velocities.*, We also confirmed, by fitting theory to experimental data, that the size of the cohesive/fracture zone is very small (between 1 angstrom and 1 nm), so neither of these length scales can realistically represent the size of the dissipation zone (the lower bound is the length of a polymer chain between cross-links as established by Lake and Thomas [51]). By computing the local dissipation rate, we have been able to determine the shape and size of dissipation zone based on a criterion of relative contribution to the total dissipation. Our result shows that the dissipation zone size is about 10 times the minimum cohesive zone size d (i.e., $10d \sim 10$ nm if $d \sim 1$ nm) in the limit of slow crack velocity. However, the size of the dissipation zone increases with crack velocity and can be as large as $10^8 d$ at large crack velocities as shown in Fig.15B. It should be noted that this result is for a SS solid, and quantitative result could be different for more realistic viscoelastic behavior. More complex viscoelastic behavior will be considered in a future work.

Finally, we emphasize that this work focuses on steady-state crack propagation in an infinite viscoelastic domain. While de Gennes [20] and Saulnier et al. [21] suggested that effect of finite specimen size would result in a critical velocity beyond which the fracture energy decreases with crack velocity, different opinion has been raised [47]. Although the finite size effect is not the focus of this work, we note two points regarding the implications of our analyses. First, the underlying physics of finite size effect is essentially how the viscoelastic dissipation zone interacts

with the boundary condition. To this end, it is critical to have a well-defined method to compute energy dissipation, which would enable clear identification of the viscoelastic dissipation zone. Second, the assumption of steady state crack propagation should be examined with caution in case of finite-sized specimen. In principle, the method to define dissipation rate, as presented in Section 7, can be extended to finite-sized geometry or even non-steady state crack propagation. Combining such definition with computational methods (e.g., finite element analysis) or experimental methods (e.g., imaging-based strain field mapping) may lead to a more precise understanding on the finite size effect.

Acknowledgement: C.Y. Hui is supported by the National Science Foundation, under Grant No. CMMI-1903308. R. Long is supported by a National Science Foundation CAREER award (NSF CMMI-1752449).

References

[1] Knauss WG. A review of fracture in viscoelastic materials. Int J Fract 2015;196:99–146. doi:10.1007/s10704-015-0058-6.

[2] Williams ML. Initiation and Growth of Viscoelastic Fracture. Int J Fract Mech 1965;1:292–310. doi:10.1007/bf03545561.

[3] Mueller HK, Knauss WG. Crack propagation in a linearly viscoelastic strip. J Appl Mech Trans ASME 1971;38:483–8. doi:10.1115/1.3408801.

[4] Kostrov B V, Nikitin L V. Some general problems of mechanics of brittle fracture. Arch Mech Stosow 1970;22:749–75.

[5] Willis JR. Crack propagation in viscoelastic media. J Mech Phys Solids 1967;15:229–40. doi:10.1016/0022-5096(67)90013-0.

[6] Dugdale DS. Yielding of steel sheets containing slits. J Mech Phys Solids 1960;8:100–4. doi:10.1016/0022-5096(60)90013-2.

[7] Barenblatt GI. The Mathematical Theory of Equilibrium Cracks in Brittle Fracture. Adv Appl Mech 1962;7:55–129. doi:10.1016/S0065-2156(08)70121-2.

[8] Knauss WG. On the steady propagation of a crack in a viscoelastic sheet: experiments and analysis. In: Kausch HH, Hassell JA, Jaffee RI, editors. Deform. Fract. High Polym., Springer US; 1973, p. 501–41. doi:10.1007/978-1-4757-1263-6_27.

[9] Schapery RA. A theory of crack initiation and growth in viscoelastic media - I. Theoretical development. Int J Fract 1975;11:141–59. doi:10.1007/BF00034721.

[10] Schapery RA. A theory of crack initiation and growth in viscoelastic media II. Approximate methods of analysis. Int J Fract 1975;11:369–88. doi:10.1007/BF00033526.

[11] Schapery RA. A theory of crack initiation and growth in viscoelastic media - III. Analysis of continuous growth. Int J Fract 1975;11:549–62. doi:10.1007/BF00116363.

[12] Graham GAC. The correspondence principle of linear viscoelasticity theory for mixed boundary value problems involving time-dependent boundary regions. Q Appl Math 1968;26:167–74. doi:10.1090/qam/99860.

[13] Rice JR. The mechanics of quasi-static crack growth. In: Kelly RE, editor. Proceedins 8th U.S. Natl. Congr. Appl. Mech., Western Periodicals CO.; 1978, p. 191–126.

[14] Christensen RM. A rate-dependent criterion for crack growth. Int J Fract 1979;15:3–21. doi:10.1007/BF00115904.

[15] McCartney LN. Discussion: “A rate-dependent criterion for crack growth,” by R. M. christensen. Int J Fract 1980;16:3–5. doi:10.1007/BF00016587.

[16] Christensen RM. Response: Discussion of "A rate-dependent criterion for crack growth," by L. N. McCartney. Int J Fract 1980;16:R233–7. doi:10.1007/BF00016588.
[17] McCartney LN. Response to discussion concerning kinetic criteria for crack in viscoelastic materials. Int J Fract 1981;17:R161–R161. doi:10.1007/BF00681562.
[18] Christensen RM. Viscoelastic crack growth - A response note. Int J Fract 1981;17:R169–76. doi:10.1007/BF00681563.
[19] Christensen RM, McCartney LN. Viscoelastic crack growth. Int J Fract 1983;23:11–3. doi:10.1007/BF00020162.
[20] de Gennes PG. Soft Adhesives †. Langmuir 1996;12:4497–500. doi:10.1021/la950886y.
[21] Saulnier F, Ondarçuhu T, Aradian A, Raphaël E. Adhesion between a viscoelastic material and a solid surface. Macromolecules 2004;37:1067–75. doi:10.1021/ma021759t.
[22] Persson BNJ, Brener EA. Crack propagation in viscoelastic solids. Phys Rev E - Stat Nonlinear, Soft Matter Phys 2005;71:036123. doi:10.1103/PhysRevE.71.036123.
[23] Gent AN, Lai S-M. Interfacial bonding, energy dissipation, and adhesion. J Polym Sci Part B Polym Phys 1994;32:1543–55. doi:10.1002/polb.1994.090320826.
[24] Gent AN. Adhesion and strength of viscoelastic solids. Is there a relationship between adhesion and bulk properties? Langmuir 1996;12:4492–5. doi:10.1021/la950887q.
[25] Abramowitz M, Stegun IA. Handbook of mathematical functions with formulas, graphs, and mathematical tables. vol. 55. US Government printing office; 1964.
[26] Zehnder AT. Fracture Mechanics. Springer; 2012.
[27] Long R, Hui CY. Crack tip fields in soft elastic solids subjected to large quasi-static deformation - A review. Extrem Mech Lett 2015;4:131–55. doi:10.1016/j.eml.2015.06.002.
[28] Ferry JD. Viscoelastic properties of polymers. third. John Wiley & Sons; 1980.
[29] Christensen R. Theory of viscoelasticity: an introduction. second. Elsevier; 1982.
[30] Bagley RL. Power law and fractional calculus model of viscoelasticity. AIAA J 1989;27:1412–7. doi:10.2514/3.10279.
[31] Bonfanti A, Kaplan JL, Charras G, Kabla A. Fractional viscoelastic models for power-law materials. Soft Matter 2020;16:6002–20. doi:10.1039/d0sm00354a.
[32] Loy RJ, de Hoog FR, Anderssen RS. Interconversion of Prony series for relaxation and creep. J Rheol (N Y N Y) 2015;59:1261–70. doi:10.1122/1.4929398.
[33] Williams ML. Structural analysis of viscoelastic materials. AIAA J 1964;2:785–808. doi:10.2514/3.2447.
[34] Gradshteyn IS, Ryzhik IM. Table of integrals, series, and products. Academic Press; 1965.
[35] Erdelyi A, Magnus W, Oberhettinger F, Tricomi FG. Tables of Integral Transforms, Bateman Manuscript Project Volume II. McGraw-Hill New York; 1954.
[36] MacKinnon RF. The Asymptotic Expansions of Hankel Transforms and Related Integrals. Math Comput 1972;26:515. doi:10.2307/2005179.
[37] Livne A, Bouchbinder E, Svetlizky I, Fineberg J. The Near-Tip Fields of Fast Cracks. Science (80-) 2010;327:1359–63. doi:10.1126/science.1180476.
[38] Mzabi S, Berghezan D, Roux S, Hild F, Creton C. A critical local energy release rate criterion for fatigue fracture of elastomers. J Polym Sci Part B Polym Phys 2011;49:1518–24. doi:10.1002/polb.22338.
[39] Zhang T, Lin S, Yuk H, Zhao X. Predicting fracture energies and crack-tip fields of soft tough materials. Extrem Mech Lett 2015;4:1–8. doi:10.1016/j.eml.2015.07.007.
[40] Liu M, Guo J, Hui CY, Zehnder A. Crack tip stress based kinetic fracture model of a PVA dual-crosslink hydrogel. Extrem Mech Lett 2019;29:100457.

doi:10.1016/j.eml.2019.100457.
[41] Mai TT, Okuno K, Tsunoda K, Urayama K. Crack-Tip Strain Field in Supershear Crack of Elastomers. ACS Macro Lett 2020;9:762–8. doi:10.1021/acsmacrolett.0c00213.
[42] Mai TT, Okuno K, Tsunoda K, Urayama K. Anisotropic stress-softening effect on fast dynamic crack in filler-reinforced elastomers. Mech Mater 2021;155:103786. doi:10.1016/j.mechmat.2021.103786.
[43] Corre T, Coret M, Verron E, Leblé B, Le Lay F. Experimental full field analysis for dynamic fracture of elastomer membranes. Int J Fract 2020;224:83–100. doi:10.1007/s10704-020-00447-1.
[44] Qi Y, Zou Z, Xiao J, Long R. Mapping the nonlinear crack tip deformation field in soft elastomer with a particle tracking method. J Mech Phys Solids 2019;125:326–46. doi:10.1016/j.jmps.2018.12.018.
[45] Luo F, Sun TL, Nakajima T, Kurokawa T, Zhao Y, Ihsan A Bin, et al. Crack Blunting and Advancing Behaviors of Tough and Self-healing Polyampholyte Hydrogel. Macromolecules 2014;47:6037–46. doi:10.1021/ma5009447.
[46] Holzapfel GA. Nonlinear solid mechanics : a continuum approach for engineering. Wiley; 2000.
[47] Persson BNJ. On Opening Crack Propagation in Viscoelastic Solids. Tribol Lett 2021;69:1–8. doi:10.1007/S11249-021-01494-Y/FIGURES/6.
[48] Ciavarella M, Cricri G, McMeeking R. A comparison of crack propagation theories in viscoelastic materials. Theor Appl Fract Mech 2021;116:103113. doi:10.1016/J.TAFMEC.2021.103113.
[49] Greenwood JA. The theory of viscoelastic crack propagation and healing. J Phys D Appl Phys 2004;37:2557–69. doi:10.1088/0022-3727/37/18/011.
[50] Slootman J, Waltz V, Yeh CJ, Baumann C, Göstl R, Comtet J, et al. Quantifying Rate-and Temperature-Dependent Molecular Damage in Elastomer Fracture. Phys Rev X 2020;10:041045. doi:10.1103/PHYSREVX.10.041045/FIGURES/9/MEDIUM.
[51] Lake GJ, Thomas AG. The strength of highly elastic materials. Proc R Soc London Ser A Math Phys Sci 1967;300:108–19. doi:10.1098/rspa.1967.0160.

Supplementary Information

Steady state crack growth in viscoelastic solids: a comparative study

Chung-Yuen Hui[1*], Bangguo Zhu[1,2], Rong Long[3*]

[1]Sibley School of Mechanical and Aerospace Engineering, Field of Theoretical and Applied Mechanics, Cornell University, Ithaca, New York, 14853, USA

[2]Department of Modern Mechanics, University of Science and Technology of China, Hefei, Anhui, 230027, China

[3]Department of Mechanical Engineering, University of Colorado Boulder, Boulder, Colorado, 80309, USA

*Corresponding Authors: ch45@cornell.edu, rong.long@colorado.edu

Table of Contents

S1. Stress field for a crack with a Dugdale-Barenblatt cohesive zone

We follow the geometry and coordinate system defined in Fig.1A of the main text. A Dugdale-Barenblatt cohesive zone with constant cohesive stress σ_D occupies the line segment: $0 \le X \le \alpha$ and $Y = 0$. To describe the stress field, we introduce the complex variable $z = X + \mathrm{i}Y$ where $i = \sqrt{-1}$. In general, one can write the stress fields in terms of a stress function $\phi(z)$ [1]:

$$\sigma_{11} = 2\mathrm{Re}[\phi'(z)] - \mathrm{Re}[(\bar{z} - z)\phi''(z)], \tag{S1a}$$

$$\sigma_{22} = 2\mathrm{Re}[\phi'(z)] + \mathrm{Re}[(\bar{z} - z)\phi''(z)], \tag{S1b}$$

$$\sigma_{12} = \mathrm{Im}[(\bar{z} - z)\phi''(z)]. \tag{S1c}$$

For the SSC problem shown in Fig.1A, the complex stress function ϕ is given by:

$$\phi'(z) = \frac{\sigma_D}{\pi}\tan^{-1}\left[\sqrt{\frac{\alpha}{z-\alpha}}\right] \tag{S2a}$$

$$\phi''(z) = -\frac{\sigma_D}{2\pi}\frac{1}{z}\sqrt{\frac{\alpha}{z-\alpha}} \tag{S2b}$$

Substituting eq. (S2a)-(S2b) into eq. (S1a)-(S1c), we obtain

$$\sigma_{11} = \frac{\sigma_D}{\pi}\mathrm{Re}\left[2\tan^{-1}\sqrt{\frac{\alpha}{(X-\alpha)+iY}} - \frac{iY}{X+iY}\sqrt{\frac{\alpha}{(X-\alpha)+iY}}\right] \tag{S3a}$$

$$\sigma_{22} = \frac{\sigma_D}{\pi}\mathrm{Re}\left[2\tan^{-1}\sqrt{\frac{\alpha}{(X-\alpha)+iY}} + \frac{iY}{X+iY}\sqrt{\frac{\alpha}{(X-\alpha)+iY}}\right] \tag{S3b}$$

$$\sigma_{12} = \frac{\sigma_D}{\pi}\mathrm{Im}\left[\frac{iY}{X+iY}\sqrt{\frac{\alpha}{(X-\alpha)+iY}}\right] \tag{S3c}$$

The stress field given in eq. (S3a)-(S3b) is valid for both linear elastic and viscoelastic materials. Note that the stress field is independent of modulus.

S2. Derivation of eq. (11a)-(11b)

In Schapery's analysis, he defined a creep function $C_v(t)$ which is 4 times the uniaxial tensile creep function in *plane strain* (see discussion after equation (4) of Schapery [2]). In our notation, $C_v(t) = 4(1-\nu^2)J(t)$, where ν is the Poisson's ratio. Since we focus on results for *plane stress*, $C_v(t)$ should be $4J(t)$. Schapery [2] assumed a power law form of the creep compliance function $C_v(t)$, and obtained the following expression connecting the local energy release rate G_0 and the stress intensity factor K_I (see his equation (47) [2]):

$$\frac{G_0}{2} = \frac{1}{8}C_v\left(\tilde{t}_\alpha\right)K_I^2, \qquad \tilde{t}_\alpha = \lambda\frac{\alpha}{v}, \tag{S4a}$$

where α is the cohesive zone length and λ (denoted as "$\lambda_n^{1/n}$" in Schapery [2]) has a weak dependence on the power parameter of the creep function $C_V(t)$ and is found to be approximately 1/3 by Schapery [2]. Note that the local fracture energy, denoted as "Γ" in Schapery [2], is equivalent to $G_0/2$ in our notation, since its definition only involves the upper half of the cohesive zone separation. Regarding the cohesive zone length α, Schapery considered arbitrary distribution of cohesive stress in the cohesive zone and found that [2]:

$$\alpha = \frac{\pi}{2}\left(\frac{K_I}{\sigma_m I_S}\right)^2, \tag{S4b}$$

where σ_m is the maximum cohesive stress and I_S is a constant reflecting the effect of non-uniform cohesive stress (ranging from 0 to 2 and given in equation (2b) of Schapery [2]). In our work, since we consider only the Dugdale-Barenblatt cohesive zone with a constant cohesive stress σ_D, we have $\sigma_m = \sigma_D$ and $I_S = \int_0^1 \xi^{-1/2} d\xi = 2$. As a result, eq. (S4b) reduces to

$$\alpha = \frac{\pi K_I^2}{8\sigma_D^2}, \tag{S4c}$$

which is identical to that given by Knauss's theory (see eq.(4a) of the main text).

Assuming plane stress condition, we can cast eq. (S4a) in terms of our notation using eq. (6d), (7a), (8b) of the main text, i.e.,

$$\frac{G_0}{G} \equiv 1 - \Lambda^S = \frac{1}{J_\infty} J\left(\lambda \frac{\alpha}{v}\right) = 1 + \frac{1}{J_\infty} \Delta\tilde{J}\left(\lambda \frac{\alpha}{v t_c}\right), \tag{S5a}$$

where $\Delta\tilde{J}\,(t/t_c) = \Delta J = J(t) + J_\infty$ and $\lambda \approx 1/3$. To simplify notation, we absorb the factor $\lambda \approx 1/3$ into α and define

$$\alpha^S \equiv \lambda\alpha = \lambda \frac{\pi K_I^2}{8\sigma_D^2} = \lambda \frac{\pi G}{8 J_\infty \sigma_D^2} = \frac{G}{G_0} d^S, \qquad d^S \equiv \lambda \frac{\pi G_0}{8 J_\infty \sigma_D^2}. \tag{S5b}$$

This is equivalent to increasing the cohesive stress σ_D by a factor of approximately $\sqrt{3}$. Therefore, eq. (S5a) becomes:

$$\Lambda^S = -\frac{1}{J_\infty} \Delta\tilde{J}\left(\frac{\alpha^S}{v t_c}\right) = -\frac{1}{J_\infty} \Delta\tilde{J}\left(\beta^S\right), \qquad \beta^S = \frac{\alpha^S}{v t_c}, \tag{S5c}$$

which is eq. (11a) of the main text.

S3. Derivation for Table 1

In standard notation of viscoelasticity [3,4], the stress and strain relation under uniaxial tension is

$$\varepsilon(t) = \int_{-\infty}^{t} J(t-\tau)\frac{d\sigma(\tau)}{d\tau}d\tau\,. \tag{S6a}$$

Using integration by parts we obtain

$$\varepsilon(t) = J(t-\tau)\sigma(\tau)\Big|_{-\infty}^{t} - \int_{-\infty}^{t}\frac{J(t-\tau)}{d\tau}\sigma(\tau)d\tau = J_0\sigma(t) + \int_{-\infty}^{t} J'(t-\tau)\sigma(\tau)d\tau\,, \tag{S6b}$$

where $J'(t) = dJ/dt$. In the PB's work, the compliance function $C_{PB}(t)$ is defined such that

$$\varepsilon(t) = \int_{-\infty}^{t} C_{PB}(t-\tau)\sigma(\tau)d\tau\,. \tag{S7a}$$

By comparing eq. (S6a) and (S7a), we conclude

$$C_{PB}(t) = J_0\delta_+(t) + J'(t)\,. \tag{S7b}$$

where $\delta_+(t)$ is the Dirac delta function with the property that $\int_0^\infty \delta_+(t)dt = 1$.

The connection between the complex moduli (i.e., according to the standard notation and PB's notation) is simple but more difficult to show. First, we take the time Fourier transform of the strain and stress in eq. (S6b) according to PB's notation:

$$\hat{\varepsilon}(\omega) \equiv \frac{1}{2\pi}\int_{-\infty}^{\infty} e^{i\omega t}\varepsilon(t)dt\,, \quad \hat{\sigma}(\omega) \equiv \frac{1}{2\pi}\int_{-\infty}^{\infty} e^{i\omega t}\sigma(t)dt\,. \tag{S8a}$$

It should be noted that eq. (S8a) is different from the standard notation. For example, in the standard notation the Fourier transform of the strain is defined as $\tilde{\varepsilon}(\omega) \equiv \int_{-\infty}^{\infty} e^{-i\omega t}\varepsilon(t)dt$ [5], where the pre-factor $1/(2\pi)$ is absent and the exponential term is $e^{-i\omega t}$ rather than $e^{i\omega t}$ as in eq. (S8a). We follow PB's notation and substitute eq. (S8a) into eq. (S6b), which gives

$$\begin{aligned}\hat{\varepsilon}(\omega) &= J_0\hat{\sigma}(\omega) + \frac{1}{2\pi}\int_{-\infty}^{\infty} e^{i\omega t}\left[\int_{-\infty}^{t} J'(t-\tau)\sigma(\tau)d\tau\right]dt \\ &= J_0\hat{\sigma}(\omega) + \int_0^\infty e^{i\omega s}J'(s)\underbrace{\left[\frac{1}{2\pi}\int_{-\infty}^{\infty} e^{i\omega(t-s)}\sigma(t-s)dt\right]}_{\hat{\sigma}(\omega)}ds = \left[J_0 + \int_0^\infty J'(t)e^{i\omega t}dt\right]\hat{\sigma}(\omega)\end{aligned}\,. \tag{S8b}$$

PB defined their complex creep compliance C_{PB}^* using $\hat{\varepsilon}(\omega) = C_{PB}^*\hat{\sigma}(\omega)$. Using eq. (S8b), we see that it is related to the standard creep function $J(t)$ by

$$C^*_{PB}(\omega) = J_0 + \int_0^\infty J'(t) e^{i\omega t} dt \,. \tag{S8c}$$

Integration by parts give

$$C^*_{PB}(\omega) = J_0 + \left[J(t) - J_\infty\right] e^{i\omega t}\Big|_0^\infty - i\omega \int_0^\infty \left[J(t) - J_\infty\right] e^{i\omega t} dt = J_\infty - i\omega \int_0^\infty \Delta J(t) e^{i\omega t} dt \,. \tag{S8d}$$

Comparing this with the standard notation where the complex creep compliance is

$$J^*(\omega) = J_\infty + i\omega \int_0^\infty \left[J(t) - J_\infty\right] e^{-i\omega t} dt = J_\infty + i\omega \int_0^\infty \Delta J(t) e^{-i\omega t} dt \,, \tag{S8e}$$

we find

$$C^*_{PB}(\omega) = J^*(-\omega) \tag{S8f}$$

Since the imaginary part of $1/E^*_{PB}(\omega) = C^*_{PB}(\omega)$ and $J^*(\omega)$ has *opposite* signs, the dissipation rate *would be negative* if the standard complex modulus $E^*(\omega)$ is used in PB's formulation. Note that the sign change in ω has no effect on the storage modulus since it is an even function of the frequency.

S4. Derivation of eq. (13a) and (13b)

Using eq. (S8d), we can convert the integral in eq. (12a) to

$$\int_0^1 \frac{\sqrt{1-\xi^2}}{\xi} \mathrm{Im}\left(\frac{1}{E^*_{PB}(\omega_c \xi)}\right) d\xi = -\omega_c \int_0^\infty \Delta J(t) dt \int_0^1 \cos\left(\omega_c \xi t\right) \sqrt{1-\xi^2}\, d\xi \,, \tag{S9a}$$

where $\omega_c = 2\pi v / \alpha^{PB} \equiv 1/(\beta^{PB} t_c)$ is the cut-off frequency in PB's theory. It is well known that

$$\int_0^1 \cos\left(\omega_c \xi t\right) \sqrt{1-\xi^2}\, d\xi = \frac{\pi}{2\omega_c t} J_1\left(\omega_c t\right) \tag{S9b}$$

where J_1 is the Bessel function of the first kind of order one. Substituting eq. (S9b) into eq. (S9a) gives

$$\int_0^1 \frac{\sqrt{1-\xi^2}}{\xi} \mathrm{Im}\left(\frac{1}{E^*_{PB}(\omega_c \xi)}\right) d\xi = -\frac{\pi}{2} \int_0^\infty \frac{\Delta J(t)}{t} J_1\left(\omega_c t\right) dt = -\frac{\pi}{2} \int_0^\infty \frac{\Delta \tilde{J}(\eta)}{\eta} J_1\left(\frac{\eta}{\beta^{PB}}\right) d\eta \,, \tag{S9c}$$

where $\overline{t} = t/t_c$, $\Delta J(t) = \Delta \tilde{J}(t/t_c)$, and $\beta^{PB} = 1/(\omega_c t_c)$. The standard definition of Hankel transform of a generic function $f(\eta)$, denote by $H_1\left(f(\eta), \lambda\right)$ is [6]

$$H_1\left(f(\eta),\lambda\right)\equiv\int_0^\infty f(\eta)J_1(\eta\lambda)\sqrt{\lambda\eta}dt\,. \tag{S10a}$$

By identifying $f(\eta)=\Delta J(\eta)/\left(\eta\sqrt{\eta}\right)$ and $\lambda=1/\beta^{PB}$, we have

$$\int_0^1\frac{\sqrt{1-\xi^2}}{\xi}\mathrm{Im}\left(\frac{1}{E^*_{PB}(\omega_c\xi)}\right)d\xi=-\frac{\pi}{2}\sqrt{\beta^{PB}}H_1\left(\frac{\Delta J(\eta)}{\eta^{3/2}},\frac{1}{\beta^{PB}}\right). \tag{S10b}$$

Recall that $\omega_c=2\pi v/\alpha^{PB}$. Substituting eq. (S10b) into eq.(12a) gives eq. (13a).

The derivation of eq. (13b) proceeds in the same way. The integral in eq. (12b) can be rewritten as

$$\int_0^1\mathrm{Im}\left(\frac{1}{E^*\left(\omega_{\max}\xi\right)}\right)\frac{d\xi}{\xi}=-\omega_{\max}\int_0^\infty\Delta J(t)dt\int_0^1\cos\left(\omega_{\max}\xi t\right)d\xi=-\int_0^\infty\frac{\Delta J(t)}{t}\left(1-\cos\left(\omega_{\max}t\right)\right)dt\,, \tag{S11a}$$

where $\omega_{\max}=v/\alpha$. Therefore, the FDR of de Gennes is:

$$\Lambda^{dG}\equiv\frac{G_D}{G}=-E^*\left(\omega=0\right)\int_0^\infty\left[\frac{1-\cos\left(\omega_{\max}t\right)}{t}\right]\Delta J(t)dt=-\frac{1}{J_\infty}\int_0^\infty\left[\frac{1-\cos\left(vt/\alpha\right)}{t}\right]\Delta J(t)dt\,, \tag{S11b}$$

where we have used $E^*\left(\omega=0\right)=1/J_\infty$.

S5. Derivation of eq. (18c)

We apply integration by parts to the integral $I(\beta)$:

$$I\left(\beta\right)\equiv-\int_0^1e^{-\beta\xi}F'\left(\xi\right)d\xi=\frac{1}{\beta}\int_0^1F'\left(\xi\right)d\left(e^{-\beta\xi}-1\right)=-\frac{1}{\beta}\int_0^1F''\left(\xi\right)\left(e^{-\beta\xi}-1\right)d\xi=-\frac{1}{4\beta}\int_0^1\frac{e^{-\beta\xi}-1}{\xi\sqrt{1-\xi}}d\xi \tag{S12a}$$

where we have used $F'\left(\xi\right)$ given in eq. (6b) to obtain

$$F''\left(\xi\right)=\frac{1}{4\sqrt{1-\xi}}\frac{1}{\xi} \tag{S12b}$$

The integrand in eq. (S12a) has a removable singularity at $\xi=0$. Expanding the numerator in a power series, we find

$$\begin{aligned}I\left(\beta\right)&=-\frac{1}{4\beta}\int_0^1\frac{e^{-\beta\xi}-1}{\xi\sqrt{1-\xi}}d\xi=\frac{1}{4}\sum_{i=0}^\infty\frac{(-1)^i\beta^i}{(i+1)!}\int_0^1\frac{\xi^i}{\sqrt{1-\xi}}d\xi\\&=\frac{\sqrt{\pi}}{4}\sum_{i=0}^\infty\frac{(-1)^i\beta^i}{(i+1)!}\frac{i!}{\Gamma\left(i+3/2\right)}=\frac{\sqrt{\pi}}{4}\sum_{i=0}^\infty\frac{(-1)^i\beta^i}{(i+1)\Gamma\left(i+3/2\right)}\end{aligned}\,. \tag{S12c}$$

The series in eq. (S12c) has infinite radius of convergence and converges rapidly. We can also express $I(\beta)$ in terms of Kummer's Confluent Hypergeometric function by writing

$$I(\beta)=\frac{1}{4\beta}\lim_{\varepsilon\to 0}\left[\int_0^1 \frac{\exp(-\beta\xi)-1}{\xi^{1-\varepsilon}\sqrt{1-\xi}}d\xi\right]. \tag{S13a}$$

The integral in eq. (S13a) can be evaluated using the following identities (see 3.383 on Page 318 of [7])

$$\int_0^1 \frac{\exp(-\beta\xi)}{\xi^{1-\varepsilon}\sqrt{1-\xi}}d\xi=\frac{\Gamma(\varepsilon)\Gamma(1/2)}{\Gamma(\varepsilon+1/2)}M\left(\varepsilon,\frac{1}{2}+\varepsilon,-\beta\right), \tag{S13b}$$

and

$$-\int_0^1 \frac{1}{\xi^{1-\varepsilon}\sqrt{1-\xi}}d\xi=-\frac{\Gamma(\varepsilon)\Gamma(1/2)}{\Gamma(\varepsilon+1/2)}. \tag{S13c}$$

Adding eq. (S13b) and (S13c) and taking the limit of ε going to zero gives eq. (13c) in the main text. One can also use the series expansion of the Kummer's Confluent Hypergeometric function to obtain the power series in eq. (S12c) or eq. (18c) of the main text.

S6. Derivation of eq. (18d) and (18e)

We first use Watson's Lemma to determine the asymptotic behavior of $I(\beta)$ for large β.

$$I(\beta)\equiv\frac{1}{4}\int_0^1 e^{-\beta\xi}F'(\xi)d\xi=\frac{1}{4}\int_0^1 e^{-\beta\xi}\ln\left|\frac{\sqrt{1-\xi}+1}{\sqrt{1-\xi}-1}\right|d\xi \Rightarrow I(\beta>>1)\approx\frac{1}{4}\int_0^\infty e^{-\beta\xi}\ln\left|\frac{\sqrt{1-\xi}+1}{\sqrt{1-\xi}-1}\right|d\xi. \tag{S14a}$$

Equation (S14a) can be further expanded as follows:

$$\begin{aligned}
I(\beta>>1)&\approx\frac{1}{4}\left\{\int_0^\infty e^{-\beta\xi}\ln\left(\sqrt{1-\xi}+1\right)d\xi-\int_0^\infty e^{-\beta\xi}\ln\left|1-\sqrt{1-\xi}\right|d\xi\right\}\\
&\approx\frac{1}{4}\left\{\int_0^\infty e^{-\beta\xi}\ln\left[2\left(1-\frac{\xi}{4}+\ldots\right)\right]d\xi-\int_0^\infty e^{-\beta\xi}\ln\left[\frac{\xi}{2}\left(1+\frac{\xi}{4}+\ldots\right)\right]d\xi\right\}\\
&=\frac{1}{4}\left\{\left(\frac{\ln 2}{\beta}-\frac{1}{4\beta^2}+\ldots\right)-\int_0^\infty e^{-\beta\xi}\ln\left(\frac{\xi}{2}\right)dr-\int_0^\infty e^{-\beta\xi}\ln\left(1+\frac{\xi}{4}+\ldots\right)d\xi\right\}
\end{aligned}. \tag{S14b}$$

We note

$$\int_0^\infty e^{-\beta\xi}\ln\left(\frac{\xi}{2}\right)d\xi=-\frac{\ln 2}{\beta}+\int_0^\infty e^{-\beta\xi}\left(\ln(\xi\beta)-\ln\beta\right)d\xi=\frac{-\gamma-\ln 2}{\beta}-\frac{\ln\beta}{\beta}, \tag{S14c}$$

where $\gamma = 0.5772156649...$ is the Euler constant, and

$$\int_0^\infty e^{-\beta\xi} \ln\left[\left(1+\frac{\xi}{4}+..\right)\right] d\xi = \frac{1}{4\beta^2} + O\left(\beta^{-3}\right). \tag{S14d}$$

By combining eq. (S14b)-(S14d), we obtain

$$I\left(\beta >> 1\right) \approx \frac{1}{4}\left\{\left[\frac{\ln 2}{\beta} - \frac{1}{4\beta^2} + ..\right] + \frac{\gamma + \ln 2}{\beta} + \frac{\ln\beta}{\beta} - \frac{1}{4\beta^2} + ..\right\} = \frac{\ln\beta + \gamma + 2\ln 2}{4\beta} - \left(\frac{1}{8\beta^2}\right) + \ldots \tag{S14e}$$

Replacing the generic β by β_n^K and substituting eq. (S14e) into eq. (18a), we obtain eq. (18d).

In the limit of small β, we use the first three terms of the power series in eq. (18c) in the main text to compute $I(\beta)$ and derive eq. (18e) by replacing the generic β in $I(\beta)$ by β_n^K and using eq. (18a).

S7. Derivation of eq. (20a)

Using PB's definition of complex modulus E_{PB}^*, it is easy to show the following relation for GMS:

$$\mathrm{Im}\, C_{PB}^*\left(\omega\right) = \mathrm{Im}\frac{1}{E_{PB}^*\left(\omega\right)} = \left(J_\infty - J_0\right)\sum_{n=1}^{N}\frac{a_n\omega t_n}{1+\left(\omega t_n\right)^2}. \tag{S15a}$$

Substituting eq. (S15a) into the integral of eq. (12a) of the main text and using $E_{PB}^*\left(\omega = 0\right) = E_\infty = 1/J_\infty$, we get

$$\int_0^1 \mathrm{Im}\left(\frac{1}{E_{PB}^*(\omega_c\xi)}\right)\frac{\sqrt{1-\xi^2}}{\xi}d\xi = \left(J_\infty - J_0\right)\sum_{n=1}^{N}\int_0^1 \frac{a_n\omega_c t_n\sqrt{1-\xi^2}}{1+\left(\omega_c\xi t_n\right)^2}d\xi = \left(J_\infty - J_0\right)\frac{\pi}{2}\sum_{n=1}^{N}a_n\left(\sqrt{1+\left(\omega_c t_n\right)^{-2}} - \left(\omega_c t_n\right)^{-1}\right) \tag{S15b}$$

where $\omega_c = 2\pi\nu/\alpha^{PB}$ is the cut-off frequency in PB's theory. Combining eq. (S15b) and eq. (12a) of the main text, we obtain eq. (20a).

S8. Derivation of eq. (22a)

To derive eq. (22a), we plug the creep compliance function for the PLS (in eq. (17)) in eq. (10a):

$$\Lambda^K = \frac{2}{J_\infty}\int_0^1 \Delta\tilde{J}\left(\beta^K\xi\right)F'\left(\xi\right)d\xi = -2\kappa\int_0^1 \frac{F'\left(\xi\right)d\xi}{\left[1+\beta^K\xi\right]^m} \equiv -2\kappa I_{PL}. \tag{S16a}$$

Integration by parts gives

$$I_{PL} = \frac{1}{(1-m)\beta^K}\int_0^1 F'(\xi)\, d\left(\left[1+\beta^K\xi\right]^{1-m}-1\right)$$

$$= \frac{1}{(1-m)\beta^K}\left[\underbrace{F'(\xi)\left(\left[1+\beta^K\xi\right]^{1-m}-1\right)\Big|_0^1}_{0} - \int_0^1\left(\left[1+\beta^K\xi\right]^{1-m}-1\right)F''(\xi)\,dr\right] \quad . \tag{S16b}$$

$$= \frac{-1}{(1-m)4\beta^K}\int_0^1 \frac{\left[1+\beta^K\xi\right]^{1-m}-1}{\xi\sqrt{1-\xi}}d\xi = \frac{-1}{4(1-m)\beta^K}\lim_{\varepsilon\to 0}\left[\int_0^1 \frac{\left[1+\beta^K\xi\right]^{1-m}-1}{\xi^{1-\varepsilon}\sqrt{1-\xi}}d\xi\right]$$

The integral in eq. (S16b) can be determined by using

$$\int_0^1 \frac{\left[1+\beta^K\xi\right]^{1-m}}{\xi^{1-\varepsilon}\sqrt{1-\xi}}d\xi = \frac{\Gamma(\varepsilon)\Gamma(1/2)}{\Gamma\left(\frac{1}{2}+\varepsilon\right)}\,{}_2F_1\left(-1+m,\varepsilon,\frac{1}{2}+\varepsilon,-\beta^K\right) \tag{S16c}$$

and

$$\int_0^1 \frac{1}{\xi^{1-\varepsilon}\sqrt{1-\xi}}d\xi = \frac{\Gamma(\varepsilon)\Gamma(1/2)}{\Gamma(\varepsilon+1/2)}, \tag{S16d}$$

where ${}_2F_1$ is the Gauss Hypergeometric function. Combining eq. (S16c) and (S16d), we have

$$I_{PL} = \frac{-1}{4(1-m)\beta^K}\lim_{\varepsilon\to 0}\left[\Gamma(\varepsilon)\left\{{}_2F_1\left(-1+m,\varepsilon,\frac{1}{2}+\varepsilon,-\beta^K\right)-1\right\}\right]. \tag{S17}$$

Substituting eq. (S17) into eq. (S16a) gives eq.(22a).

S9. Derivation of eq. (22b) and (22c)

For $\beta^K \le 1$, the hypergeometric function in eq. (S17) can be expanded as a convergent power series,

$$\begin{aligned} {}_2F_1\left(-1+m,\varepsilon,\frac{1}{2}+\varepsilon,-\beta^K\right) &= \sum_{k=0}^{\infty}\frac{(\varepsilon)_k(-1+m)_k}{(1/2+\varepsilon)_k}\frac{\left(-\beta^K\right)^k}{k!} \\ &= 1-\frac{\varepsilon(-1+m)}{1/2+\varepsilon}\beta^K + \frac{\varepsilon(1+\varepsilon)(-1+m)(m)}{(1/2+\varepsilon)(3/2+\varepsilon)}\frac{\left(\beta^K\right)^2}{2!}-.... \end{aligned} \quad , \tag{S18a}$$

where we have used the notation: $(a)_k \equiv \Gamma(a+k)/\Gamma(a)$. Equation (S18a) implies the following result as $\varepsilon \to 0^+$:

$$\lim_{\varepsilon\to 0}\left[{}_2F_1\left(-1+m,\varepsilon,\frac{1}{2}+\varepsilon,-\beta^K\right)-1\right]$$
$$=\varepsilon\left[-\frac{(-1+m)}{1/2}\beta^K+\frac{(-1+m)(m)}{(1/2)(3/2)}\frac{(\beta^K)^2}{2!}+\ldots\right]=\varepsilon\sum_{k=1}^{\infty}\frac{(-1+m)_k}{(1/2)_k\,k}\left(-\beta^K\right)^k \quad \text{(S18b)}$$

Recall that $(a)_k\equiv\Gamma(a+k)/\Gamma(a)$. Since $\varepsilon\Gamma(\varepsilon)\to 1$ as $\varepsilon\to 0^+$, combining eq. (S17) and (S18b), we obtain

$$I_{PL}\left(\beta^K,m\right)=-\frac{1}{4(1-m)\beta^K}\sum_{k=1}^{\infty}\frac{(-1+m)_k}{(1/2)_k\,k}\left(-\beta^K\right)^k=-\frac{1}{2}\left[1-\frac{m}{3}\beta^K+\ldots\right],\qquad \left|\beta^K\right|\le 1. \quad \text{(S18c)}$$

In the limit of $\beta^K<<1$ (large crack velocity), using eq. (S18c) and (S16a), we obtain

$$\Lambda^K\left(\beta^K<<1\right)\approx\kappa\left(1-\frac{m}{3}\beta^K+\ldots.\right), \quad \text{(S18d)}$$

which is eq. (22b) in the main text.

For $\beta^K>1$, we use the linear transformation formula for hypergeometric functions to evaluate eq.(S17). Specifically,

$${}_2F_1\left(-1+m,\varepsilon,\frac{1}{2}+\varepsilon,-\beta^K\right)-1=\frac{\Gamma(1/2+\varepsilon)\Gamma(\varepsilon+1-m)}{\Gamma(\varepsilon)\Gamma\left(\frac{3}{2}+\varepsilon-m\right)}\left(\beta^K\right)^{1-m}{}_2F_1\left(-1+m,m-\varepsilon-\frac{1}{2},m-\varepsilon,\frac{1}{-\beta^K}\right)$$
$$+\frac{\Gamma(1/2+\varepsilon)\Gamma(-1+m-\varepsilon)}{\Gamma(-1+m)\Gamma(1/2)}\left(\beta^K\right)^{-\varepsilon}{}_2F_1\left(\varepsilon,\frac{1}{2},2-m+\varepsilon,\frac{1}{-\beta^K}\right)-1 \quad \text{(S19a)}$$

Since $1/\beta^K<1$, we can use the power series expansion of the hypergeometric function and after taking the limit of $\varepsilon\to 0$, we obtain

$$I_{PL}=\frac{-1}{4(1-m)}\left[\frac{\sqrt{\pi}\Gamma(1-m)}{\Gamma\left(\frac{3}{2}-m\right)}\left(\beta^K\right)^{-m}{}_2F_1\left(-1+m,m-\frac{1}{2},m,\frac{1}{-\beta^K}\right)-\frac{1}{2-m}\frac{1}{2\left(\beta^K\right)^2}\left\{1-\frac{1\cdot(3/2)}{(3-m)}\frac{1}{2!\left(\beta^K\right)}+\ldots\right\}\right] \quad \text{(S19b)}$$

Substituting eq. (S19b) into eq. (S16a) and keeping the dominant term for $\beta^K>>1$, we have

$$\Lambda^K\left(\beta^K>>1\right)\approx\frac{\kappa}{2(1-m)}\left[\frac{\sqrt{\pi}\Gamma(1-m)}{\Gamma(3/2-m)}\left(\beta^K\right)^{-m}\right] \quad \text{(S19c)}$$

which is eq. (22c).

S10. Derivation of eq. (23a)-(23c)

For the special case of PLS with $m = 1/2$, we have

$$I_{PL}\left(\beta^K, m=\frac{1}{2}\right)=\frac{-1}{2\beta^K}\int_0^1\frac{\sqrt{1+\beta^K\xi}-1}{\xi\sqrt{1-\xi}}d\xi=\frac{-1}{\beta_K}\int_0^1\frac{\sqrt{\left(1+\beta^K\right)-\beta^K r^2}-1}{\left(1-r^2\right)}dr \quad , \tag{S20}$$

where we have implemented a change of variable: $\xi = 1-r^2$. The integrand has a removable singularity at $r = 1$. We divide the integral in eq. (S20) into two integrals and evaluate each with upper limit at $r = s < 1$. The first integral is

$$\int_0^s\frac{\sqrt{\left(1+\beta^K\right)-\beta^K r^2}}{\left(1-r^2\right)}dr=\sqrt{1+\beta_K}\int_0^s\frac{\sqrt{1-\lambda^* r^2}}{\left(1-r^2\right)}dr=\frac{1}{2}\sqrt{1+\beta_K}\left[\underbrace{\int_0^s\frac{\sqrt{1-\lambda^* r^2}}{1-r}dr}_{I_1}+\underbrace{\int_0^s\frac{\sqrt{1-\lambda^* r^2}}{1+r}dv}_{I_2}\right] \tag{S21a}$$

where $\lambda^* = \beta^K/(1+\beta^K)$ or $\sqrt{1+\beta^K}=1/\sqrt{1-\lambda^*}$. The two integrals in eq. (S21a) can be carried out exactly, i.e.,

$$I_1=1-\sqrt{1-\lambda^* s^2}+\sqrt{\lambda^*}\sin^{-1}\left(s\sqrt{\lambda^*}\right)-\sqrt{1-\lambda^*}\ln\left(\frac{1+\sqrt{1-\lambda^*}}{1-\lambda^* s+\sqrt{1-\lambda^*}\sqrt{1-\lambda^* s^2}}\right)-\sqrt{1-\lambda^*}\ln\left(1-s\right) \tag{S21b}$$

$$\lim_{s\to 1} I_2=\sqrt{1-\lambda^*}-1+\sqrt{\lambda^*}\sin^{-1}\left(\sqrt{\lambda^*}\right)+\sqrt{1-\lambda^*}\ln\left(1+\sqrt{1-\lambda^*}\right) \tag{S21c}$$

Adding eq. (S21b) and (S21c) and taking the limit of $s \to 1$, we have

$$\frac{\sqrt{1+\beta^K}}{2}\lim_{s\to 1}\left(I_1+I_2\right)=\frac{\sqrt{\lambda^*}}{\sqrt{1-\lambda^*}}\sin^{-1}\left(\sqrt{\lambda^*}\right)+\frac{1}{2}\ln\left[2\left(1-\lambda^*\right)\right]-\frac{1}{2}\ln\left(1-s\right), \tag{S21d}$$

where we have used $\sqrt{1+\beta^K}=1/\sqrt{1-\lambda^*}$. The last term on the right hand side of eq. (S21d) is singular as $s \to 1$, which should be canceled by the second integral from eq. (S20), which is

$$-\int_0^s\frac{1}{1-r^2}dr=-\frac{1}{2}\ln\left(\frac{1+r}{1-r}\right)\Bigg|_0^s=\frac{1}{2}\ln\left(1-s\right)-\frac{1}{2}\ln\left(1+s\right) \tag{S21e}$$

Adding eq. (S21d) and eq. (S21e), we cancel the singular term $\ln(1-s)$ and then take limit of $s \to 1$, which gives

$$\int_0^1\frac{\sqrt{\left(1+\beta^K\right)-\beta^K r^2}}{\left(1-r^2\right)}dr=\frac{\sqrt{\lambda^*}}{\sqrt{1-\lambda^*}}\sin^{-1}\left(\sqrt{\lambda^*}\right)+\frac{1}{2}\ln\left(1-\lambda^*\right)=\sqrt{\beta^K}\sin^{-1}\sqrt{\frac{\beta^K}{1+\beta^K}}-\ln\sqrt{1+\beta^K} \tag{S21f}$$

Substituting eq.(S21f) into eq. (S20) and (S16a) gives:

$$\Lambda^K = -2\kappa\left[\frac{1}{\beta^K}\ln\sqrt{1+\beta^K} - \frac{1}{\sqrt{\beta^K}}\sin^{-1}\sqrt{\frac{\beta^K}{1+\beta^K}}\right]. \tag{S22}$$

Note that when $\beta^K \to 0$, we have

$$\begin{aligned}\Lambda^K\left(\beta^K \to 0\right) &\approx -2\kappa\left[\frac{1}{2\beta^K}\left(\beta^K - \frac{\left(\beta^K\right)^2}{2} + \ldots\right) - \frac{1}{\sqrt{\beta^K}}\left(\sqrt{\frac{\beta^K}{1+\beta^K}} + \frac{1}{6}\left(\frac{\beta^K}{1+\beta^K}\right)^{3/2} + \ldots\right)\right] \\ &= -2\kappa\left[\left(\frac{1}{2} - \frac{\beta^K}{4} + \ldots\right) - \left(1 - \frac{\beta^K}{2} + \frac{\beta^K}{6} + o(\beta^K)\right)\right] = -2\kappa\left[-\frac{1}{2} + \frac{\beta^K}{12} + \ldots\right] = \kappa\left(1 - \frac{\beta^K}{6} + ..\right)\end{aligned} \tag{S23}$$

which is consistent with eq. (S18c) when $m = 1/2$.

S11. FDR for PLS with different *m*

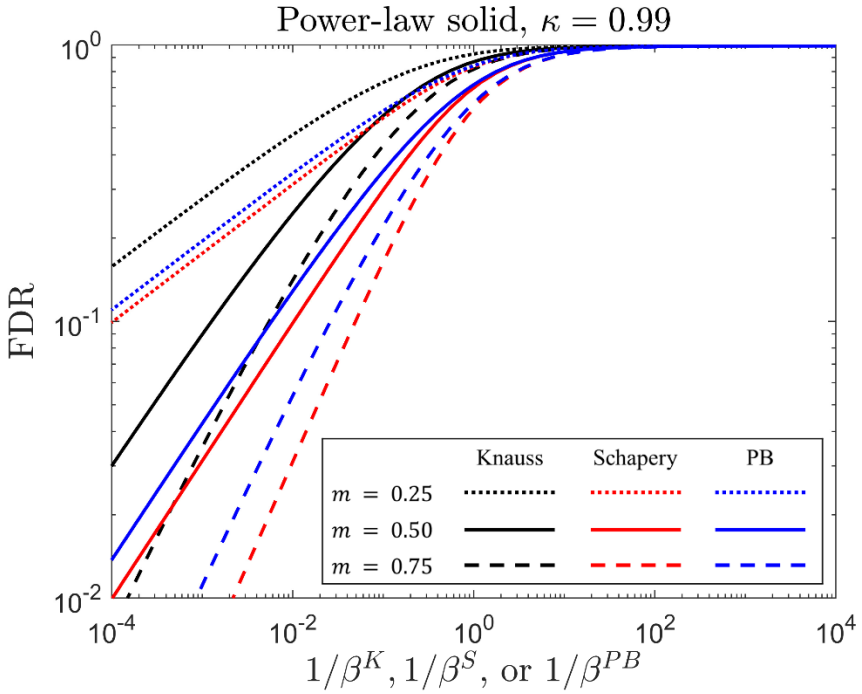

Figure S1 FDR for PLS with $\kappa = 0.99$ and m = 0.25, 0.5 or 0.75. Results for the case of m = 0.5 are identical to those in Fig.3 of the main text, while results for the cases of m = 0.25 and 0.75 are obtained using eq. (22a), eq. (24a) and eq. (25a) of the main text for Knauss, Schapery and PB, respectively.

S12. Derivation of eq. (31a) and (31b)

In the limit of $\beta^K >> 1$ (i.e., $\bar{v}^K << 1$), we combine eq. (22c) and (27) and use the definition that $\beta^K = \bar{G}d^K / vt_c = \bar{G}/\bar{v}^K$, which results in

$$\frac{\bar{G}-1}{\bar{G}} \approx \underbrace{\frac{\kappa}{2(1-m)} \frac{\sqrt{\pi}\Gamma(1-m)}{\Gamma(3/2-m)}}_{c_m} \left(\frac{\bar{G}}{\bar{v}^K}\right)^{-m} = c_m \left(\frac{\bar{G}}{\bar{v}^K}\right)^{-m}, \tag{S24a}$$

where we have introduced the symbol c_m to simplify notation. Solving $\bar{v}^K$ from eq. (S24a), we obtain

$$\bar{v}^K = \bar{G}\left(\frac{\bar{G}-1}{c_m \bar{G}}\right)^{1/m} = \left(\frac{\bar{G}-1}{c_m}\right)^{1/m} \bar{G}^{(m-1)/m}, \qquad \bar{v}^K << 1, \tag{S24b}$$

which is eq. (31a) in the main text.

In the limit of $\beta^K << 1$ (i.e., $\bar{v}^K >> 1$), combing eq. (22b) and eq. (27), we have

$$\frac{\bar{G}-1}{\bar{G}} \approx \kappa\left(1-\frac{m}{3}\beta^K\right) = \kappa\left(1-\frac{m}{3}\frac{\bar{G}}{\bar{v}^K}\right). \tag{S25a}$$

Using the definition that $\kappa = 1 - J_0/J_\infty$, we obtain

$$\bar{v}^K = \left(\frac{m\kappa}{3}\frac{J_\infty}{J_0}\right)\frac{\bar{G}^2}{(J_\infty/J_0)-\bar{G}}, \qquad \bar{v}^K >> 1, \tag{S25b}$$

which is eq. (31b) in the main text.

S13. Derivation of eq. (32c)

We start from the exact solution in eq. (32a). In the limit of $\bar{v}^S >> 1$, we expect $\bar{G}$ to approach $J_\infty/J_0 = 1/(1-\kappa)$. Therefore, we assume $\bar{G} = (1-\varepsilon)/(1-\kappa)$ where ε is a small positive value (i.e., $\varepsilon << 1$). Substituting it into eq. (32a) and keeping only leading order term of ε, we obtain

$$\bar{v}^S = \frac{(1-\varepsilon)/(1-\kappa)}{\left((1-\varepsilon)/(1-\varepsilon/\kappa)\right)^{1/m}-1} \approx \frac{(1-\varepsilon)/(1-\kappa)}{\left((1-\varepsilon)(1+\varepsilon/\kappa)\right)^{1/m}-1} \approx \frac{m\kappa}{(1-\kappa)^2\varepsilon}. \tag{S26a}$$

Using $\varepsilon = 1-(1-\kappa)\bar{G}$ and $\kappa = 1 - J_0/J_\infty$, we have

$$\bar{v}^S \approx m\kappa\left(\frac{J_\infty}{J_0}\right)^2\left(1-\frac{J_0}{J_\infty}\bar{G}\right)^{-1}, \qquad \bar{v}^S >> 1, \tag{S26b}$$

which is eq. (32c) in the main text.

S14. Comparison with Gent & Lai's data

We extract the experimental data of dynamic shear modulus μ' and loss modulus μ'' versus effective frequency ω for a styrene-butadiene copolymer in Figure 14 of Gent and Lai [8]. Specifically, we divide the frequencies into small equal intervals $\delta\omega = \omega_{i+1} - \omega_i$ and extract $\mu'(\omega_i)$ and $\mu''(\omega_i)$ from Figure 14 of Gent and Lai [8] at the nodal points ω_i. This information allows us to determine the complex shear modulus $\mu^*(\omega) = \mu'(\omega) + i\mu''(\omega)$ at ω_i. The complex compliances at these frequencies are obtained by $J^*(\omega) = 1/3\mu^*(\omega)$ assuming the polymer is incompressible. In GMS, the complex compliance is:

$$J^*(\omega) = J_\infty - i\omega(J_\infty - J_0)\sum_{n=1}^{N}\frac{a_n t_n}{1+i\omega t_n} \tag{S27}$$

where $\sum_{n=1}^{N} a_n = 1$. For convenience, we take $N = 5$ in eq. (S27) to determine the material constants a_n and t_n. The relax and instant compliance J_∞ and J_0 can be decided easily and directly by the lower and upper limits of complex compliance, i.e., $J_0 = 5.81 \times 10^{-7}\text{Pa}^{-1}$ and $J_\infty = 4.00 \times 10^{-10}\text{Pa}^{-1}$. To impose the constraint $\sum_{n=1}^{N} a_n = 1$, we set $a_1 = 1 - \sum_{n=2}^{5} a_n$ and determine a_2 to a_5 and t_1 to t_5 through fitting. The fitting of a_2 to $a_5$and t_1 to t_5 is done by using the "*lsqnonlin*" function in the optimization toolbox of MATLAB. The fitting curve and parameters are shown in Fig.S2.

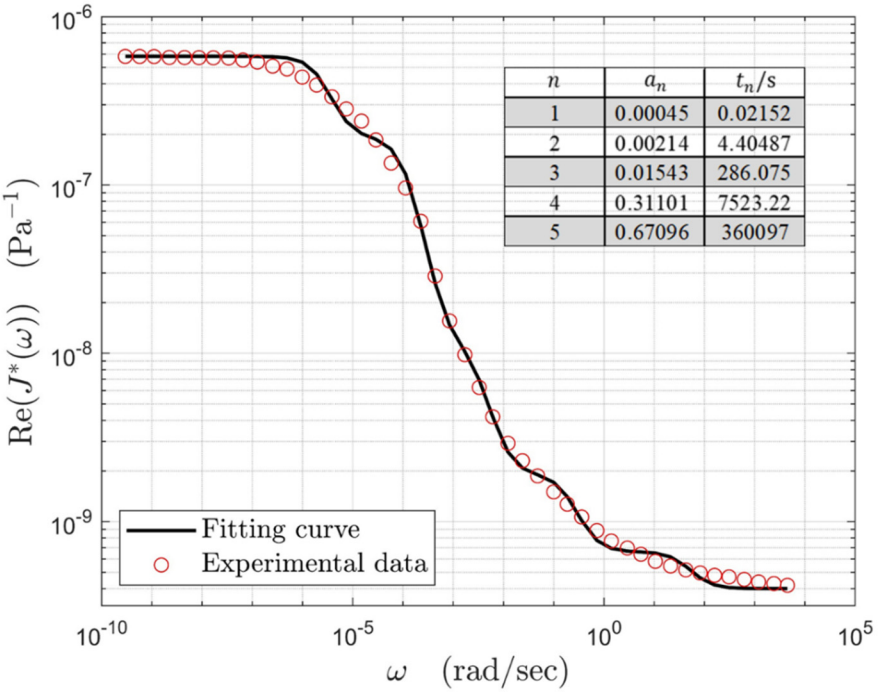

n	a_n	t_n/s
1	0.00045	0.02152
2	0.00214	4.40487
3	0.01543	286.075
4	0.31101	7523.22
5	0.67096	360097

Figure S2 Experimental data of Gent and Lai [8] for the real part of $J^*(\omega)$ and the fit using a GMS with 5 viscous branches. Fitted values of a_n and t_n (n = 1 to 5) are shown in the inset table.

S15. Comparison with Knauss's data

We use the power law model given by eq. (17) to fit the data of "Batch number 1" in Figure 3 of Knauss [9]. We choose the instantaneous and relaxed compliance to be the lower and upper limits. The results are $J_0 = 6.026 \times 10^{-7}\text{Pa}^{-1}$ and $J_\infty = 3.491 \times 10^{-4}\text{Pa}^{-1}$. As a result, m and t_c are the only two fitting parameters. We use the fitting function "*nlinfit*" in MATLAB to determine the optimal values for m and t_c. The results are shown in Fig.S3 below.

In Figure 12 of [9], Knauss plotted ε_∞, which denotes the strain imposed on the pure shear fracture specimen against the crack velocity v. For plane stress and incompressible solid, the applied energy release rate for a pure shear fracture specimen $G = 4b_t E_\infty \varepsilon_\infty^2 / 3$, where b_t is the specimen thickness and E_∞ is the relaxed modulus. This equation allows us to convert Knauss's strain data ε_∞ to G. To compare the experimental data with theory, G and v should be normalized by $\bar{G} = G / G_0$ and $\bar{v} = v t_c / d$. We chose G_0 to be the minimum fracture energy in Knauss's data. The value of t_c is determined by the fitting procedure described above (see Fig.S3). The only adjustable parameter in Schapery's theory is d^S. We found that d^S = 0.9 nm provides the best fit for Knauss's fracture test data as shown in Fig. 7 of the main text.

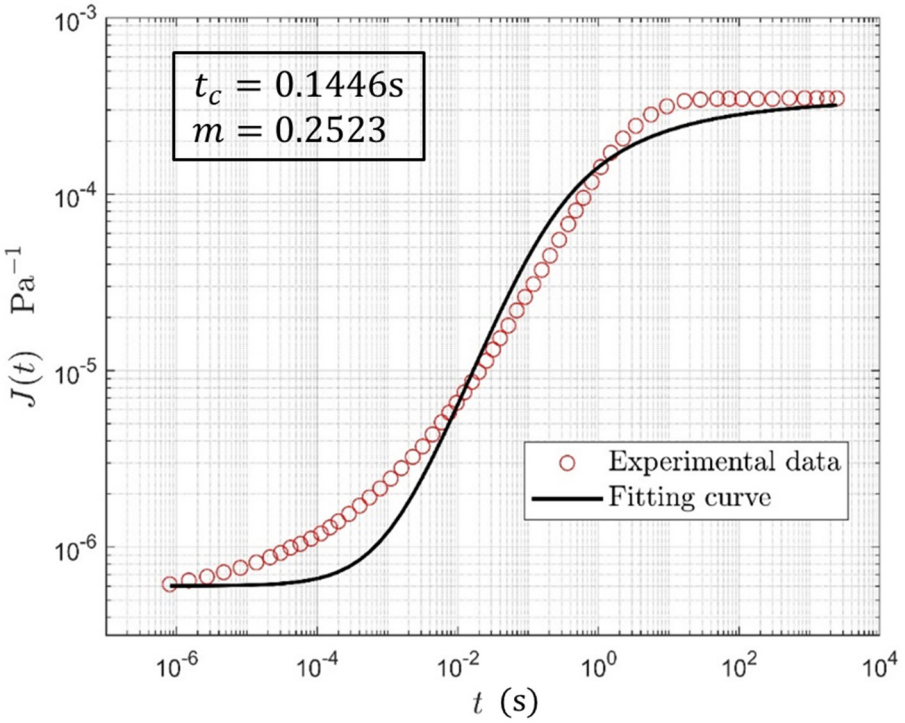

Figure S3 Experimental data of Knauss [9] for $J(t)$ and the fit using the PLS compliance function given by eq.(17). Fitted values of t_c and m are shown in the inset table.

S16. Derivation of eq. (38a)

Using the stress field with the DB cohesive zone model (see eq. (S3a)-(S3c) in Section S1), we find the following stress distribution directly ahead of the cohesive zone tip:

$$\sigma_{11}\left(X>\alpha,Y=0\right)=\sigma_{22}\left(X>\alpha,Y=0\right)=\frac{2\sigma_D}{\pi}\tan^{-1}\sqrt{\frac{\alpha}{X-\alpha}},\qquad \sigma_{12}=0\,, \tag{S28}$$

where α is the cohesive zone length. The strain directly ahead of the cohesive zone tip is obtained by substituting eq. (S28) into the viscoelastic constitutive relation for plane stress deformation, i.e.,

$$\varepsilon_{22}\left(X,Y=0\right)=\int_{-\infty}^{t}J(t-\tau)\frac{\partial}{\partial\tau}\left(\sigma_{22}-\frac{\sigma_{11}}{2}\right)d\tau=-\frac{1}{2}\int_{X}^{\infty}J\left(\frac{X'-X}{v}\right)\frac{\partial\sigma_{22}}{\partial X'}dX'\,, \tag{S29a}$$

where we have used the steady state crack growth condition and the incompressibility condition (i.e., Poisson's ratio = 1/2). For GMS, we substitute the creep function in eq. (16a) of the main text into eq.(S29a) results in:

$$\varepsilon_{22}\left(\bar{X}\ge 1,Y=0\right)=\frac{\sigma_D}{2\pi}\int_{\bar{X}}^{\infty}\left[J_\infty-\left(J_\infty-J_0\right)\sum_{n=1}^{N}a_n\exp\left(-\beta_n(\eta-\bar{X})\right)\right]\frac{1}{\eta\sqrt{\eta-1}}d\eta\,, \tag{S29b}$$

where we have used $\sum_{n=1}^{N}a_n=1$, $\beta_n=\alpha/vt_n$, $\bar{X}=X/\alpha$, $\eta=X'/\alpha$, and

$$\frac{\partial\sigma_{22}}{\partial X}=-\frac{\sigma_D}{\pi}\frac{\sqrt{\alpha}}{X\sqrt{X-\alpha}}\quad. \tag{S29c}$$

We apply the following identify

$$\int_{\bar{X}}^{\infty}\frac{1}{\eta\sqrt{\eta-1}}d\eta=\pi-2\tan^{-1}\left(\sqrt{\bar{X}-1}\right),\qquad \bar{X}\ge 1\,, \tag{S30a}$$

and introduce the integral function

$$\Psi\left(\bar{X}\ge 1,\beta_n\right)\equiv\int_{\bar{X}}^{\infty}\frac{e^{-\beta_n\eta}}{\eta\sqrt{\eta-1}}d\eta=\int_{1}^{\infty}\frac{e^{-\beta_n\eta}}{\eta\sqrt{\eta-1}}d\eta-\int_{1}^{\bar{X}}\frac{e^{-\beta_n\eta}}{\eta\sqrt{\eta-1}}d\eta\,. \tag{S30b}$$

The first integral on the right hand side of eq. (30b) can be related to the complementary error function:

$$\int_{1}^{\infty}\frac{e^{-\beta_n\eta}}{\eta\sqrt{\eta-1}}d\eta=2e^{-\beta_n}\int_{0}^{\infty}\frac{e^{-\beta_n s}}{s^2+1}ds=2e^{-\beta_n}\frac{\pi}{2}e^{\beta_n}erfc\left(\sqrt{\beta_n}\right)=\pi erfc\left(\sqrt{\beta_n}\right). \tag{S30c}$$

Equation (S30b) and (S30c) suggest that $\Psi\left(\bar{X}=1,\beta_n\right)=\pi erfc\left(\sqrt{\beta_n}\right)$. Using eq. (S30a) and (S30b), the strain in eq. (S29b) is:

$$\varepsilon_{22}\left(\bar{X}\ge 1,Y=0\right)=\frac{\sigma_D}{2\pi E_\infty}\left[\left\{\pi-2\tan^{-1}\left(\sqrt{\bar{X}-1}\right)\right\}-\kappa\sum_{n=1}^{N}a_n\exp\left(\beta_n\bar{X}\right)\Psi\left(\bar{X},\beta_n\right)\right], \tag{S30d}$$

where we used $E_\infty = 1/J_\infty$. Equation eq. (S30d) is eq. (38a) in the main text.

S17. Derivation of eq. (39c)

We first consider the asymptotic behavior of $\Psi\left(\bar{X},\beta_n\right)$ for $\bar{X}>>1$, which is obtained using integration by parts, i.e.,

$$\Psi\left(\bar{X}>>1,\beta_n\right)\approx\int_{\bar{X}}^{\infty}\frac{e^{-\beta_n\eta}}{\eta^{3/2}}d\eta=\frac{e^{-\beta_n\bar{X}}}{\beta_n\bar{X}^{3/2}}-\frac{3}{2}\int_{\bar{X}}^{\infty}\frac{e^{-\beta_n\eta}}{\eta^{5/2}}d\eta=\frac{e^{-\beta_n\bar{X}}}{\beta_n\bar{X}^{3/2}}+O\left(\bar{X}^{-5/2}e^{-\beta_n\bar{X}}\right). \tag{S31a}$$

Using eq. (S31a), we obtain the following asymptotic behavior for the numerator of eq. (39a)

$$\kappa\sum_{n=1}^{N}a_n\exp\left(\beta_n\bar{X}\right)\Psi\left(\bar{X},\beta_n\right)\approx\frac{\kappa}{\bar{X}^{3/2}}\sum_{n=1}^{N}\frac{a_n}{\beta_n},\quad \bar{X}>>1. \tag{S31b}$$

The denominator in eq. (39a) approaches the following limit for $\bar{X}>>1$:

$$\lim_{\bar{X}\to\infty}\left[\pi-2\tan^{-1}\left(\sqrt{\bar{X}-1}\right)\right]=\frac{2}{\sqrt{\bar{X}}}\ . \tag{S31c}$$

Substituting eq. (S31b) and (31c) into eq. (39a), we obtain the eq. (39c) for the asymptotic behavior of χ_{strain} for $\bar{X}>>1$.

S18. Derivation of eq. (41a)

We use the stress distribution given in eq. (37b) of the main text (i.e., approximation based on the *K*-field) and obtain

$$\frac{\partial\sigma_{22}}{\partial X}=-\frac{\sigma_D\sqrt{\alpha}}{2X\sqrt{X}}. \tag{S32a}$$

Substituting eq. (S32a) into eq. (S29a) using the creep function for GMS (see eq. (16a) of the main text), we obtain the following equation for ε_{22}^{*},

$$\varepsilon_{22}^{*}\left(\bar{X}\geq1,Y=0\right)=\frac{J_\infty}{2}\frac{\sigma_D}{\sqrt{\bar{X}}}-\frac{J_\infty\kappa\sigma_D}{4}\sum_{n=1}^{N}a_n\exp\left(\beta_n\bar{X}\right)\int_{\bar{X}}^{\infty}\exp\left(-\beta_n\eta\right)\frac{1}{\eta^{3/2}}d\eta, \tag{S32b}$$

where we have used $\bar{X}=X/\alpha$ and $\beta_n=\alpha/vt_n$. The integral in eq. (S32b) can be readily evaluated using integration by parts, which results in

$$\varepsilon_{22}^{*}\left(\bar{X}\geq1,Y=0\right)=\frac{\sigma_D}{2E_\infty\sqrt{\bar{X}}}\left[1-\kappa\left\{1-\sum_{n=1}^{N}a_n\sqrt{\pi\bar{X}\beta_n}\exp\left(\beta_n\bar{X}\right)erfc\left(\sqrt{\beta_n\bar{X}}\right)\right\}\right], \tag{S32c}$$

which is eq. (41a).

S19. Asymptotic behavior of eq. (41a) and (41b)

Using the asymptotic behavior of the complementary error function, i.e.,

$$erfc\left(\sqrt{\beta_n \bar{X}}\right) \approx \frac{\exp\left(-\beta_n \bar{X}\right)}{\sqrt{\pi \beta_n \bar{X}}}\left(1-\frac{1}{2\beta_n \bar{X}}\right) \quad \text{for } \bar{X}\beta_n >> 1, \tag{S33a}$$

we found the following asymptotic behavior of ε_{22}^* in eq. (41a):

$$\varepsilon_{22}^*\left(\bar{X} \geq 1, Y=0\right) \approx \frac{\sigma_D}{2E_\infty \sqrt{\bar{X}}}\left[1-\frac{\kappa}{2\bar{X}}\sum_{n=1}^{N}\frac{a_n}{\beta_n}\right] \quad \text{for } \bar{X}\beta_n >> 1. \tag{S33b}$$

Using eq. (S33b), we can also evaluate the asymptotic behavior of χ_{strain}^*:

$$\chi_{strain}^*\left(\bar{X}\right) = \kappa\left\{1-\sum_{n=1}^{N}\sqrt{\pi \bar{X}\beta_n}\exp\left(\beta_n \bar{X}\right) erfc\left(\sqrt{\beta_n \bar{X}}\right)\right\} \approx \frac{\kappa}{2\bar{X}}\sum_{n=1}^{N}\frac{a_n}{\beta_n} \text{ for } \beta_{ave}\bar{X} >> 1, \tag{S33c}$$

which is identical to eq. (39c) in the main text.

S20. Asymptotic behavior of eq. (40a) and (41c)

Here we examine the asymptotic behavior of eq. (40a) and (41c) in the main text for the SS (i.e., GMS with $N = 1$). In this case, there is only one retardation time $t_c = t_1$ and hence one β ($= \alpha/vt_c$). In the limit of high crack velocity ($\beta \rightarrow 0$), using the series expansion of the complementary error function, we find:

$$\varepsilon_{22}\left(\bar{X}=1, \beta \rightarrow 0\right) = \frac{\sigma_D}{2E_\infty}\left[1-\kappa\left(1-\frac{2\sqrt{\beta}}{\sqrt{\pi}}+..\right)\right], \tag{S34a}$$

$$\varepsilon_{22}^*\left(\bar{X}=1, \beta \rightarrow 0\right) = \frac{\sigma_D}{2E_\infty}\left[1-\kappa\left(1-\sqrt{\pi\beta}+....\right)\right], \tag{S34b}$$

Comparing eq. (34a) and (34b), we notice that in the limit of high crack velocity (i.e., $\beta \rightarrow 0$), the first order terms in the strains given by the interacting and non-interacting models agree exactly as expected. However, the second order terms do not agree as β increases. In the limit of low crack velocity ($\beta \rightarrow \infty$), we have:

$$\varepsilon_{22}\left(\bar{X}=1, \beta \rightarrow \infty\right) = \frac{\sigma_D}{2E_\infty}\left[1-\kappa\left(\frac{1}{\sqrt{\pi\beta}}+O\left(\beta^{-3/2}\right)\right)\right], \tag{S35a}$$

$$\varepsilon_{22}^*\left(\bar{X}=1, \beta \rightarrow \infty\right) = \frac{\sigma_D}{2E_\infty}\left[1-\frac{\kappa}{2\beta}+O\left(\beta^{-2}\right)\right] \quad . \tag{S35b}$$

In this limit, again the first order terms in the strains for both interacting and non-interacting models agree exactly. However, the rate of convergence is quite different as reflected by the second term in the expansion. Note that in Fig. 7, the discrepancy at $\bar{X} = 1$ for small and large β is partly due to our effort to bring the two theories into agreement, i.e., the blue dash line is (41a) multiplied by 2/π.

S21. Derivation of eq. (43a), (43b) and (43c)

The integral $\Psi_{PL}(\bar{X},\beta,m)$ given eq. (42b) can be rewritten in the following form after a change of variable $w = 1/\eta$:

$$\Psi_{PL}(\bar{X},\beta,m) = \frac{1}{\beta^m}\int_0^{1/\bar{X}}\left[1+\left(\frac{1-\beta\bar{X}}{\beta}\right)w\right]^{-m}\frac{w^{m-1/2}}{\sqrt{1-w}}dw\,. \tag{S36a}$$

For the special case of m = 1/2, we have

$$\Psi_{PL}(\bar{X},\beta,m=1/2) = \frac{1}{\sqrt{\beta}}\int_0^{1/\bar{X}}\left[1+\left(\frac{1-\beta\bar{X}}{\beta}\right)w\right]^{-1/2}\frac{1}{\sqrt{1-w}}dw\,. \tag{S36b}$$

To evaluate the integral in eq. (S36b), we implement another change of variable, $1-w=\xi^2$, which leads to

$$\Psi_{PL}(\bar{X},\beta,m=1/2) = \frac{2}{\sqrt{\beta}}\int_{\sqrt{1-1/\bar{X}}}^{1}\left[1+A\left(1-\xi^2\right)\right]^{-1/2}d\xi = \frac{2}{\sqrt{\beta}}\int_{\sqrt{1-1/\bar{X}}}^{1}\frac{1}{\sqrt{(1+A)-A\xi^2}}d\xi\,, \tag{S36c}$$

where

$$A=\left(\frac{1-\beta\bar{X}}{\beta}\right)\Rightarrow\frac{A}{1+A}=\frac{1-\beta\bar{X}}{\beta+1-\beta\bar{X}}\,, \tag{S36d}$$

The value of A can be positive, negative or zero, depending on the sign of $1-\beta\bar{X}$. The integral in eq. (S36c) depends on the sign of A. For $A < 0$ (i.e., $\beta\bar{X} > 1$), we have

$$\begin{aligned}\Psi_{PL}(\bar{X},\beta,m=1/2) &= \frac{2}{\sqrt{\beta}}\frac{1}{\sqrt{-A}}\ln\left(\xi\sqrt{-A}+\sqrt{(1+A)-A\xi^2}\right)\Big|_{\sqrt{1-1/\bar{X}}}^{1}\\ &= 2\sqrt{\frac{1}{\bar{X}\beta-1}}\ln\left(\frac{\sqrt{\dfrac{\bar{X}\beta-1}{\beta}}+1}{\sqrt{\dfrac{(\bar{X}\beta-1)(\bar{X}-1)}{\bar{X}\beta}}+\sqrt{\dfrac{1}{\bar{X}\beta}}}\right)\end{aligned} \qquad \text{for } \bar{X}\beta > 1. \tag{S37a}$$

For $A > 0$ (i.e., $\beta\bar{X} < 1$), we have

$$\Psi_{PL}(\bar{X},\beta,m=1/2)=\frac{2}{\sqrt{\beta}}\frac{1}{\sqrt{A}}\sin^{-1}\left(\sqrt{\frac{A}{1+A}}\xi\right)\Bigg|_{\sqrt{1-1/\bar{X}}}^{1}$$
$$=\frac{2}{\sqrt{1-\bar{X}\beta}}\left[\sin^{-1}\left(\sqrt{\frac{1-\beta\bar{X}}{\beta+1-\beta\bar{X}}}\right)-\sin^{-1}\left(\sqrt{\frac{1-\beta\bar{X}}{\beta+1-\beta\bar{X}}\left(1-1/\bar{X}\right)}\right)\right] \quad \text{for } \beta\bar{X}<1\,. \tag{S37b}$$

For $A = 0$ (i.e., $\beta\bar{X}=1$), we have

$$\Psi_{PL}(\bar{X},\beta,m=1/2)=\frac{2}{\sqrt{\beta}}\left(1-\sqrt{1-\frac{1}{\bar{X}}}\right)=\frac{2}{\sqrt{\beta}}\left(1-\sqrt{1-\beta}\right) \quad \text{for } \beta\bar{X}=1\,. \tag{S37c}$$

Substituting eq. (S37a), (37b) and (37c) into eq. (42c) gives eq. (43a), (43b) and (43c), respectively.

S22. Derivation of eq. (46a)

Using the approximate stress distribution based on the *K*-field given in eq. (37b) and the compliance function for PLS in eq. (17), the strain ε_{22}^{*} in eq. (S29a) is

$$\varepsilon_{22}^{*}\left(\bar{X}\ge 1,Y=0\right)=\frac{1}{2}J_{\infty}\frac{\sigma_D}{\sqrt{\bar{X}}}+\frac{1}{2}\int_{\bar{X}}^{\infty}\Delta\tilde{J}\left(\beta\left(\eta-\bar{X}\right)\right)\frac{\partial\sigma_{22}}{\partial\eta}d\eta=\frac{1}{2}J_{\infty}\frac{\sigma_D}{\sqrt{\bar{X}}}\left(1-\frac{\kappa\sqrt{\bar{X}}}{2}\int_{\bar{X}}^{\infty}\left[1+\beta\left(\eta-\bar{X}\right)\right]^{-m}\eta^{-3/2}d\eta\right) \tag{S38a}$$

To evaluate the integral on the right hand side of eq. (S38a), we implement a change of variable $w=\bar{X}/\eta$:

$$\int_{\bar{X}}^{\infty}\left[1+\beta\left(\eta-\bar{X}\right)\right]^{-m}\eta^{-3/2}d\eta=\frac{\left(\beta\bar{X}\right)^{-m}}{\sqrt{\bar{X}}}\int_{0}^{1}\left[1-\left(\frac{\beta\bar{X}-1}{\beta\bar{X}}\right)w\right]^{-m}w^{m-1/2}dw$$
$$=\frac{\left(\beta\bar{X}\right)^{-m}}{\sqrt{\bar{X}}}\frac{1}{m+1/2}\,{}_2F_1\left(m,m+1/2,m+3/2,\frac{\beta\bar{X}-1}{\beta\bar{X}}\right) \tag{S38b}$$

Substituting (S38b) in (S38a) and using $E_\infty = 1/J_\infty$, we obtain

$$\varepsilon_{22}^{*}\left(\bar{X}\ge 1,Y=0\right)=\frac{\sigma_D}{2E_{\infty}\sqrt{\bar{X}}}\left(1-\frac{\kappa}{2m+1}\left(\beta\bar{X}\right)^{-m}\,{}_2F_1\left(m,m+1/2,m+3/2,\frac{\beta\bar{X}-1}{\beta\bar{X}}\right)\right), \tag{S38c}$$

which is eq. (46a) in the main text.

S23. Derivation of eq. (47a) and (47b)

Here we derive the asymptotic behavior of χ^*_{strain} given in eq. (46b) of the main text. In the limit of $\beta\bar{X} >> 1$, we have $\left(\beta\bar{X} - 1\right)/\beta\bar{X} \to 1$ within the hypergeometric function in eq. (46b). Therefore, we obtain first-order behavior for $\beta\bar{X} >> 1$ by evaluating the hypergeometric function at 1, which gives eq. (47a), i.e.,

$$\chi^*_{strain}\left(\bar{X} \geq 1, \bar{X}\beta >> 1, m\right) = \frac{\kappa\left(\beta\bar{X}\right)^{-m}}{2m+1} {}_2F_1\left(m, m+\frac{1}{2}, m+\frac{3}{2}, 1\right) = \frac{\kappa\left(\beta\bar{X}\right)^{-m}}{2m+1} \frac{2\Gamma\left(m+3/2\right)\Gamma\left(1-m\right)}{\sqrt{\pi}}, \tag{S39a}$$

which is eq. (47a) in the main text.

In the limit of $\beta\bar{X} << 1$, we use the linear transformation formulae for hypergeometric functions to obtain

$$\begin{aligned} &{}_2F_1\left(m, m+1/2, m+3/2, \frac{\beta\bar{X}-1}{\beta\bar{X}}\right) \\ &= \left(2m+1\right)\left(\frac{1-\beta\bar{X}}{\beta\bar{X}}\right)^{-m} {}_2F_1\left(m, -1/2, 1/2; \frac{\beta\bar{X}}{\beta\bar{X}-1}\right) - \frac{2\sqrt{\pi}\Gamma\left(m+3/2\right)}{\Gamma\left(m\right)}\left(\frac{1-\beta\bar{X}}{\beta\bar{X}}\right)^{-m-1/2}. \end{aligned} \tag{S39b}$$

Using the condition $\beta\bar{X} << 1$, we expand the hypergeometric function in eq. (S39b) in power series and keep only the first term which is 1. This gives

$${}_2F_1\left(m, m+\frac{1}{2}, m+\frac{3}{2}, \frac{\beta\bar{X}-1}{\beta\bar{X}}\right) \approx \left(2m+1\right)\left(\frac{1-\beta\bar{X}}{\beta\bar{X}}\right)^{-m} - \frac{2\sqrt{\pi}\Gamma\left(m+3/2\right)}{\Gamma\left(m\right)}\left(\frac{1-\beta\bar{X}}{\beta\bar{X}}\right)^{-m-1/2} \approx \left(2m+1\right)\left(\beta\bar{X}\right)^{m} \tag{S39c}$$

Substituting eq. (S39c) into eq. (46b) of the main text, we have

$$\chi^*_{strain}\left(\bar{X} \geq 1, \beta\bar{X} \leq 1, m\right) \approx \frac{\kappa\left(\beta\bar{X}\right)^{-m}}{2m+1}\left(2m+1\right)\left(\beta\bar{X}\right)^{m} = \kappa, \tag{S39d}$$

which is eq. (47b) of the main text.

S24. Derivation of eq. (49a)

As before, we assume plane stress condition (for plane strain condition, the strain ε_{22} should be reduced by a factor of 3/4). Directly behind the crack ($X < 0$, $Y = 0$), we have $\sigma_{11} = \sigma_{22}$ and $\sigma_{12} = 0$ according to the stress field given in Section S1 of the SI. Similar to eq. (36) of the main text, the general expression for the residual strain behind the crack tip is:

$$\varepsilon_{22}\left(X<0,Y=0\right)=-\frac{1}{2}\int_{X}^{\infty}J\left(\frac{X'-X}{v}\right)\frac{\partial\sigma_{22}}{\partial X'}dX' \quad . \tag{S40a}$$

Since $\sigma_{22}=0$ on the crack surface ($X<0$, $Y=0$) and is equal to a constant σ_D within the cohesive zone ($0\le X\le\alpha$, $Y=0$), the residual strain on the crack surface is

$$\varepsilon_{22}\left(X\le 0,Y=0\right)=-\frac{1}{2}\int_{\alpha}^{\infty}J\left(\frac{X'-X}{v}\right)\frac{\partial\sigma_{22}}{\partial X'}dX'-\frac{\sigma_D}{2}\int_{X}^{\alpha}J\left(\frac{X'-X}{v}\right)\frac{\partial H\left(X'\right)}{\partial X'}dX' \tag{S40b}$$

where H is the Heaviside function. The second integral represents the sudden unloading as a material point pass through the crack tip at $X=0$ (where the stress suddenly vanishes, recall the stress is constant inside the cohesive zone). Hence on the crack surface, the strain is

$$\varepsilon_{22}\left(X\le 0,y=0\right)=-\frac{1}{2}\int_{\alpha}^{\infty}J\left(\frac{X'-X}{v}\right)\frac{\partial\sigma_{22}}{\partial X'}dX'-\frac{\sigma_D}{2}J\left(\frac{-X}{v}\right). \tag{S40c}$$

Using eq. (S29c) and the normalization that $\bar{X}=X/\alpha$ and $\eta=X'/\alpha$, the first integral in eq. (S40c) is

$$\frac{\sigma_D}{2\pi}\int_{1}^{\infty}J\left(\alpha\frac{\eta-\bar{X}}{v}\right)\frac{1}{\eta\sqrt{\eta-1}}d\eta\,. \tag{S40d}$$

For a GMS, the tensile creep function $J(t)$ is given by eq. (16a) of the main text. Substituting eq. (16a) into eq. (S40c) gives:

$$\varepsilon_{22}\left(\bar{X}<0,Y=0\right)=\frac{\sigma_D J_\infty}{2\pi}\int_{1}^{\infty}\left(\frac{1-\kappa\sum_{n=1}^{N}a_n\exp\left(-\beta_n\eta-\beta_n\left|\bar{X}\right|\right)}{\eta\sqrt{\eta-1}}\right)d\eta-\frac{\sigma_D J_\infty}{2}\left[\left(1-\kappa\sum_{n=1}^{N}a_n\exp\left(-\beta_n\left|\bar{X}\right|\right)\right)\right] \tag{S41}$$

To evaluate the integral in eq. (S41), we use the following two identities:

$$\int_{1}^{\infty}\frac{1}{\eta\sqrt{\eta-1}}d\eta=\pi\,, \tag{S42a}$$

$$\int_{1}^{\infty}\frac{\exp\left(-\beta\eta\right)}{\eta\sqrt{\eta-1}}d\eta=2e^{-\beta}\int_{0}^{\infty}\frac{\exp\left(-\beta s^2\right)}{\left(1+s^2\right)}ds=2e^{-\beta}\frac{\pi}{2}e^{\beta}erfc\left(\sqrt{\beta}\right)=\pi erfc\left(\sqrt{\beta}\right). \tag{S42b}$$

Combining eq. (S42a) and (42b), eq. (S41) becomes

$$\begin{aligned}\varepsilon_{22}\left(\bar{X}<0,y=0\right)&=\frac{\sigma_D J_\infty}{2}\left[1-\kappa\sum_{n=1}^{N}a_n erfc\left(\sqrt{\beta_n}\right)\exp\left(-\beta_n\left|\bar{X}\right|\right)\right]+\frac{\sigma_D J_\infty}{2}\left[1-\kappa\sum_{n=1}^{N}a_n\exp\left(-\beta_n\left|\bar{X}\right|\right)\right],\\&=\frac{\sigma_D}{2E_\infty}\kappa\sum_{n=1}^{N}a_n\exp\left(-\beta_n\left|\bar{X}\right|\right)erf\left(\sqrt{\beta_n}\right)\end{aligned} \tag{S42c}$$

which is eq. (49a) of the main text. The residual strain at the crack tip (i.e., at $X = 0$) is obtained by taking the limit of $\bar{X}$ to zero in eq. (S42c), which results in

$$\varepsilon_{22}\left(\bar{X}=0^{-}, y=0\right)=\frac{\sigma_D \kappa}{2E_\infty}\sum_{n=1}^{N} a_n erf\left(\sqrt{\beta_n}\right), \tag{S42d}$$

which is eq. (49c) of the main text. At very slow crack speed (i.e., β_n >>1 and $erf\left(\sqrt{\beta_n}\right)\to 1$, the residue strain at the crack tip reaches a maximum of $\sigma_D\kappa/(2E_\infty)$, which decays to zero almost immediately due to the exponential function $\exp\left(-\beta_n\left|\bar{X}\right|\right)$.

S25. Derivation of eq. (50a)

Substituting eq. (17) of the main text into eq. (S40c), the residual strain for the PLS is:

$$\begin{aligned}\varepsilon_{22}\left(\bar{X}\le 0, Y=0\right)&=\frac{\sigma_D}{2\pi}\int_1^\infty\left[J_\infty-\frac{\left(J_\infty-J_0\right)}{\left[1+\beta\left(\eta-\bar{X}\right)\right]^m}\right]\frac{1}{\eta\sqrt{\eta-1}}d\eta-\frac{\sigma_D}{2}\left[J_\infty-\frac{\left(J_\infty-J_0\right)}{\left[1-\beta\bar{X}\right]^m}\right]\\&=-\frac{\sigma_D\kappa}{2\pi E_\infty}\underbrace{\int_1^\infty\left[\frac{1}{\left[1+\beta\left(\eta-\bar{X}\right)\right]^m}\right]\frac{1}{\eta\sqrt{\eta-1}}d\eta}_{\varphi\left(\beta,\bar{X}\right)}+\frac{\sigma_D\kappa}{2E_\infty}\frac{1}{\left[1-\beta\bar{X}\right]^m}\end{aligned}. \tag{S43}$$

The next step is to evaluate the integral $\varphi\left(\beta,\bar{X}\right)$ in eq. (S43), i.e.,

$$\begin{aligned}\varphi\left(\beta,\bar{X}<0\right)&=\int_1^\infty\frac{1}{\left[1+\beta\left(\eta-\bar{X}\right)\right]^m}\frac{1}{\eta\sqrt{\eta-1}}d\eta\underset{\eta=1/w}{=}\beta^{-m}\int_0^1\left[1-w\left(\frac{\beta\bar{X}-1}{\beta}\right)\right]^{-m}\left(1-w\right)^{-1/2}w^{m-1/2}dw\\&=\beta^{-m}\frac{\Gamma\left(m+1/2\right)\Gamma\left(1/2\right)}{\Gamma\left(m+1\right)}{}_2F_1\left(m,m+\frac{1}{2},m+1,\frac{-\beta\left|\bar{X}\right|-1}{\beta}\right)\end{aligned}, \tag{S44}$$

where ${}_2F_1$ is the hypergeometric function. Combining eq. (S43) and (S44), we obtain eq. (50a) in the main text.

S26. Derivation of eq. (52a) and (52b)

To examine the asymptotic behavior of eq. (51) of the main text, we first obtain an alternative form of $\varphi\left(\beta,\bar{X}\le 0\right)$ by using the linear transformation of the hypergeometric function in eq. (S44), i.e.,

$$
{}_2F_1\left(m,m+\frac{1}{2},m+1,-z\right)=\frac{\Gamma(m+1)\Gamma(1/2)}{\Gamma(m+1/2)}(z)^{-m}\,{}_2F_1\left(m,0,\frac{1}{2},-z\right)
$$
$$
+\frac{\Gamma(m+1)\Gamma(-1/2)}{\Gamma(m)\Gamma(1/2)}\left(\frac{\beta\left|\bar{X}\right|+1}{\beta}\right)^{-m-1/2}{}_2F_1\left(m+\frac{1}{2},\frac{1}{2},\frac{3}{2},-\frac{1}{z}\right), \tag{S45}
$$

where $z\equiv(\beta\left|\bar{X}\right|+1)/\beta$. Since ${}_2F_1\left(m,0,1/2,-z\right)=1$, eq. (S45) reduces to

$$
F\left(m,m+\frac{1}{2},m+1,-z\right)=\frac{\Gamma(m+1)\Gamma(1/2)}{\Gamma(m+1/2)}z^{-m}+\frac{\Gamma(m+1)\Gamma(-1/2)}{\Gamma(m)\Gamma(1/2)}z^{-m-1/2}F\left(m+\frac{1}{2},\frac{1}{2},\frac{3}{2},\frac{-1}{z}\right). \tag{S46}
$$

Equation (S46) results in two equivalent forms of φ:

$$
\varphi\left(\beta,\bar{X}<0\right)=\beta^{-m}\frac{\Gamma\left(m+1/2\right)\Gamma\left(1/2\right)}{\Gamma\left(m+1\right)}F\left(m,m+\frac{1}{2},m+1,\frac{-\beta\left|\bar{X}\right|-1}{\beta}\right), \tag{S47a}
$$

or

$$
\varphi\left(\beta,\bar{X}<0\right)=\pi\left(\beta\left|\bar{X}\right|+1\right)^{-m}+\frac{\Gamma\left(m+1/2\right)\Gamma(-1/2)}{\Gamma(m)}\beta^{-m}\left(\frac{\beta}{\beta\left|\bar{X}\right|+1}\right)^{m+1/2}F\left(m+\frac{1}{2},\frac{1}{2},\frac{3}{2},\frac{\beta}{-\beta\left|\bar{X}\right|-1}\right). \tag{S47b}
$$

The maximum residual strain occurs at the crack tip (i.e., $\bar{X}=0^-$). Using eq. (S43), we find

$$
\varepsilon_{22}\left(\bar{X}=0^-,Y=0\right)=\frac{\sigma_D\kappa}{2E_\infty}\left(1-\frac{\varphi\left(\beta,\left|\bar{X}\right|=0\right)}{\pi}\right). \tag{S48a}
$$

For $\beta<1$, we use eq. (S47b) to obtain

$$
\varphi\left(\beta,\left|\bar{X}\right|=0\right)=\pi+\frac{\Gamma\left(m+1/2\right)\Gamma(-1/2)}{\Gamma(m)}\sqrt{\beta}\,{}_2F_1\left(m+\frac{1}{2},\frac{1}{2},\frac{3}{2},-\beta\right). \tag{S48b}
$$

Substituting eq. (S48b) into eq. (S48a), we find that for high crack velocity ($\beta<<1$), the maximum residual strain is:

$$
\varepsilon_{22}\left(\bar{X}=0^-,Y=0,\beta<<1\right)\approx\frac{\sigma_D\kappa}{2E_\infty}\frac{2\Gamma\left(m+1/2\right)\sqrt{\pi}}{\Gamma(m)}\sqrt{\beta}, \tag{S48c}
$$

which is eq. (52a) in the main text. Therefore, the maximum residual strain vanishes as the reciprocal of the square root of the crack velocity since $\beta=\alpha/vt_c$. For $\beta>1$, we use eq. (S47a) to evaluate φ at $\left|\bar{X}\right|=0$ and obtain

$$\varphi\left(\beta,\left|\bar{X}\right|=0,\right)=\beta^{-m}\frac{\Gamma\left(m+1/2\right)\Gamma\left(1/2\right)}{\Gamma\left(m+1\right)}F\left(m,m+\frac{1}{2},m+1,\frac{-1}{\beta}\right)\ . \tag{S49a}$$

For low crack velocity (i.e., $\beta>>1$), the maximum residual strain is given by taking the limit of $1/\beta\to 0$ in eq. (S49a), i.e.,

$$\varepsilon_{22}\left(\bar{X}=0^{-},Y=0,\beta>>1\right)\approx\frac{\sigma_D\kappa}{2E_\infty}\left(1-\frac{1}{\sqrt{\pi}}\beta^{-m}\frac{\Gamma\left(m+1/2\right)}{\Gamma\left(m+1\right)}\right), \tag{S49b}$$

which is eq. (52b) in the main text.

S27. Derivation of eq. (53a) and (53b)

To derive eq. (53a), we use the alternative form of φ in eq. (S47b) and note that

$$\frac{\left[1+\beta\left|\bar{X}\right|\right]^m\varphi\left(\beta,\bar{X}\right)}{\pi}=1+\frac{\Gamma\left(m+1/2\right)\Gamma(-1/2)}{\pi\Gamma(m)}\sqrt{\frac{\beta}{\beta\left|\bar{X}\right|+1}}\,{}_2F_1\left(m+1/2,1/2,3/2,\frac{\beta}{-\beta\left|\bar{X}\right|-1}\right). \tag{S50a}$$

Combining eq. (S40a) with eq. (50a) of the main text, we obtain

$$\varepsilon_{22}\left(\bar{X}<0,Y=0\right)=-\frac{\sigma_D\kappa}{2E_\infty\left[1+\beta\left|\bar{X}\right|\right]^m}\frac{\Gamma\left(m+1/2\right)\Gamma(-1/2)}{\pi\Gamma(m)}\sqrt{\frac{\beta}{\beta\left|\bar{X}\right|+1}}\,{}_2F_1\left(m+\frac{1}{2},\frac{1}{2},\frac{3}{2},\frac{\beta}{-\beta\left|\bar{X}\right|-1}\right), \tag{S50b}$$

which is eq. (53a) of the main text. In the limit of $\beta\left|\bar{X}\right|>>1$, $\beta/(1+\beta\,|\,X\,|)$ approaches zero. Since ${}_2F_1\left(m+1/2,1/2,3/2,0\right)=1$ and $\Gamma(-1/2)=-2\sqrt{\pi}$, the first order behavior of the right hand side of eq. (S50b) is

$$\varepsilon_{22}\left(\left|\beta\bar{X}\right|>>1,Y=0\right)\approx\frac{\sigma_D\kappa}{E_\infty\left(\beta\left|\bar{X}\right|\right)^{m+1/2}}\frac{\Gamma\left(m+1/2\right)}{\pi\Gamma(m)}\sqrt{\pi\beta}\ , \tag{S50c}$$

which is eq. (53b) of the main text.

S28. Derivation of eq. (54)

For the special case of PLS with m = 1/2, we use eq. (S47a) to show that the function φ can be reduced to an elementary function. As shown in 15.15 of Abramowitz and Stegun [10], for the following set of parameters the hypergeometric function is elementary:

$$\varphi\left(\beta,\bar{X}<0,m=\frac{1}{2}\right)=2\beta^{-1/2}\,{}_2F_1\left(\frac{1}{2},1,\frac{3}{2},\frac{-\beta\left|\bar{X}\right|-1}{\beta}\right)=2\beta^{-1/2}\sqrt{\frac{\beta}{1+\beta\bar{X}}}\tan^{-1}\left(\sqrt{\frac{1+\beta\left|\bar{X}\right|}{\beta}}\right)$$
$$=2\sqrt{\frac{1}{1+\beta\left|\bar{X}\right|}}\tan^{-1}\left(\sqrt{\frac{1+\beta\left|\bar{X}\right|}{\beta}}\right) \quad \text{(S51a)}$$

Therefore, the residual strain for m = 1/2 is given by the following using eq. (50a) of the main text

$$\varepsilon_{22}\left(\bar{X}<0,Y=0,m=\frac{1}{2}\right)=\frac{\sigma_D\kappa}{2E_\infty\left[1+\beta\left|\bar{X}\right|\right]^{1/2}}\left[1-\frac{\left[1+\beta\bar{X}\right]^{1/2}\varphi\left(\beta,\bar{X}\right)}{\pi}\right]$$
$$=\frac{\sigma_D\kappa}{2E_\infty\left[1+\beta\left|\bar{X}\right|\right]^{1/2}}\left[1-\frac{2}{\pi}\tan^{-1}\left(\sqrt{\frac{1+\beta\left|\bar{X}\right|}{\beta}}\right)\right], \quad \text{(S51b)}$$

which is eq. (54) of the main text.

S29. Derivation of eq. (55a)

The normalized crack opening displacement $\bar{u}_{cod}$ in eq.(6a) for the case of GMS is

$$\bar{u}_{cod}\left(\bar{X}\le 1\right)\equiv\frac{u_{cod}}{\delta_0}=\frac{G}{G_0}F(\bar{X})+\frac{G}{G_0}\kappa\sum_{n=1}^{N}a_n\exp\left(\beta_n\bar{X}\right)\int_{\bar{X}}^{1}\exp\left(-\beta_n\xi\right)F'\left(\xi\right)d\xi\ , \quad \text{(S52a)}$$

where $\beta_n=\alpha/vt_n$. The integral in eq. (S52a) is

$$\int_{\bar{X}}^{1}\exp\left(-\beta_n\xi\right)F'\left(\xi\right)d\xi=-\frac{1}{\beta_n}\int_{\bar{X}}^{1}F'\left(\xi\right)d\left[\exp\left(-\beta_n\xi\right)-1\right]$$
$$=-\frac{1}{\beta_n}\left[\left[\exp\left(-\beta_n\xi\right)-1\right]F'\left(\xi\right)\Big|_{\bar{X}}^{1}-\int_{\bar{X}}^{1}F''\left(\xi\right)\left[\exp\left(-\beta_n\xi\right)-1\right]d\xi\right], \quad \text{(S52b)}$$
$$=-\frac{1}{\beta_K^{(n)}}\left\{\left[1-\exp\left(-\beta_n\bar{X}\right)\right]F'\left(\bar{X}\right)-\frac{Q\left(\beta_n,\bar{X}\right)}{4}\right\}$$

where

$$Q\left(\beta_n,\bar{X}\right)\equiv 4\int_{\bar{X}}^{1}F''\left(\xi\right)\left[\exp\left(-\beta_K^{(n)}\xi\right)-1\right]d\xi=\int_{\bar{X}}^{1}\frac{\exp\left(-\beta_n\xi\right)-1}{\xi\sqrt{1-\xi}}d\xi\ . \quad \text{(S52c)}$$

Recall that $F'(\bar{X})$ is given in eq. (6b) of the main text and $F''(\xi)$ is given in eq. (S12b). Substituting eq. (S52b) into eq. (S52a), we obtain eq. (55a) of the main text:

$$\bar{u}_{cod}\left(\bar{X}\le 1\right)=\frac{G}{G_0}F(\bar{X})+\frac{G}{G_0}\kappa\sum_{n=1}^{N}a_n\exp\left(\beta_n\bar{X}\right)\left\{\left[\frac{1-\exp\left(-\beta_n\bar{X}\right)}{-\beta_n}\right]F'\left(\bar{X}\right)+\frac{Q\left(\beta_n,\bar{X}\right)}{4\beta_n}\right\}. \quad \text{(S53)}$$
$$=\frac{G}{G_0}\left[F(\bar{X})+\kappa\sum_{n=1}^{N}a_n\left[\frac{1-\exp\left(\beta_n\bar{X}\right)}{\beta_n}\right]F'\left(\bar{X}\right)+\kappa\sum_{n=1}^{N}\frac{a_n\exp\left(\beta_n\bar{X}\right)}{4\beta_n}Q\left(\beta_n,\bar{X}\right)\right]$$

Note the first two terms of eq. (S53) is elementary while the last term cannot be integrated in closed form.

S30. Derivation of eq. (57a) and (57b)

Here we propose an approximation that allows us to evaluate the integral $Q\left(\beta_n,\bar{X}\right)$ in eq. (S52c). Although eq. (S52a) and (S52c) are defined for $\bar{X}\le 1$, i.e., including both the crack surface and the cohesive zone, here we are interested in the COD for $\bar{X}\le 0$ (i.e., behind the crack tip). Therefore, we can write $Q\left(\beta_n,\bar{X}\right)$ as the sum of two integrals:

$$Q\left(\beta_n,\bar{X}\le 0\right)=\underbrace{\int_0^1\frac{\left[\exp\left(-\beta_n\xi\right)-1\right]}{\xi\sqrt{1-\xi}}d\xi}_{Q_1(\beta_n)}+\underbrace{\int_{\bar{X}}^0\frac{\left[\exp\left(-\beta_n\xi\right)-1\right]}{\xi\sqrt{1-\xi}}d\xi}_{Q_2(\beta_n,\bar{X})}. \quad \text{(S54)}$$

The first integral, $Q_1\left(\beta_n\right)$ is independent of $\bar{X}$ and reflects the effect of cohesive stress on the crack opening displacement. From eq. (S12c), (S13a) and (S13b), we see that

$$Q_1\left(\beta_n\right)=\lim_{\varepsilon\to 0}\frac{\Gamma\left(\varepsilon\right)\Gamma\left(1/2\right)}{\Gamma\left(\varepsilon+1/2\right)}\left[M\left(\varepsilon,\frac{1}{2}+\varepsilon,-\beta_n\right)-1\right]=-\beta_n\sqrt{\pi}\sum_{k=0}^{\infty}\frac{\left(-\beta_n\right)^k}{\left(k+1\right)\Gamma\left(k+3/2\right)}. \quad \text{(S55)}$$

which depends only on β_n. This term contributes little to the COD at large distances from the crack tip since it decays exponentially fast due to the factor $\exp\left(\beta_n\bar{X}\right)$ in the last term of eq. (S53) (recall that $\bar{X}<0$). The relevant term is $Q_2\left(\beta_n\bar{X}\right)$ which can be written as, after changing the integration variable ξ to $\bar{X}(1-w)$:

$$Q_2\left(\beta_n\bar{X}\right)=-\frac{e^{\beta_n|\bar{X}|}}{\sqrt{1+|\bar{X}|}}\int_0^1\frac{\left[e^{-\beta_n|\bar{X}|w}-e^{-\beta_n|\bar{X}|}\right]}{(1-w)\sqrt{1-\frac{|\bar{X}|w}{1+|\bar{X}|}}}dw. \quad \text{(S56)}$$

Next, we assume $|\bar{X}|$ to be sufficiently large so that $1-|\bar{X}|w/\left(1+|\bar{X}|\right)\approx 1-w$, then

$$Q_2\left(\beta_n \bar{X}\right) \approx -\frac{e^{\beta_n|\bar{X}|}}{\sqrt{1+|\bar{X}|}} \int_0^1 \frac{\left[e^{-\beta_n|\bar{X}|w} - e^{-\beta_n|\bar{X}|}\right]}{(1-w)^{3/2}} dw = -\frac{1}{\sqrt{1+|\bar{X}|}} \int_0^1 \frac{\left[e^{\beta_n|\bar{X}|\eta} - 1\right]}{\eta^{3/2}} d\eta$$

$$= \frac{-2}{\sqrt{1+|\bar{X}|}} \left\{ \underbrace{\eta^{-1/2}\left[e^{\beta_n|\bar{X}|\eta} - 1\right]\Big|_0^1}_{e^{\beta_n|\bar{X}|}-1} - \beta_n|\bar{X}| \int_0^1 \frac{e^{\beta_n|\bar{X}|\eta}}{\eta^{1/2}} d\eta \right\} = \frac{-2}{\sqrt{1+|\bar{X}|}} \left(\left[e^{\beta_n|\bar{X}|} - 1\right] - \beta_n|\bar{X}| e^{\beta_n|\bar{X}|} \int_0^1 \frac{e^{-\beta_n|\bar{X}|s}}{\sqrt{1-s}} ds \right) \tag{S57}$$

For $\beta_n|\bar{X}| >> 1$, we have, neglecting exponentially small terms,

$$Q_2\left(\beta_n \bar{X}\right) \approx \frac{-2e^{\beta_n|\bar{X}|}}{\sqrt{1+|\bar{X}|}} \left(1 - \beta_n|\bar{X}| \left(\frac{1}{\beta_n|\bar{X}|} + \frac{1}{2\left(\beta_n|\bar{X}|\right)^2} + ... \right) \right) = \frac{-e^{\beta_n|\bar{X}|}}{\sqrt{1+|\bar{X}|}} \left(\frac{1}{\beta_n|\bar{X}|} + ... \right) . \tag{S58}$$

Substituting eq. (S58) into eq. (S53) and noting that $\beta_1 > .... > \beta_N$, we have

$$\bar{u}_{cod}\left(\bar{X} < 0, \beta_N|\bar{X}| >> 1\right) \approx \frac{G}{G_0} \left[F(\bar{X}) + \kappa \sum_{n=1}^{N} \frac{a_n}{\beta_n} F'\left(\bar{X}\right) + \kappa \sum_{n=1}^{N} \frac{a_n}{4\beta_n} \frac{-1}{\sqrt{1+|\bar{X}|}} \left(\frac{1}{\beta_n|\bar{X}|} + ... \right) \right] , \tag{S59}$$

which is eq. (57a) of the main text.

In particular, the ratio χ_{cod} defined in eq. (56a) of the main text in this limit is:

$$\chi_{cod}\left(\bar{X} < 0, \beta_N|\bar{X}| >> 1\right) \approx \frac{-\kappa \sum_{n=1}^{N} \frac{a_n}{\beta_n} F'\left(\bar{X}\right) + \frac{\kappa}{4\sqrt{1+|\bar{X}|}} \sum_{n=1}^{N} \frac{a_n}{\beta_n} \left(\frac{1}{\beta_n|\bar{X}|} + ... \right)}{F\left(\bar{X}\right)}$$

$$\approx \frac{\frac{\kappa}{2\sqrt{|\bar{X}|}} \sum_{n=1}^{N} \frac{a_n}{\beta_n} + \frac{\kappa}{4\sqrt{|\bar{X}|}} \sum_{n=1}^{N} \frac{a_n}{\beta_n} \left(\frac{1}{\beta_n|\bar{X}|} + ... \right)}{\sqrt{|\bar{X}|}} = \frac{\kappa}{2} \sum_{n=1}^{N} \frac{a_n}{\beta_n|\bar{X}|} \left(1 + \frac{1}{2\beta_n|\bar{X}|} + ... \right) \tag{S60}$$

which is eq. (57b) in the main text.

S31. Derivation of eq. (59): asymptotic behavior of COD for PLS

To understand the asymptotic behavior of COD in eq. (58) of the main text, the key integral to be studied is

$$Q_{PL}\left(\bar{X}\le 1,\beta,m\right)\equiv\int_{\bar{X}}^{1}\frac{F'\left(\xi\right)d\xi}{\left(1+\beta\left(\xi-\bar{X}\right)\right)^{m}}\ . \tag{S61a}$$

We are primarily interested in the COD for $\bar{X}<0$. In particular, for $\left|\bar{X}\right|>1$ (so we are at least one cohesive distance away behind the crack tip), we write

$$Q_{PL}\left(\bar{X}\le 0,\beta,m\right)=\int_{0}^{1}\frac{F'\left(\xi\right)d\xi}{\left(1+\beta\left(\xi-\bar{X}\right)\right)^{m}}+\int_{\bar{X}}^{0}\frac{F'\left(\xi\right)d\xi}{\left(1+\beta\left(\xi-\bar{X}\right)\right)^{m}}. \tag{S61b}$$

The first integral is,

$$\int_{0}^{1}\frac{F'\left(\xi\right)d\xi}{\left(1+\beta\left(\xi-\bar{X}\right)\right)^{m}}=\int_{0}^{1}\frac{F'\left(\xi\right)d\xi}{\left(1+\beta\left|\bar{X}\right|+\beta\xi\right)^{m}}=\frac{1}{\left(1+\beta\left|\bar{X}\right|\right)^{m}}\int_{0}^{1}\frac{F'\left(\xi\right)d\xi}{\left(1+\frac{\beta\xi}{1+\beta\left|\bar{X}\right|}\right)^{m}}. \tag{S62a}$$

As long as $g\equiv\beta/\left(1+\beta\left|\bar{X}\right|\right)<1$ (for example when $\left|\bar{X}\right|\ge 1$ or $\beta<1$), the power series expansion

$$\left(1+g\xi\right)^{-m}=1-\frac{m\beta\xi}{1+\beta\left|\bar{X}\right|}+\ldots=\sum_{k=0}^{\infty}\frac{\left(m\right)_{k}}{k!}\left(-g\xi\right)^{k} \tag{S62b}$$

is uniformly convergent in $g\xi\in\left[0,1\right]$ and hence can be integrated term by term. Note that $\left(m\right)_{k}=\Gamma(m+k)/\Gamma(m)$. Therefore, the integral in eq. (S62a) is

$$\begin{aligned}\int_{0}^{1}\frac{F'\left(\xi\right)d\xi}{\left(1+\beta\left(\xi-\bar{X}\right)\right)^{m}}&=\frac{1}{\left(1+\beta\left|\bar{X}\right|\right)^{m}}\sum_{k=0}^{\infty}\frac{\left(m\right)_{k}}{k!}\left(-g\right)^{k}\int_{0}^{1}\xi^{k}F'\left(\xi\right)d\xi\\&=\frac{-\sqrt{\pi}}{4\left(1+\beta\left|\bar{X}\right|\right)^{m}}\sum_{k=0}^{\infty}\frac{\left(m\right)_{k}\left(-1\right)^{k}\beta^{k}}{\left(k+1\right)\Gamma\left(k+3/2\right)}\left(1+\beta\left|\bar{X}\right|\right)^{-k}\end{aligned} \tag{S62c}$$

This is because

$$\begin{aligned}\int_{0}^{1}\xi^{k}F'\left(\xi\right)dr&=\frac{1}{k+1}\int_{0}^{1}F'\left(\xi\right)d\xi^{k+1}=\frac{1}{k+1}\left[\underbrace{F'\left(\xi\right)\xi^{k+1}\Big|_{0}^{1}}_{0}+\frac{1}{4}\int_{0}^{1}\xi^{k+1}d\ln\left(\frac{\sqrt{1-\xi}+1}{1-\sqrt{1-\xi}}\right)\right]\\&=\frac{-1}{4\left(k+1\right)}\left[\int_{0}^{1}\xi^{k+1}\frac{d\xi}{\xi\sqrt{1-\xi}}\right]=\frac{-1}{4\left(k+1\right)}\left[\int_{0}^{1}\frac{\xi^{k}d\xi}{\sqrt{1-\xi}}\right]=\frac{-1}{4\left(k+1\right)}\frac{\Gamma\left(k+1\right)\sqrt{\pi}}{\Gamma\left(k+3/2\right)}\end{aligned}. \tag{S62d}$$

Note that eq. (S62c) is *exact* for all $-\bar{X}\ge 1$. For $\beta\left|\bar{X}\right|>>1$, the first order behavior is obtained by keeping the first term of the series,

$$\int_0^1 \frac{F'(\xi)\,d\xi}{\left(1+\beta\left(\xi-\bar{X}\right)\right)^m} \approx \frac{-1}{2\left(1+\beta\left|\bar{X}\right|\right)^m}. \tag{S62e}$$

This result shows that the effect of cohesive stress on the COD decays rather slowly for the PLS, especially for fast cracks where β is small. Since we are interested in $\left|\bar{X}\right|>1$, $\beta\left|\bar{X}\right| \ll 1 \Rightarrow \beta \ll 1$ from eq. (S62c), we see that eq. (S62e) holds also for this case.

The asymptotic behavior of the second integral in eq. (S61b) requires more work. Integration by parts leads to

$$\begin{aligned}
\int_{\bar{X}}^0 \frac{F'(\xi)\,d\xi}{\left(1+\beta\left(\xi-\bar{X}\right)\right)^m} &= \frac{1}{\beta(1-m)} \int_{-\left|\bar{X}\right|}^0 F'(\xi) d\left[\left(1+\beta\left(\xi-\bar{X}\right)\right)^{1-m} - \left(1+\beta\left|\bar{X}\right|\right)^{1-m}\right] \\
&= \frac{1}{\beta(1-m)}\left\{-F'\left(-\left|\bar{X}\right|\right)\left[1-\left(1+\beta\left|\bar{X}\right|\right)^{1-m}\right] - \frac{1}{4}\int_{-\left|\bar{X}\right|}^0 \frac{\left(1+\beta\left(\xi-\bar{X}\right)\right)^{1-m} - \left(1+\beta\left|\bar{X}\right|\right)^{1-m}}{\xi\sqrt{1-\xi}}\,d\xi\right\} \qquad \text{(S63a)} \\
&= \frac{1}{\beta(1-m)}\left\{-F'\left(-\left|\bar{X}\right|\right)\left[1-\left(1+\beta\left|\bar{X}\right|\right)^{1-m}\right] - \frac{\left(1+\beta\left|\bar{X}\right|\right)^{1-m}}{4}\int_{-\left|\bar{X}\right|}^0 \frac{(1+g\xi)^{1-m}-1}{\xi\sqrt{1-\xi}}\,d\xi\right\}
\end{aligned}$$

where $g \equiv \beta/(1+\beta\left|\bar{X}\right|)$. Note the removable singularity of the integrand at the upper integration limit. Next, we make the change of variable $\xi = -\left|X\right|\eta$ and eq. (S63a) becomes:

$$\int_{\bar{X}}^0 \frac{F'(\xi)\,d\xi}{\left(1+\beta\left(\xi-\bar{X}\right)\right)^m} = \frac{1}{\beta(1-m)}\left\{-F'\left(-\left|\bar{X}\right|\right)\left[1-\left(1+\beta\left|\bar{X}\right|\right)^{1-m}\right] + \frac{\left(1+\beta\left|\bar{X}\right|\right)^{1-m}}{4}\int_0^1 \frac{\left(1-g\left|\bar{X}\right|\eta\right)^{1-m}-1}{\eta\sqrt{1+\left|\bar{X}\right|\eta}}\,d\eta\right\} \tag{S63b}$$

Note that $g\left|\bar{X}\right| = \beta\left|\bar{X}\right|/(1+\beta\left|\bar{X}\right|) < 1$ for all β. Hence we can expand $\left(1-g\left|\bar{X}\right|\eta\right)^{1-m}$ as a uniformly convergent power series in $[0,1]$, i.e.,

$$\left(1-g\left|\bar{X}\right|\eta\right)^{1-m} = \sum_{k=0}^{\infty} \frac{(1-m)_k}{k!}\left(g\left|\bar{X}\right|\right)^k. \tag{S64a}$$

Therefore, $\left[\left(1-g\left|\bar{X}\right|\eta\right)^{1-m}-1\right]/\eta$ is analytic at zero since the numerator has a simple zero there. We can develop a power series solution since term by term integration is legitimate. The series solution of the last integral in eq. (S63b) is

$$\int_0^1 \frac{\left(1-g\left|\bar{X}\right|\eta\right)^{1-m}-1}{\eta\sqrt{1+\left|\bar{X}\right|\eta}}d\eta=\sum_{k=1}^{\infty}\frac{(m-1)_k\left(g\left|\bar{X}\right|\right)^k}{k!}\int_0^1\frac{\eta^{k-1}d\eta}{\sqrt{1+\left|\bar{X}\right|\eta}}=\sum_{n=0}^{\infty}\frac{(m-1)_{n+1}\,c_n\left(g\left|\bar{X}\right|\right)^{n+1}}{(n+1)!}, \tag{S64b}$$

where

$$c_n=\int_0^1\frac{\eta^n d\eta}{\sqrt{1+\left|\bar{X}\right|\eta}}=\frac{2}{\left|\bar{X}\right|^{n+1}}\sum_{k=0}^{n}\frac{(-1)^k}{2n-2k+1}\binom{n}{k}\left[\left(1+\left|\bar{X}\right|\right)^{n-k+1/2}-1\right]. \tag{S64c}$$

So far, eq. (S64b) is exact.

To get asymptotic behavior for $\beta\left|\bar{X}\right|\ll 1$, we note that

$$\beta\left|\bar{X}\right|\ll 1\Rightarrow g\left|\bar{X}\right|=\frac{\beta\left|\bar{X}\right|}{1+\beta\left|\bar{X}\right|}\to 0 \tag{S65a}$$

Hence the first order behavior of the integral in eq. (S64b) is

$$\int_0^1\frac{\left(1-g\left|\bar{X}\right|\eta\right)^{1-m}-1}{\eta\sqrt{1+\left|\bar{X}\right|\eta}}d\eta\approx-(1-m)c_0 g\left|\bar{X}\right|=-2(1-m)\frac{\beta\left|\bar{X}\right|}{1+\beta\left|\bar{X}\right|}\left(\sqrt{1+\left|\bar{X}\right|}-1\right),\ \ \beta\left|\bar{X}\right|\ll 1 \tag{S65b}$$

Combining eq. (S65b) with eq. (S63b), we have, for $\beta\left|\bar{X}\right|\ll 1$ (or small β since $\left|\bar{X}\right|>1$):

$$\int_{\bar{X}}^{0}\frac{F'(\xi)d\xi}{\left(1+\beta\left(\xi-\bar{X}\right)\right)^m}\approx\frac{1}{\beta(1-m)}\left\{-F'\left(-\left|\bar{X}\right|\right)\left[1-\left(1+\beta\left|\bar{X}\right|\right)^{1-m}\right]-\frac{(1-m)\beta\left|\bar{X}\right|\left(1+\beta\left|\bar{X}\right|\right)^{-m}}{2}\left(\sqrt{1+\left|\bar{X}\right|}-1\right)\right\}$$

$$\approx\left\{\left|\bar{X}\right|F'\left(-\left|\bar{X}\right|\right)-\frac{\left|\bar{X}\right|}{2}\left(\sqrt{1+\left|\bar{X}\right|}-1\right)\right\} \tag{S65c}$$

Surprisingly, the asymptotic behavior for small $\beta\left|\bar{X}\right|$ is approximately independent of *m*.

Next, consider the behavior where $\beta\left|\bar{X}\right|\gg 1\Rightarrow g\left|\bar{X}\right|\to 1$, the last integral in eq. (S63b) is

$$\int_0^1\frac{\left(1-g\left|\bar{X}\right|\eta\right)^{1-m}-1}{\eta\sqrt{1+\left|\bar{X}\right|\eta}}d\eta\approx\int_0^1\frac{(1-\eta)^{1-m}-1}{\eta\sqrt{1+\left|\bar{X}\right|\eta}}d\eta\,. \tag{S66a}$$

This means in this limit the integral in eq. (S66a) is independent of β. We are mostly interested in $\left|\bar{X}\right|>>1$, so eq. (S66a) can be approximated by

$$\int_0^1 \frac{\left(1-g\left|\bar{X}\right|\eta\right)^{1-m}-1}{\eta\sqrt{1+\left|\bar{X}\right|\eta}}d\eta \approx \frac{1}{\sqrt{\left|\bar{X}\right|}}\int_0^1 \frac{(1-\eta)^{1-m}-1}{\eta^{3/2}}d\eta = \frac{-2}{\sqrt{\left|\bar{X}\right|}}\int_0^1 \left((1-\eta)^{1-m}-1\right)d\eta^{-1/2}$$

$$= \frac{-2}{\sqrt{\left|\bar{X}\right|}}\left\{\left((1-\eta)^{1-m}-1\right)\eta^{-1/2}\Big|_0^1 + (1-m)\int_0^1 (1-\eta)^{-m}\eta^{-1/2}d\eta\right\} \tag{S66b}$$

$$= \frac{-2}{\sqrt{\left|\bar{X}\right|}}\left\{-1+(1-m)\frac{\Gamma(1/2)\Gamma(1-m)}{\Gamma(3/2-m)}\right\} = \frac{-2}{\sqrt{\left|\bar{X}\right|}}\left(\frac{\sqrt{\pi}\Gamma(2-m)}{\Gamma(3/2-m)}-1\right)$$

Substituting eq. (S66b) into eq. (S63b) and using the asymptotic behavior of $F'\left(-\left|\bar{X}\right|\right)$ for large $\left|\bar{X}\right|$ gives, for large $\beta\left|\bar{X}\right|$,

$$\int_{\bar{X}}^0 \frac{F'(\xi)d\xi}{\left(1+\beta\left(\xi-\bar{X}\right)\right)^m} = \frac{-\sqrt{\pi}\Gamma(2-m)}{2(1-m)\Gamma(3/2-m)}\frac{\left(\beta\left|\bar{X}\right|\right)^{\frac{1}{2}-m}}{\sqrt{\beta}}. \tag{S66c}$$

Combining eq. (S66c) and (S62e), we have

$$Q_{PL}\left(\bar{X}<0,\beta\left|\bar{X}\right|>>1,\beta,m\right) \approx \frac{-1}{2\left(\beta\left|\bar{X}\right|\right)^m} - \frac{\sqrt{\pi}\Gamma(2-m)}{2(1-m)\Gamma(3/2-m)}\frac{\left(\beta\left|\bar{X}\right|\right)^{\frac{1}{2}-m}}{\sqrt{\beta}} \tag{S67}$$

Therefore, the COD for $\beta\left|\bar{X}\right|>>1$ is :

$$\bar{u}_{cod}\left(\bar{X}<0,\beta\left|\bar{X}\right|>>1\right) = \bar{G}\sqrt{\left|\bar{X}\right|}\left[1-\kappa\left\{\frac{\sqrt{\beta}}{2\left(\beta\left|\bar{X}\right|\right)^{m+1/2}} + \frac{\sqrt{\pi}\Gamma(2-m)}{2(1-m)\Gamma(3/2-m)}\frac{1}{\left(\beta\left|\bar{X}\right|\right)^m}\right\}\right], \tag{S68}$$

which is eq. (59) of the main text.

S32. Derivation of eq. (60b) and (60c): exact solution for the special case *m* = 1/2

In the special case of $m = 1/2$, the integral in eq. (S61b) becomes:

$$Q_{PL}\left(\bar{X}\le 0,\beta,m=\frac{1}{2}\right) = \int_{\bar{X}}^1 \frac{F'(\xi)d\xi}{\left[1+\beta\left(\xi-\bar{X}\right)\right]^{1/2}} = \underbrace{\int_0^1 \frac{F'(\xi)d\xi}{\left[1+\beta\left(\xi-\bar{X}\right)\right]^{1/2}}}_{Q_{PL1}} + \underbrace{\int_{-|\bar{X}|}^0 \frac{F'(\xi)d\xi}{\left[1+\beta\left(\xi-\bar{X}\right)\right]^{1/2}}}_{Q_{PL1}} \tag{S69}$$

We apply integration by parts to the integral Q_{PL1}:

$$Q_{PL1} = \frac{2}{\beta}\int_0^1 F'(\xi)\, d\left(\left[1+\beta\left(\xi-\bar{X}\right)\right]^{1/2} - \sqrt{1+\beta\left|\bar{X}\right|}\right)$$

$$= \frac{2}{\beta}\left\{\underbrace{\left[F'(\xi)\left(\left[1+\beta\left(\xi-\bar{X}\right)\right]^{1/2} - \sqrt{1+\beta\left|\bar{X}\right|}\right)\right]_0^1}_{0} - \frac{1}{4}\int_0^1 \frac{\left(\left[1+\beta\left(\xi-\bar{X}\right)\right]^{1/2} - \sqrt{1+\beta\left|\bar{X}\right|}\right)}{\xi\sqrt{1-\xi}}\, d\xi\right\}, \quad \text{(S70)}$$

$$= -\frac{1}{2\beta}\int_0^1 \frac{\left(\sqrt{1+\beta\left(\xi-\bar{X}\right)} - \sqrt{1+\beta\left|\bar{X}\right|}\right)}{\xi\sqrt{1-\xi}}\, d\xi = -\frac{1}{\beta}\int_0^1 \frac{\left(\sqrt{1+\beta\left(1+\left|\bar{X}\right|-w^2\right)} - \sqrt{1+\beta\left|\bar{X}\right|}\right)}{\left(1-w^2\right)}\, dw$$

where we have used $F'(\xi=1)=0$, eq. (S12b) and the change of variable $\xi = 1-w^2$. Note that the integrand has no singularity at $w = 1$ (i.e., a removable singularity). To proceed further, we separate the two integrals, evaluate them at $s < 1$, then take limit as s approaches 1. The last integral in eq. (S70) is

$$-\sqrt{1+\beta\left|\bar{X}\right|}\int_0^s \frac{1}{\left(1-w^2\right)}dw = \frac{\sqrt{1+\beta\left|\bar{X}\right|}}{2}\ln\left(\frac{1-s}{1+s}\right). \quad \text{(S71)}$$

The first integral in eq. (S70) is

$$\int_0^s \frac{\sqrt{1+\beta\left(1+\left|\bar{X}\right|-w^2\right)}}{\left(1-w^2\right)}dw = \frac{1}{2}\left[\underbrace{\int_0^s \frac{\sqrt{1+\beta\left(1+\left|\bar{X}\right|-w^2\right)}}{(1-w)}dw}_{H_1} + \underbrace{\int_0^1 \frac{\sqrt{1+\beta\left(1+\left|\bar{X}\right|-w^2\right)}}{1+w}dw}_{H_2}\right]. \quad \text{(S72)}$$

Note that the second integral in eq. (S72) has no singularity at $w = 1$, and so we have set $s = 1$. The first integral is

$$H_1 = \int_{1-s}^1 \frac{\sqrt{1+\beta\left(1+\left|\bar{X}\right|-(1-q)^2\right)}}{q}dq = \int_{1-s}^1 \frac{\sqrt{1+\beta\left|\bar{X}\right|+2\beta q-\beta v^2}}{q}dq\,. \quad \text{(S73)}$$

This integral can be evaluated exactly (see 2.267 on Page 84 of [7]) and is

$$H_1 = \left(\sqrt{1+\beta\left(1+\left|\bar{X}\right|\right)} - \sqrt{1+\beta\left|\bar{X}\right|}\right) + \sqrt{\beta}\sin^{-1}\left(\frac{\sqrt{\beta}}{\sqrt{1+\beta\left(1+\left|\bar{X}\right|\right)}}\right)$$
$$-\sqrt{1+\beta\left|\bar{X}\right|}\ln\left(\frac{\left(1+\beta\left|\bar{X}\right|\right)+\beta+\sqrt{1+\beta\left|\bar{X}\right|}\sqrt{1+\beta\left(1+\left|\bar{X}\right|\right)}}{2\left(1+\beta\left|\bar{X}\right|\right)}(1-s)\right). \quad \text{(S74)}$$

Next, we compute H_2 in eq. (S72). Using a change of variable $q = 1+w$, we have

$$H_2 = \int_0^1 \frac{\sqrt{1+\beta\left(1+\left|\bar{X}\right|-w^2\right)}}{1+w}dw = \int_1^2 \frac{\sqrt{1+\beta\left(1+\left|\bar{X}\right|-(q-1)^2\right)}}{q}dq\,. \tag{S75a}$$

Again, this integral can be evaluated exactly:

$$H_2 = \left(\sqrt{1+\beta\left|\bar{X}\right|}-\sqrt{1+\beta\left(1+\left|\bar{X}\right|\right)}\right)-\sqrt{1+\beta\left|\bar{X}\right|}\ln\left(\frac{\left(1+\beta\left|\bar{X}\right|\right)+\beta}{\left(\left(1+\beta\left|\bar{X}\right|\right)+\beta+\sqrt{1+\beta\left|\bar{X}\right|}\sqrt{1+\beta\left(1+\left|\bar{X}\right|\right)}\right)}\right) \tag{S75b}$$
$$+\sqrt{\beta}\sin^{-1}\left(\frac{\sqrt{\beta}}{\sqrt{1+\beta\left(1+\left|\bar{X}\right|\right)}}\right)$$

Adding eq. (S74) and (S75b), we have

$$\frac{H_1+H_2}{2} = -\frac{\sqrt{1+\beta\left|\bar{X}\right|}}{2}\ln\left(\frac{\beta+\left(1+\beta\left|\bar{X}\right|\right)}{2\left(1+\beta\left|\bar{X}\right|\right)}\right)+\sqrt{\beta}\sin^{-1}\left(\frac{\sqrt{\beta}}{\sqrt{1+\beta\left(1+\left|\bar{X}\right|\right)}}\right)-\frac{\sqrt{1+\beta\left|\bar{X}\right|}}{2}\ln(1-s)\,. \tag{S76}$$

Adding eq. (S76) to eq. (S71) and noting that the singular terms proportional to $\ln(1-s)$ are canceled, we obtain the integral in eq. (S72), i.e.,

$$\int_0^1 \frac{\left(\sqrt{1+\beta\left(1+\left|\bar{X}\right|-w^2\right)}-\sqrt{1+\beta\left|\bar{X}\right|}\right)}{\left(1-w^2\right)}dw$$
$$= -\frac{\sqrt{1+\beta\left|\bar{X}\right|}}{2}\ln\left(\frac{\beta+\left(1+\beta\left|\bar{X}\right|\right)}{2\left(1+\beta\left|\bar{X}\right|\right)}\right)+\sqrt{\beta}\sin^{-1}\left(\frac{\sqrt{\beta}}{\sqrt{1+\beta\left(1+\left|\bar{X}\right|\right)}}\right)-\frac{\sqrt{1+\beta\left|\bar{X}\right|}}{2}\ln(2)\ . \tag{S77}$$
$$= -\frac{\sqrt{1+\beta\left|\bar{X}\right|}}{2}\ln\left(1+\frac{\beta}{1+\beta\left|\bar{X}\right|}\right)+\sqrt{\beta}\sin^{-1}\left(\frac{\sqrt{\beta}}{\sqrt{1+\beta\left(1+\left|\bar{X}\right|\right)}}\right)$$

Therefore,

$$Q_{PL1} = \frac{\sqrt{1+\beta\left|\bar{X}\right|}}{2\beta}\ln\left(1+\frac{\beta}{1+\beta\left|\bar{X}\right|}\right)-\frac{1}{\sqrt{\beta}}\sin^{-1}\left(\frac{\sqrt{\beta}}{\sqrt{1+\beta\left(1+\left|\bar{X}\right|\right)}}\right) \tag{S78}$$
$$= \frac{\sqrt{b}}{2\beta}\ln\left(\frac{b+\beta}{b}\right)-\frac{1}{\sqrt{\beta}}\sin^{-1}\left(\frac{\sqrt{\beta}}{\sqrt{b+\beta}}\right)$$

where $b = 1 + \beta\left|\bar{X}\right|$. Equation (S78) is eq. (60b) of the main text. Here we consider the asymptotic behavior of eq. (S78) in the limit of $\beta\left|\bar{X}\right| >> 1$. For $\beta\left|\bar{X}\right| >> 1$, we have

$$\frac{\sqrt{1+\beta\left|\bar{X}\right|}}{2\beta}\ln\left(1+\frac{\beta}{1+\beta\left|\bar{X}\right|}\right) \approx \frac{\sqrt{\left|\bar{X}\right|}}{2\sqrt{\beta}}\ln\left(1+\frac{1}{\left|\bar{X}\right|}\right), \tag{S79a}$$

$$\frac{1}{\sqrt{\beta}}\sin^{-1}\left(\frac{\sqrt{\beta}}{\sqrt{1+\beta\left(1+\left|\bar{X}\right|\right)}}\right) \approx \frac{1}{\sqrt{\beta}}\sin^{-1}\left(\frac{1}{\sqrt{1+\left|\bar{X}\right|}}\right) \quad . \tag{S79b}$$

Therefore,

$$Q_{PL1}\left(\beta\left|\bar{X}\right| >> 1, m=\frac{1}{2}\right) \approx \frac{1}{\sqrt{\beta}}\left\{\frac{\sqrt{\left|\bar{X}\right|}}{2}\ln\left(1+\frac{1}{\left|\bar{X}\right|}\right) - \sin^{-1}\left(\frac{1}{\sqrt{1+\left|\bar{X}\right|}}\right)\right\} \tag{S79c}$$

In particular, if $\left|\bar{X}\right| >> 1$, then

$$Q_{PL1}\left(\beta\left|\bar{X}\right| >> 1, m=\frac{1}{2}\right) \approx \frac{1}{\sqrt{\beta}}\left\{\frac{1}{2\sqrt{\left|\bar{X}\right|}} - \frac{1}{\sqrt{\left|\bar{X}\right|}}\right\} = \frac{-1}{2\sqrt{\beta\left|\bar{X}\right|}} \quad . \tag{S79d}$$

Next, we evaluate Q_{PL2} in eq. (S69). Using integration by parts, we obtain

$$\begin{aligned}
Q_{PL2} &= \frac{2}{\beta}\int_{-\left|\bar{X}\right|}^{0} F'(\xi)\, d\left(\left[1+\beta\left(\xi-\bar{X}\right)\right]^{1/2} - \sqrt{1+\beta\left|\bar{X}\right|}\right) \\
&= \frac{2}{\beta}\left\{\underbrace{\left[F'(\xi)\left(\left[1+\beta\left(\xi-\bar{X}\right)\right]^{1/2} - \sqrt{1+\beta\left|\bar{X}\right|}\right)\right]_{-\left|\bar{X}\right|}^{0}}_{-F'\left(-\left|\bar{X}\right|\right)\left(1-\sqrt{1+\beta\left|\bar{X}\right|}\right)} - \frac{1}{4}\int_{-\left|\bar{X}\right|}^{0}\frac{\left(\left[1+\beta\left(\xi-\bar{X}\right)\right]^{1/2} - \sqrt{1+\beta\left|\bar{X}\right|}\right)}{\xi\sqrt{1-\xi}}d\xi\right\} \\
&= \frac{2}{\beta}F'\left(-\left|\bar{X}\right|\right)\left(\sqrt{1+\beta\left|\bar{X}\right|}-1\right) - \frac{1}{2\beta}\int_{-\left|\bar{X}\right|}^{0}\frac{\left(\sqrt{1+\beta\left(r-\bar{X}\right)} - \sqrt{1+\beta\left|\bar{X}\right|}\right)}{\xi\sqrt{1-\xi}}d\xi \\
&= \frac{2}{\beta}F'\left(-\left|\bar{X}\right|\right)\left(\sqrt{1+\beta\left|\bar{X}\right|}-1\right) + \underbrace{\frac{1}{\beta}\int_{1}^{\sqrt{1+\left|\bar{X}\right|}}\frac{\left(\sqrt{1+\beta\left(1+\left|\bar{X}\right|-w^2\right)} - \sqrt{1+\beta\left|\bar{X}\right|}\right)}{\left(w^2-1\right)}dw}_{H_3}
\end{aligned} \tag{S80a}$$

where we have used the change of variable: $\xi = 1 - w^2$. Therefore,

$$Q_{PL2} = \frac{2}{\beta} F'\left(-\left|\bar{X}\right|\right)\left(\sqrt{1+\beta\left|\bar{X}\right|}-1\right)+\frac{1}{\beta}H_3 . \tag{S80b}$$

We break H_3 into two integrals, i.e.,

$$H_3 = \int_1^{\sqrt{1+|\bar{X}|}} \frac{\left(\sqrt{1+\beta\left(1+\left|\bar{X}\right|-w^2\right)}-\sqrt{1+\beta\left|\bar{X}\right|}\right)}{\left(w^2-1\right)}dw = \lim_{\varepsilon\to 0}\left[\underbrace{\int_{1+\varepsilon}^{\sqrt{1+|\bar{X}|}} \frac{\sqrt{1+\beta\left(1+\left|\bar{X}\right|-w^2\right)}}{\left(w^2-1\right)}dw}_{P} - \int_{1+\varepsilon}^{\sqrt{1+|\bar{X}|}} \frac{\sqrt{1+\beta\left|\bar{X}\right|}}{\left(w^2-1\right)}dw\right] \tag{S81}$$

The last integral in eq. (S81) is

$$\begin{aligned} &-\int_{1+\varepsilon}^{\sqrt{1+|\bar{X}|}} \frac{\sqrt{1+\beta\left|\bar{X}\right|}}{\left(w^2-1\right)}dw = -\frac{\sqrt{b}}{2}\ln\left(\frac{w-1}{w+1}\right) = -\frac{\sqrt{b}}{2}\ln\left(\frac{\sqrt{1+\left|\bar{X}\right|}-1}{\sqrt{1+\left|\bar{X}\right|}+1}\frac{2}{\varepsilon}\right) \\ &= -\frac{\sqrt{b}}{2}\ln\left(2\frac{\sqrt{1+\left|\bar{X}\right|}-1}{\sqrt{1+\left|\bar{X}\right|}+1}\right)+\frac{\sqrt{b}}{2}\ln\varepsilon \end{aligned} \tag{S82a}$$

Recall that $b = 1+\beta\left|\bar{X}\right|$. The integral P in eq. (S81) is

$$\int_{1+\varepsilon}^{\sqrt{1+|\bar{X}|}} \frac{\sqrt{1+\beta\left(1+\left|\bar{X}\right|-w^2\right)}}{\left(w^2-1\right)}dw = \frac{1}{2}\left[\underbrace{\int_{1+\varepsilon}^{\sqrt{1+|\bar{X}|}} \frac{\sqrt{1+\beta\left(1+\left|\bar{X}\right|-w^2\right)}}{w-1}dw}_{P_1} - \underbrace{\int_{1+\varepsilon}^{\sqrt{1+|\bar{X}|}} \frac{\sqrt{1+\beta\left(1+\left|\bar{X}\right|-w^2\right)}}{w+1}dw}_{P_2}\right] \tag{S82b}$$

To proceed, let us use the notations that $b = 1+\beta\left|\bar{X}\right|$. By taking the limit $\varepsilon \to 0$ judiciously, we obtain

$$\begin{aligned} P_1 &= \int_{1+\varepsilon}^{\sqrt{1+|\bar{X}|}} \frac{\sqrt{1+\beta\left(1+\left|\bar{X}\right|-w^2\right)}}{w-1}dw = \int_{\varepsilon}^{\sqrt{1+|\bar{X}|}-1} \frac{\sqrt{1+\beta\left(1+\left|\bar{X}\right|-(1+r)^2\right)}}{r}dr \\ &= 1-\sqrt{b}-\sqrt{b}\ln\left[\frac{b-\beta\left(\sqrt{1+\left|\bar{X}\right|}-1\right)+\sqrt{b}}{2\omega\left(\sqrt{1+\left|\bar{X}\right|}-1\right)}\varepsilon\right]-\sqrt{\beta}\left[\sin^{-1}\left(\frac{\sqrt{b+\beta-1}}{\sqrt{b+\beta}}\right)-\sin^{-1}\left(\frac{\sqrt{\beta}}{\sqrt{b+\beta}}\right)\right] \end{aligned} \tag{S82c}$$

and

$$P_2 = \int_{1+\varepsilon}^{\sqrt{1+|\bar{X}|}} \frac{\sqrt{1+\beta\left(1+|\bar{X}|-w^2\right)}}{w+1}dw = \int_{2}^{1+\sqrt{1+|\bar{X}|}} \frac{\sqrt{1+\beta\left(1+|\bar{X}|-(v-1)^2\right)}}{v}dv$$

$$= \left[1-\sqrt{b}\right] - \sqrt{b}\ln\left[\frac{b+\beta\left(1+\sqrt{1+|\bar{X}|}\right)+\sqrt{b}}{\left(1+\sqrt{1+|\bar{X}|}\right)(b+\beta)}\right] + \sqrt{\beta}\left[\sin^{-1}\left(\frac{\sqrt{b+\beta-1}}{\sqrt{\beta+b}}\right) - \sin^{-1}\left(\frac{\sqrt{\beta}}{\sqrt{\beta+b}}\right)\right] \quad \text{(S82d)}$$

Combining eq. (S82d) and (S82d), we obtain

$$P = \frac{P_1 - P_2}{2} = \frac{\sqrt{b}}{2}\ln\left[\frac{b+\beta\left(1+\sqrt{1+|\bar{X}|}\right)+\sqrt{b}}{\left(1+\sqrt{1+|\bar{X}|}\right)(b+\beta)}\frac{2b\left(\sqrt{1+|\bar{X}|}-1\right)}{b-\beta\left(\sqrt{1+|\bar{X}|}-1\right)+\sqrt{b}}\right] - \frac{\sqrt{b}}{2}\ln\varepsilon$$
$$-\sqrt{\beta}\left[\sin^{-1}\left(\frac{\sqrt{\omega+\beta-1}}{\sqrt{\beta+\omega}}\right) - \sin^{-1}\left(\frac{\sqrt{\beta}}{\sqrt{\beta+\omega}}\right)\right] \quad \text{(S82e)}$$

Substituting eq. (S82e) into eq. (S81), we obtain

$$H_3 = P - \frac{\sqrt{b}}{2}\ln\left(2\frac{\sqrt{1+|\bar{X}|}-1}{\sqrt{1+|\bar{X}|}+1}\right) + \frac{\sqrt{b}}{2}\ln\varepsilon$$
$$= \frac{\sqrt{b}}{2}\ln\left[\frac{b+\beta\left(1+\sqrt{1+|\bar{X}|}\right)+\sqrt{b}}{b-\beta\left(\sqrt{1+|\bar{X}|}-1\right)+\sqrt{b}}\frac{b}{(b+\beta)}\right] - \sqrt{\beta}\left[\sin^{-1}\left(\frac{\sqrt{b+\beta-1}}{\sqrt{\beta+b}}\right) - \sin^{-1}\left(\frac{\sqrt{\beta}}{\sqrt{\beta+b}}\right)\right] \quad \text{(S82f)}$$

Substituting eq. (S82f) into eq. (S80b), we obtain eq. (60c) of the main text, which is

$$Q_{PL2} = \frac{2}{\beta}F'\left(-|\bar{X}|\right)\left(\sqrt{1+\beta|\bar{X}|}-1\right) + \frac{H_3}{\beta} = -\frac{1}{2\beta}\ln\left|\frac{\sqrt{1+|\bar{X}|}+1}{\sqrt{1+|\bar{X}|}-1}\right|\left(\sqrt{b}-1\right) + \frac{H_3}{\beta}$$
$$= -\frac{\left(\sqrt{b}-1\right)}{2\beta}\ln\left|\frac{\sqrt{1+|\bar{X}|}+1}{\sqrt{1+|\bar{X}|}-1}\right| + \frac{\sqrt{b}}{2\beta}\ln\left[\frac{b+\beta\left(1+\sqrt{1+|\bar{X}|}\right)+\sqrt{b}}{b-\beta\left(\sqrt{1+|\bar{X}|}-1\right)+\sqrt{b}}\frac{b}{(b+\beta)}\right] - \frac{1}{\sqrt{\beta}}\left[\sin^{-1}\left(\frac{\sqrt{b+\beta-1}}{\sqrt{\beta+b}}\right) - \sin^{-1}\left(\frac{\sqrt{\beta}}{\sqrt{\beta+b}}\right)\right] \quad \text{(S82g)}$$

Adding eq. (S82g) and eq. (S78), we obtain the integral in eq. (S69):

$$Q_{PL}\left(\bar{X}\le 0, m=\frac{1}{2}\right)=Q_{PL1}+Q_{PL2}=\frac{\sqrt{b}}{2\beta}\ln\left(\frac{b+\beta}{b}\right)-\frac{1}{\sqrt{\beta}}\sin^{-1}\left(\frac{\sqrt{\beta}}{\sqrt{b+\beta}}\right)$$
$$-\frac{\left(\sqrt{b}-1\right)}{2\beta}\ln\left|\frac{\sqrt{1+\left|\bar{X}\right|}+1}{\sqrt{1+\left|\bar{X}\right|}-1}\right|+\frac{\sqrt{b}}{2\beta}\ln\left[\frac{b+\beta\left(1+\sqrt{1+\left|\bar{X}\right|}\right)+\sqrt{b}}{b-\beta\left(\sqrt{1+\left|\bar{X}\right|}-1\right)+\sqrt{b}}\frac{b}{(b+\beta)}\right]-\frac{1}{\sqrt{\beta}}\left[\sin^{-1}\left(\frac{\sqrt{b+\beta-1}}{\sqrt{\beta+b}}\right)-\sin^{-1}\left(\frac{\sqrt{\beta}}{\sqrt{\beta+b}}\right)\right]$$
$$=\frac{\sqrt{b}}{2\beta}\ln\left(\frac{b+\beta}{b}\right)-\frac{\left(\sqrt{b}-1\right)}{2\beta}\ln\left|\frac{\sqrt{1+\left|\bar{X}\right|}+1}{\sqrt{1+\left|\bar{X}\right|}-1}\right|+\frac{\sqrt{b}}{2\beta}\ln\left[\frac{b+\beta\left(1+\sqrt{1+\left|\bar{X}\right|}\right)+\sqrt{b}}{b-\beta\left(\sqrt{1+\left|\bar{X}\right|}-1\right)+\sqrt{b}}\frac{b}{(b+\beta)}\right]-\frac{1}{\sqrt{\beta}}\sin^{-1}\left(\frac{\sqrt{b+\beta-1}}{\sqrt{\beta+b}}\right)$$
$$=\frac{\sqrt{b}}{2\beta}\ln\left[\frac{b+\beta\left(1+\sqrt{1+\left|\bar{X}\right|}\right)+\sqrt{b}}{b-\beta\left(\sqrt{1+\left|\bar{X}\right|}-1\right)+\sqrt{b}}\right]-\frac{\left(\sqrt{b}-1\right)}{2\beta}\ln\left|\frac{\sqrt{1+\left|\bar{X}\right|}+1}{\sqrt{1+\left|\bar{X}\right|}-1}\right|-\frac{1}{\sqrt{\beta}}\sin^{-1}\left(\frac{\sqrt{b+\beta-1}}{\sqrt{\beta+b}}\right)$$

(S83)

Recall that $b=1+\beta\left|\bar{X}\right|$**.**

S33. Local dissipation rate and dissipation zone

We first derive the local dissipation rate directly ahead of the cohesive zone tip ($X > \alpha$). Consider plane stress deformation. Material elements on the crack line are under equal bi-axial tension, and so the non-trivial strains are $\varepsilon_{11}=\varepsilon_{22}$ and they are related to the stress $\sigma_{11}=\sigma_{22}$ by eq. (S29a), i.e.,

$$\varepsilon_{22}\left(\bar{X},Y=0\right)=-\frac{1}{2}\int_{\bar{X}}^{\infty}J\left(\frac{\bar{X}'-\bar{X}}{vt_c}\right)\frac{\partial\sigma_{22}}{\partial\bar{X}'}d\bar{X}'. \tag{S84}$$

For a standard solid (SS), $J\left(t\right)$ is given by eq. (16b) of the main text, where $J_\infty=1/E_\infty$ and $J_0=1/E_0$. The viscosity η_v of the dashpot of the standard solid in bi-axial tension is related to the retardation time t_c in eq. (16b) of the main text by

$$\eta_v=2E_\infty\left(1-\frac{E_\infty}{E_0}\right)t_c. \tag{S85a}$$

We decompose the stress σ_{22} into a part that acts on the soft spring $\left(\sigma_{22s}\right)$, and the rest acts on the Maxwell element consisting of a spring (with modulus E_0-E_∞ and a dashpot with viscosity η_v) in series. The stress σ_s acting on the soft spring is (the factor of 2 comes from biaxial deformation),

$$\sigma_{22s}=\frac{2}{J_\infty}\varepsilon_{22}=2E_\infty\varepsilon. \tag{S86a}$$

Hence the viscous stress acting on the dashpot is

$$\sigma_{22}-\sigma_{22s}=\frac{2\sigma_D}{\pi}\tan^{-1}\sqrt{\frac{1}{\bar{X}-1}}-2E_\infty\varepsilon_{22}\quad , \tag{S86b}$$

where σ_{22} is given by eq. (S28). The strain in eq. (S86b) is given by eq. (38a) in the main text. Substituting the strain into eq. (S86b) gives:

$$\frac{2\sigma_D}{\pi}\tan^{-1}\sqrt{\frac{1}{\bar{X}-1}}-2E_\infty\varepsilon_{22}=\frac{\kappa\sigma_D}{\pi}\exp\left(\beta\bar{X}\right)\Psi\left(\bar{X},\beta\right), \tag{S86c}$$

where $\beta = \alpha/vt_c$ and Ψ is given in eq. (38b) of the main text. The dissipation power at a material point is:

$$2\frac{\left(\sigma_{22}-\sigma_{22s}\right)^2}{\eta_v}=\frac{\kappa}{E_\infty t_c}\left(\frac{\sigma_D}{\pi}\right)^2\left[\exp\left(\beta\bar{X}\right)\Psi\left(\bar{X},\beta\right)\right]^2 \tag{S86d}$$

The factor of 2 on the left hand side of eq.(S86d) accounts for the fact that stress work is done by both σ_{11} and σ_{22} (biaxial deformation). Due to the steady state crack growth condition, the local dissipation rate (per unit crack extension) Φ_D is obtained by dividing eq. (S86d) by the crack velocity v, which results in eq. (62a) of the main text:

$$\Phi_D\left(\bar{X}\ge 1, Y=0\right)=\frac{\kappa}{E_\infty vt_c}\left(\frac{\sigma_D}{\pi}\right)^2\left[\exp\left(\beta\bar{X}\right)\Psi\left(\bar{X},\beta\right)\right]^2 \tag{S87a}$$

The maximum dissipation rate occurs at $\bar{X}=1$. From eq. (S30b,c),

$$\Psi\left(\bar{X}=1, Y=0, \beta\right)=\pi erfc\left(\sqrt{\beta}\right) \tag{S87b}$$

If we use the non-interacting model where the stress field near the cohesive zone is approximated by the *K*-field (i.e., Persson and Brener's approach), i.e., where $\sigma_{22}=\sigma_D/\sqrt{\bar{X}}$ and the viscous stress is

$$\frac{\sigma_D}{\sqrt{\bar{X}}}-\sigma_{22s}=\frac{\kappa\sigma_D}{\sqrt{\bar{X}}}\left\{1-\sqrt{\pi\bar{X}\beta}\exp\left(\beta\bar{X}\right)erfc\left(\sqrt{\beta\bar{X}}\right)\right\}. \tag{S88a}$$

The local dissipation rate Φ_D^* for this case is obtained using eq. (S88a) and the left hand side of eq. (S86d), this results in eq. (64) of the main text:

$$\Phi_D^*=\frac{\kappa\sigma_D^2}{E_\infty vt_c\bar{X}}\left\{1-\sqrt{\pi\bar{X}\beta}\exp\left(\beta\bar{X}\right)erfc\left(\sqrt{\beta\bar{X}}\right)\right\}^2. \tag{S88b}$$

S34. Areal distribution of the local dissipation rate

Next, we calculate the 2D distribution of the local dissipation rate Φ_D assuming plane stress deformation. Because of the multiaxial stress and strain state around the crack, Φ_D is defined as

$$\Phi_D = \frac{\sigma_{ij}\dot{\varepsilon}_{ij} - \dot{W}_e}{v} \ . \tag{S89a}$$

Using steady state condition, eq. (S89a) simplifies to

$$\Phi_D = -\sigma_{ij}\frac{\partial \varepsilon_{ij}}{\partial X} + \frac{\partial W_e}{\partial X} . \tag{S89b}$$

To evaluate the elastic stress power $\dot{W}_e$, we take a generalized Maxwell element which is represented schematically in Fig.S4. $\dot{W}_e$ is evaluated by computing the time rate of change of the energy stored in the springs. The energy stored in the springs are (see Fig.S4)

$$W_e = \frac{1}{2}\left[\sigma_{ij}^{(1)}\varepsilon_{ij}^{(1)} + \sigma_{ij}^{(2)}\varepsilon_{ij}^{(2)}\right],\ i = 1,2 \tag{S90a}$$

where

$$E_1 = E_\infty \tag{S90b}$$

$$E_1 + E_2 = E_0 \tag{S90c}$$

$$\sigma_{ij}^{(1)} + \sigma_{ij}^{(2)} = \sigma_{ij}, \qquad \varepsilon_{ij}^{(1)} = \varepsilon_{ij} \tag{S90d}$$

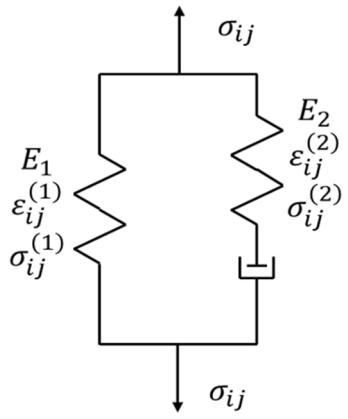

Figure S4 Schematic representation of the Standard Solid model.

Using the stress field σ_{ij} given in Section S1, we can evaluate $\sigma_{ij}^{(1)}, \sigma_{ij}^{(2)}, \varepsilon_{ij}^{(1)}, \varepsilon_{ij}^{(2)}$ given in eq. (S90d). Note that $\sigma_{ij}^{(1)}$ and $\varepsilon_{ij}^{(1)}$ are related through the linear elastic Hooke's law with Young's

modulus E_∞ and Poisson ratio = 0.5. Once $\sigma_{ij}, \varepsilon_{ij}, \frac{\partial \sigma_{ij}}{\partial X}, \frac{\partial \varepsilon_{ij}}{\partial X}$ are derived, we compute Φ_D everywhere on the plane using eq. (89a). We normalize the dissipative work rate as follows:

$$\bar{\Phi}_D = \Phi_D \Big/ \left(\frac{\kappa \sigma_D^2}{E_\infty v t_c} \right) \tag{S91}$$

The contour lines of $\bar{\Phi}_D$ shown in Fig.14 of the main text are obtained using MATLAB by dividing the region into discrete grid points and calculating the normalized local dissipation rate $\bar{\Phi}_D(\bar{X}, \bar{Y})$ at every grid point.

We used two ways to verify the accuracy of our numerical calculation. First, we compare results of the normalized local dissipation rate $\bar{\Phi}_D$ directly ahead of the cohesive zone tip (i.e., $\bar{X} \geq 1$ and $Y = 0$) from our 2D numerical calculation and eq. (62) of the main text, which is shown in Fig. S5. These two results agree well. Second, the areal integral of local dissipation rate $\iint \bar{\Phi}_D \, \mathrm{dA}$ should be equal to the total energy dissipation rate $G - G_0 = (\bar{G} - 1)G_0$. We use $\kappa \sigma_D^2 / (E_\infty v t_c)$ to normalize these two values, and then use the theory of Knauss to evaluate $\bar{G}$. The comparison of these results is shown in Fig.S6 below.

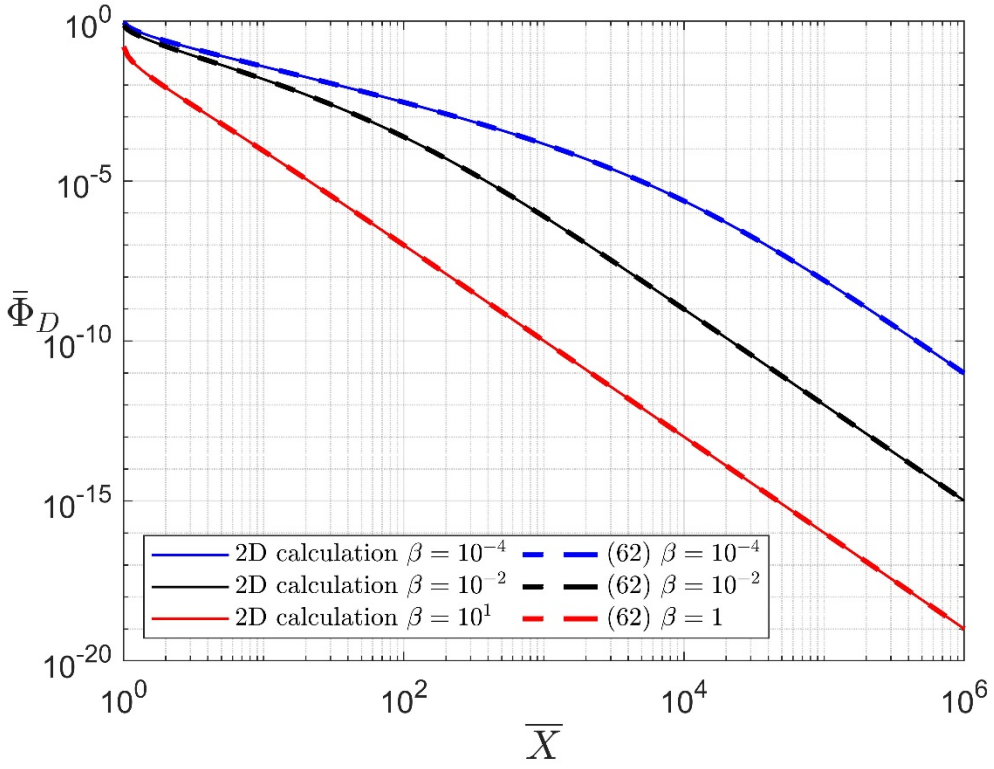

Figure S5 Normalized local dissipation rate $\bar{\Phi}_D$ directly ahead of the cohesive zone tip ($\bar{X} \geq 1$ and $Y = 0$) for different values of β. Results from the 2D numerical calculation (solid lines) agree well with those from eq. (62).

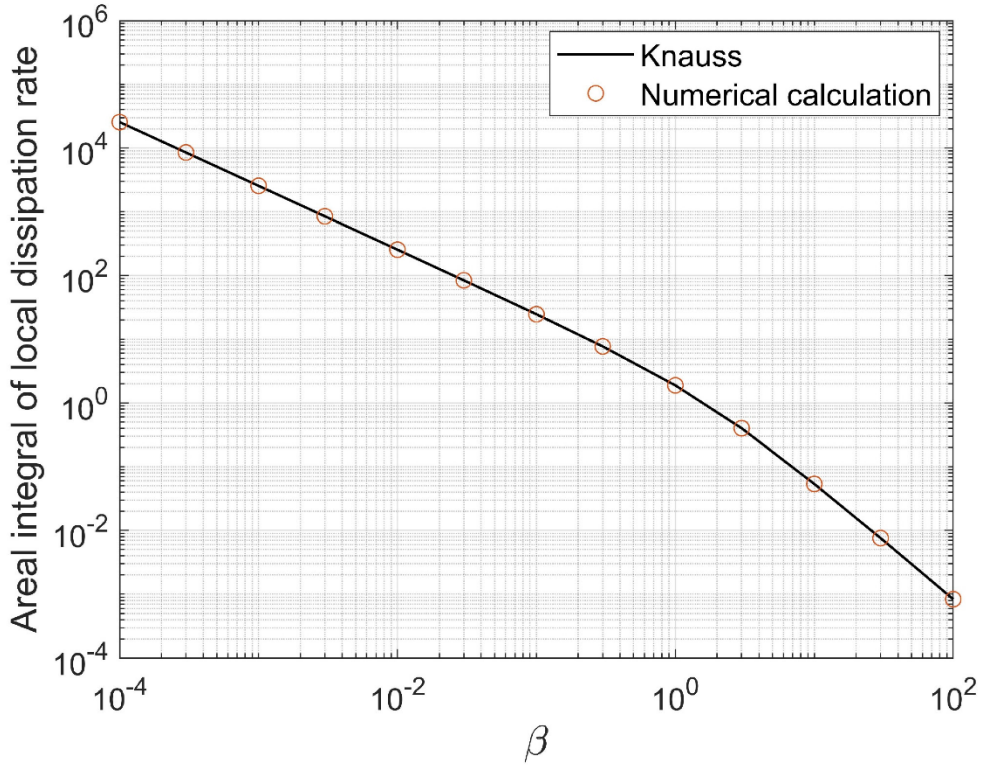

Figure S6 Comparison between the areal integral of the local dissipation rate $\iint \bar{\Phi}_D \, dA$ and the total energy dissipation rate $G - G_0$ calculated using Knauss's theory for different values of β. Results from the 2D areal integral agree well with those based on Knauss's theory.

References:

[1] Rice JR. Mathematical Analysis in the Mechanics of Fracture. In: Liebowitz H., editor. Fract. An Adv. Treatise. Vol.2, Mat, Academic Press, N.Y.; 1968, p. 191–311.

[2] Schapery RA. A theory of crack initiation and growth in viscoelastic media II. Approximate methods of analysis. Int J Fract 1975;11:369–88. doi:10.1007/BF00033526.

[3] Ferry JD. Viscoelastic properties of polymers. third. John Wiley & Sons; 1980.

[4] Christensen R. Theory of viscoelasticity: an introduction. second. Elsevier; 1982.

[5] WAPNER PG, FORSMAN WC. Fourier transform method in linear viscoelastic analysis. The vibrating viscoelastic reed. Trans Soc Rheol 1971;15:603–26. doi:10.1122/1.549216.

[6] Erdelyi A, Magnus W, Oberhettinger F, Tricomi FG. Tables of Integral Transforms, Bateman Manuscript Project Volume I. McGraw-Hill New York; 1954.

[7] Gradshteyn IS, Ryzhik IM. Table of integrals, series, and products. Academic Press; 1965.

[8] Gent AN, Lai S-M. Interfacial bonding, energy dissipation, and adhesion. J Polym Sci Part

B Polym Phys 1994;32:1543–55. doi:10.1002/polb.1994.090320826.

[9] Knauss WG. A review of fracture in viscoelastic materials. Int J Fract 2015;196:99–146. doi:10.1007/s10704-015-0058-6.

[10] Abramowitz M, Stegun IA. Handbook of mathematical functions with formulas, graphs, and mathematical tables. vol. 55. US Government printing office; 1964.